

Acta Universitatis Sapientiae

**Electrical and Mechanical
Engineering**

Volume 5, 2013

Sapientia Hungarian University of Transylvania
Scientia Publishing House

Contents

Telecommunications & Signal Processing

Cs. Simon, M. Maliosz, B. Baranyai

Network Based Caching For Near Real-Time Streaming Video5

L. Molnár, Sz. András, I. Kotta, I. Székely

New Approaches Analyzing Usage of the Telecommunication Services21

Industrial Electronics & Control Systems

L. Márton, K. György

Two-Stage Kalman Filtering for Indoor Localization of Omnidirectional Robots.....44

L. Kenéz, N. Kutasi, E. Filep, L. Jakab-Farkas, I. Á. Szőcs

Heat-Treatment of 16MnCr Steel in a Linear Non-Isotherm Plasma Reactor61

Mechanical Engineering

M. Máté

The Single-Parametric Model of the Meshing by Cutting Cylindrical Gears Having Archimedean Spiral Curved Tooth Line.....73

D. Lates, S. Noveanu, V. Csibi

Characterization Methods of a 2 DOF Micro Positioning Compliant Mechanism85

V. S. Jisa, D. Lates

Gripping Compliant Systems Operated with Bellows Actuators Used in Biomedical Engineering97



Network Based Caching for Near Real-Time Streaming Video

Csaba SIMON, Markosz MALIOSZ, Balázs BARANYAI

Department of Telecommunications and Media Informatics,
Budapest University of Technology and Economics,
1117 Budapest, Magyar T. krt. 2., Hungary,
e-mail: {simon; maliosz}@tmit.bme.hu

Manuscript received March 29, 2014; revised September 15, 2014.

Abstract: Nowadays more and more live events are being consumed via the web or smart phones rather than legacy broadcast services. In this paper we present a scenario – focusing on wireless smartphone-based nodes – that covers this trend. Starting from this scenario we introduce a novel service that can be offered on top of classical streaming media services to the users of these mobile handheld devices. Considering that the wireless infrastructure is heavily loaded by the traffic of the real-time stream itself, we propose a distributed caching solution to offload it, improving the scalability of the system. We define two heuristic algorithms to place the caching elements within the network in an optimal way – the goal was either to minimize the required number of caching nodes or the size of the cache. In our earlier work we have investigated some individual aspects covered by the scenario and built a testbed that implements these proposals. In this paper we present the extension of this integrated testbed suitable for network coding based communication, which supports the measurement based evaluation of the presented scenario and the evaluation of the implementation details. Finally we offer a measurement based assessment of the features implemented in the testbed.

Keywords: network coding, video streaming, caching.

1. Introduction

The economic success and the market share of Android devices [1] led to the situation where a significant part of the population carries a plentiful of sensors and short-range communication devices with them. These general purpose devices have an unprecedentedly high computational power, allowing the execution of complex operations in the background. The smartphones also offer the possibility to experiment with a wide variety of wireless networking issues. In our earlier work we have started to develop a generic testbed environment, as

introduced in [2] and [3]. In this testbed the Android devices may act as harvesters (mobile data collectors), communicating nodes and real-time media endpoints in distributed wireless networks. We primarily used this testbed to research the applicability of network coding techniques in sensor networks and on forwarding streaming video over wireless links [3].

In [2] we also presented several scenarios that motivated our research of network coding. The scenarios cover wireless sensor networking (WSN - [4]) communication and distributed wireless communication research issues, network coding application alternatives, real-time media streaming and communication management. For the details of the respective scenarios please refer to [2].

In this paper we extend the scenarios, introducing a novel service that can be offered on top of a classical streaming media service. The scenario focuses on crowded events, when lots of users follow the same live content. The new service is the replay of recent highlight of this real event. Considering that the wireless infrastructure is heavily loaded by the traffic of the real-time stream itself, we propose a distributed caching solution to offload it, improving the scalability of the system. We will discuss the details of such novel service and will present a model that will allow us to analyze its behavior later in Section 3. Although media distribution might use multicast in order to use efficiently the network resources, most of the devices and applications still use unicast. Therefore in the following we will focus only on unicast solutions. Because the scenarios are used as motivations for our research, which are validated by testbed experiments, the testbed development was a natural follow up of the scenario definition and analysis. We implemented both the media streaming and network coding support in our testbed that can be used to demonstrate the presented scenarios and the test implementation details. The details of this work are presented in Section 5.

As explained in this paper, the implementation of this scenario is based on network coding mechanisms, already used in earlier scenarios. Network coding (NC) mechanism re-codes packets of flows within the network at various nodes, promising overall higher throughput and/or reliability [2], [5]. Here we only shortly review the main advantage of the NC, using the widely used butterfly topology (see *Fig. 1*): “if the packets of a stream are distributed over parallel paths (flows a and b) and packets are encoded together using network coding, the original packets can be restored at the destination. This approach can be used to increase the network capacity. Let us assume that both a and b flows require the same bandwidth. In *Fig. 1* the common link carries the encoded $a+b$ flow instead of carrying both a and b flows. Now, using NC techniques, the required capacity of $a+b$ is the same as for the individual a (or b) flow. Thus we

can achieve a 50% cost saving over the common link in terms of bandwidth capacity” [2].

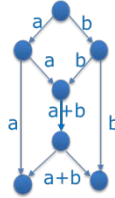


Figure 1: Network coding in a network with butterfly topology.

In our work we follow an alternative (Random Linear Network Coding - RLNC - [6]), where nodes assign coefficients to each packet randomly. All nodes using random network coding are independent and randomized, without the need of any knowledge of the rest of the network, assuring high quality transmission [7]. Early works focused on the case when the network is populated by large enough number of flows (inter-flow NC) [8], then also considered the intra-flow case [9]. Later works then further extended the area of applicability [10], [11], [12].

2. Caching of media streams – related work

The traffic volume of streaming media had exceeded that of any other traffic type, including peer-to-peer or web access and researchers tried to reduce its bandwidth demand by various methods, including caching. There is a vast available literature in this field. In what follows we highlight the most important ones.

Early caching strategies focused on the deployment of a dedicated proxy close to the consumers, and a good overview of these solutions divided them in four categories: sliding-interval caching, prefix caching, segment caching, and rate-split caching [13]. The sliding-interval caching [14] stores data at the first appearance of it (as it is arriving from the server), and delivers it to the subsequent requests. The prefix caching [15] always stores the first segments of the media, thus the proxy can immediately serve any request and starting to fetch the rest of the data in the meantime. The segment caching [16], [17], [18] offers a more advanced solution, because it assigns utilities to the segments, and caches them accordingly. The rate-split caching [19] breaks with the time-based segmentation of the stream and splits it along the rate. The lower rate component may arrive directly from the server, while the rest of the data, ensuring the premium quality of the service, uses only local networking resources.

The advent of the peer-to-peer (P2P) networks influenced this research area, as well. Several P2P based solutions were proposed: some of them are more

generic, as rely on the logical P2P overlays [20], or ones that use the specific architecture of the access network and cannot be directly applied in other networks [21].

As Content Delivery Networks (CDN) gained in popularity, researchers applied the streaming video caching mechanisms on this technology, too [22]. Similarly, caching in clouds is a promising research direction [23]. Nevertheless, both directions require heavy investments in the infrastructure. Moreover, in our scenario the problem is the overload of the access, which connects the cloud to the users, thus we still have to address this issue. The combination of network coding methods with P2P solution is a noteworthy novelty [24], but in this paper we focus on a specific service, not supported in earlier papers.

Finally we mention the new networking paradigm, the Information Centric Network, which has an advanced caching mechanism [27], integrated with its novel data forwarding mechanism. The challenging research issues gave birth to several interesting papers [25], [26] involving multicast scenarios, but our work deals with classical IP unicast networks.

The reader interested in further details of streaming video caching is directed to a thorough overview of this field [28].

3. Near-real time streaming supported by caching

A. Basic Scenarios

Before presenting our new scenario we summarize first the basic scenarios that motivated our work, because it leads to a better understanding of our testbed and also introduces the reader to Section 3.B. For a detailed description the reader is redirected to [2]. The scenarios built on the fact that the cheap short-range wireless devices (RFID and NFC tags) favor the deployment of large distributed wireless sensor networks (WSN) [4]. Nevertheless, the collection of the sensory data from such large deployed networks will be both an economical and a logistic issue. We proposed to use the ubiquitous Android smartphones to do this task and envisaged a cooperative wireless mesh to convey the sensory data to a management center. Apart of sensory data, the smartphones had to forward live video and control traffic, both required to manage and control the wireless nodes. The network coding was the technology of choice to improve the reliability and performance of the communication over the wireless mesh.

In this paper we build on the basic scenarios, reusing the ideas of forwarding live streaming video streams. Although we reuse many building blocks developed during our earlier work, this new scenario can be described and

analyzed as a standalone one. Note that this common background will be more evident when we describe our testbed, as mentioned later in Section 5. As a consequence the following sub-section contains the definition of the scenario itself, along with the motivation behind it.

B. Near real-time streaming service

In their quest to gain competitive advantage on the travel and leisure market, many cities organize large public events: city festivals or thematic events (e.g., concerts, art festivals, sporting events). In parallel with this trend more live events are being consumed via the web or smart phones rather than broadcast; the “second screen” is gaining prominence and people are multi-tasking on their devices; attendees of live events continue using their smart devices (e.g. for social media). Current access networks are hard pressed to provide the required QoS.

This scenario aims at providing various mechanisms to support the goal of increasing QoE of live media streaming while at the same time decreasing the network load. The target service is for (near) real-time streaming media distribution. Note that participants at events often want to see replays of the key moments or re-watch some recent performance, often only a few seconds after it happened. We build on the trend that attendees of live events will use their smart devices during the event – for email, social media and, more and more, for recording and consuming video.

The load in the wireless access is decreased by the use of network coding and stretching the lifetime of the network encoded packets somewhere in the network distributed in end devices or well-placed points in the distribution/access domain. The cached distribution primarily is implemented on the user's devices.

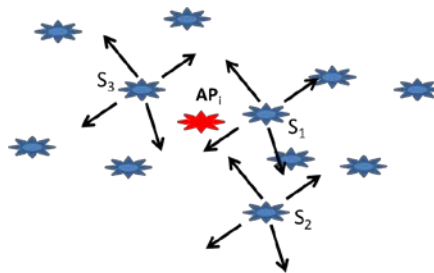


Figure 2: Media streaming with caching.

This scenario is depicted in Fig. 2. The streaming media is distributed by the AP_i Access Points. The nodes receiving the data encode it and cache it locally (S_1, \dots). Any time a node (blue stars) want a replay, they will have the data chunks readily available in their local mesh network.

The above scenario, although seems a quite limited one at first glance, it proves to be a complex one. The complexity comes from the fact that it uses many technologies and during the analysis of the scenario we have to deal both with the technical details to be solved in order to implement the scenario and with the interactions among these particular technologies. In our earlier work we have investigated some individual aspects covered by the scenario.

In our earlier paper [2] we evaluated candidate radio technologies to support the scenarios. In [3] we investigated the aspects of distributed streaming video communication in our testbed, focusing on the performance of a simplified logical ring that formed a peer-to-peer overlay over the Android devices within the testbed. In [5] we presented a simulation based performance evaluation of caching strategies. In this paper we add new elements to these series of results, addressing the particularities of this scenario introduced above. We propose two alternative algorithms that offer an optimized solution to our scenario. Then in Section 5 we present an extension of our earlier testbeds that can support the measurement based evaluation of our scenario.

4. Proposed caching model optimization

In this section we take a closer look at two alternatives to optimize the cache placement within the scenario presented in Section 3.B. The optimization problem is not trivial, because not all nodes should necessarily act as caches and even those that do, do not necessarily store every packet in their cache memory. The starting point is the all the nodes are attached to one AP_i from the set of a set of $\{AP_i\}$ Access Points and the covered area is large enough to make sure that nodes cannot communicate directly with everyone within the whole network. We also consider that the nearest caching nodes and cache hit statistics can be obtained by the requesting nodes [5].

A. Minimizing the number of caches

In the first model we search for the number of caching nodes to serve those nodes that are attached to the same AP and we allow to store unlimited number of segments in the cache. We can give the required number of caching nodes $|S_i|$ as the rounded up value of the total size of required data chunks (g_w segments are required for D_i users) divided by the direct link capacity c :

$$|S_i| = \left\lceil \frac{D_i g_w}{c} \right\rceil \quad (1)$$

Note that this solution does not allow that a node attached to AP_i to request data from a caching node attached to AP_j . *Our goal is to get the minimal number*

of caching nodes, a subset of all N nodes. c_i is the total capacity of the direct link from node i (we consider that the total incoming and outgoing capacities are equal). In [5] we gave a 0-1 Integer Linear Programming (ILP) to solve this optimization problem, but this type of ILPs are known to be NP hard [29].

Therefore we propose the following heuristic algorithm (see *Table 1*).

Table 1: The cache placement algorithm.

```

Foreach  $AP_i$ 
  Compute  $|S_i|$  based on eq. (1)
   $X_i :=$  arbitrary selection of  $|S_i|$  nodes from the vicinity of  $AP_i$ 
 $S = \bigcup X_i$ 

Foreach  $AP_i$ 
  Partition all the nodes with demands based on distance from the coverage
  area  $AP_i$  among  $X_{ij}$ 
   $C_{ij} =$  total expected demand on  $X_{ij}$ 

Do
  Flag = 0
  Foreach  $X_{ij}$ 
    If  $C_{ij} < \text{Capacity}(X_{ij})$  then
      Flag = 1
      Elect an additional X from the vicinity
      Re-partition all the nodes with demands based on distance from
      the coverage area  $AP_i$  among  $X_{ij}$ 
Until Flag == 0

```

The above heuristic algorithm takes all APs and makes an initial selection of caches as given in (1) for the simplified scenario. Then it refines this selection, introducing new caching nodes in those areas, where the existing ones cannot answer all the demands. If there are no more unanswered demands, the algorithm stops.

B. Minimizing the cache size

In Section 4.A we tried to reduce the number of caching nodes, without restricting the individual cache sizes. *Now we will try to minimize the size of the cache, but we do not restrict the number of caching nodes.* Let us keep the same notations we introduced earlier in this section, and additionally let us note the

number of chunks *stored* at node i with k_i . We proposed and ILP in [5] to solve this optimization problem, but the same reasoning presented in Section 4.A applies here, as well. Therefore we provide a heuristic algorithm that solves this problem. First we give the number of chunks a node should store, if the chunks are evenly distributed among all nodes attached to the AP_i . We keep the notation used for eq. (1), and we note with N_i the total number of attached nodes.

$$k_i = \left\lceil \frac{D_i g_w}{N_i} \right\rceil \quad (17)$$

The algorithm is given in *Table 2* below.

Table 2: The cache placement algorithm.

```

Foreach  $AP_i$ 
    Compute  $k_i$  based on eq. (17)
 $k = \min_i (k_i)$ 
Store  $k$  chunks in each node

Foreach leacher  $l$ 
    Assign the closest nodes (caches) to it
    Can't assign more than  $c_l$ 
 $g_l =$  total available chunks at these caches

Do
    Flag = 0
    Foreach leacher  $l$ 
        While  $g_l < g_w$  do
            Flag = 1
             $k_{l++}$  for the caches linked to  $l$ 
                //this can be done in parallel – increase the cache only once
                //during a single round
Until Flag == 0

```

The algorithm computes the minimal number of chunks that should be available at the nodes (i.e., caches, since every node is a potential cache) in order to satisfy the lowest demand at any AP. Then we find those leachers, which have unsatisfied demand and increase the cache size by one for its caches. The algorithm stops, if there are no new unsatisfied leachers left.

5. Video streaming environment with Android smartphones

In this section we present a testbed to support the evaluation of the proposed scenario and algorithms presented in this paper.

A. Testbed for streaming video services

Earlier in this paper we have already motivated our testbed development work by the need to obtain a platform suitable to assess our scenarios. The common point in our scenarios is the presence of a mobile node capable of communicating over IP. This node was implemented as a remote controlled vehicle, where the computational and communication functions are executed by an Android smartphone, implementing an extended distributed data network. The interface between the Android device and the motors moving the vehicle is done by a dedicated microcontroller board, the IOIO [30].



Figure 3: a) The elements of the mobile node and b) the implemented vehicle.

Fig. 3. a) presents the components of the implemented mobile node. The vehicle and the driving motors are on the left bottom, the IOIO board is one the upper left part of the figure. The Android smartphone (pictured on the upper right part of the figure) is linked to the IOIO board by Bluetooth (but we can also use USB cables for this purpose). This device is also responsible with the control tasks. A central management entity (bottom right corner) has a suitable GUI to control the movement of the node (on the downlink direction) and is connected to it over variants of WiFi (see Section 5.C for further details). As a part of the control process, live video streams are sent from the mobile node to the control station (i.e., uplink), the implementation details of this streaming service being discussed later in Section 5.B. The implemented mobile node and the management station is pictured in Fig. 3. b).

B. Streaming media over Android

The multimedia stream in the testbed is offered by an application implemented from scratch by us.

A natural choice would have been the use of Real-time Transport Protocol (RTP) for such task [31]. RTP based streaming in Android is supported by the *libstreaming* library. The encoding for RTP transmission should be done using H263 codecs instead of H264, since the latter has higher resource demands. For decoding at the destination an external library can be used (we used vlc player, which was able to decode the stream [32]). Due to the above Android environment details (e.g., the delays introduced by encapsulation and control, video handling difficulties) we decided to go for different solution.

As a first option, in order to capture the stream from the camera of the smartphone, we use the camera preview images. Then these raw images are sent to an image encoding library, and this encoded JPEG image, which corresponds to a frame of the video stream, is sent over UDP to the recipient(s). This solution makes it easier to handle the frames at the receiving peer and debug our implementation: any disturbance in the encoding/decoding process is limited to a well identifiable frame, not to a sequence of frames. The fragmentation of the video frames and the header structure of the packets have been designed to be able to carry multiple streams and/or support multiple networks encoding along the path. In our first tests we checked the viability of our solution.

A second option was to use other, older encoders developed for TV transmission in a selfcontaining mode. E.g., MPEG-2 Transport Stream (MPEG-2 TS, M2TS) has been introduced in ISO/IEC 13818-1 standard in 1995 [33]. It has the advantage that video format info is in-band. Most of Android smartphones support the playout of such streams, but the encoding of such streams officially is not supported. Some forums reported that that in some devices with Android OS above version 3.0 have unofficial support for this format (e.g., Google Nexus 4). We used this smartphone to implement and test our solution.

Fig. 4. shows the logical structure of our solution. The live feed from the camera is encoded by the Media Recorder in real time. Instead of saving this stream locally, it is written into a socket, which is used to send the stream over the Internet. On the receiver side the ideal playout method would have been to feed the read socket directly to the player, but the available players require a seekable source. Therefore the socket is read in a loop, temporarily stored in a file and the player plays the video from this file. The file is continuously filled from the socket and read by the players. We just have to make sure that the new video content is filled fast enough into the file as the player never reaches the end of the file. We made some experiments and found that a 200ms buffer is enough for this goal.

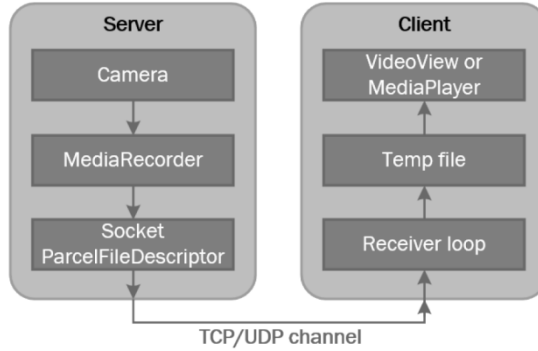


Figure 4: Client-server architecture of the MPEG-2 TS implementation.

We compared our two solutions and we found that there is a tradeoff on quality vs delay. The JPEG based solution has lower delays (avg. 300ms), but during fast moves it is blurred, while the MPEG-TS based solution offers usable picture during fast moves, too, but it has higher delays (avg. 500ms).

Finally, in *Table 3* we summarized the measured performance of the video transfer in our testbed. The first row corresponds to our first implementation, when we forward the series of JPEG still pictures captured at the source. Then we show the RTP-based solution, finally the MPEG2-TS based implementation. As we can see, the packet delays are extremely high in the case of the RTP based solution, while the other two provide similar results, with a clear advantage on the JPEG-based implementation. Note that for the MPEG based implementation we did not have packet-level statistics. The required bandwidth was similar for the first two solutions, but it came at the price of lower Quality of Experience (QoE). The highest disadvantage of the JPEG based solution was the low fps (frame per second) value. The QoE of the MPEG based solution outperformed both previous solutions.

Table 3: The performance of tested video transfer solutions.

Technology of choice	Delay [ms]	Avg. delay [ms]	Bandwidth [kilo Bytes/sec]	Avg. BW [kilo Bytes/sec]	Avg. video q. [fps]	Still picture quality (QoE)	Moving picture (video) quality (QoE)
JPEG	170-440	290	100-300	170	15	Blurry	Blurry
RTSP	1090-1570	1300	100-200	150	20	Good	Checked
MPEG-2 TS	-	500	-	250	-	Excellent (sharp)	Rarely checked

C. Communication between the mobile nodes

The Android smartphone attached to the vehicle is able to control the vehicle, to collect sensory data and to capture live streams. Nevertheless, in order to exploit these capabilities we have to assure the delivery of the data to the management center. We proposed scenarios where this is achieved through a cooperative mesh between Android smartphones (see the testbed in *Fig. 5*).



Figure 5: Mobile nodes in the distributed testbed.

The cooperative mesh is a logical construct at layer 3. In order to implement it in the testbed we used several WiFi variants. The Android SDK assures a complex API to handle WiFi related aspects [34]. Unfortunately, the WiFi ad hoc mode is not supported by Android. They introduced WiFi Direct [35] (earlier also known as WiFi P2P) instead, designed to provide seamless device-to-device WiFi connection. We implemented our testbed using this technology, the measurement results being generated with this setup. Nevertheless, we also used the infrastructure mode WiFi communication in our testbed and focus on the logical overlay to emulate distributed communication scenarios [3]. [2] introduces our RLNC implementation, and is not affected from the choice of which WiFi alternative is used.

As the proposed scenario is based on the network coding of streaming data, we evaluated the performance of the testbed by means of measurements. We

used the unsuccessful display attempts during the playout process to assess the performance of the implementation. This is a complex parameter, aggregating the events of unsuccessful decoding attempts and the de-synchronization events. This latter happens when the encoded packet streams arriving over two branches are skewed, thus the decoder cannot get enough coded segments. Note that this event may be caused by the delays caused by a slow wireless link (e.g., slowed down by interference, resent packets, etc.).

Since decoding is a computationally intensive process, we tested devices from two different generations (Google Nexus S and Nexus 4). *Table 4* presents the average results obtained after 10 experiments. We present both the encoding and decoding performance. Note that in all cases the QoE of the played video was specific to the JPEG streaming solution (i.e., it allowed to successfully control the mobile node in real-time).

Table 4: The performance of network coding of media streams.

Smartphone model	Encoding loss rate [%]	Decoding loss rate [%]
Google Nexus S	4.8	19.1
Google Nexus 4	4.1	11.5

We can see that the encoding process has significantly lower impact. Also note that the older device has only slightly lower performance than the Nexus 4. During the decoding phase the Nexus S cannot keep the pace, the performance gap between the two becoming significantly larger. A practical conclusion of these measurements is that current state-of-the art Android devices (which are 3 years newer by design compared to the Nexus 4) provide enough resources to support real-time RLNC decoding.

6. Conclusions

The spread of both WiFi capable Android devices makes feasible the design and implementation of general purpose distributed heterogeneous data networks. The high processing capacity of the smartphones makes them ideal to experiment with streaming video distribution and related services. In this paper we presented a novel streaming video service, and a method using network coding based caching to offload the wireless infrastructure. We proposed a heuristic algorithm to place the caching elements within the network.

We have built a prototype testbed based on Android smartphones which will serve as a demonstration platform for our proposal. We have implemented a mobile node, the live streaming video solution over the Android system and the random linear network coding based communication between the Android devices. We measured the performance of the implemented technologies. We

showed that the implementation of RLNC based streaming video is feasible in modern Android devices. In our future work we plan to analyze the different aspects of caching strategies in our proposed scenario.

Acknowledgements

Csaba Simon's research work was supported by the European Union and the State of Hungary, co-financed by the European Social Fund in the framework of TÁMOP 4.2.4.A/1-11-1-2012-0001 National Program of Excellence (NKP).

Markosz Maliosz's research work was carried out as part of the EITKIC_12-1-2012-0001 project, which is supported by the Hungarian Government, managed by the National Development Agency, financed by the Research and Technology Innovation Fund and was performed in cooperation with the EIT ICT Labs Budapest Associate Partner Group (www.ictlabs.elte.hu).

References

- [1] Google Android developers guide – available online from: <http://developer.android.com/guide/components/index.html>
- [2] Soos, A., Simon, Cs., Maliosz, M., “Network Coding Based Data Collection in Distributed Sensor Networks”, *The 4th International Conference on Recent Achievements in Mechatronics, Automation, Computer Sciences and Robotics, MACRo 2013*, Târgu Mureş, Romania, 2013.
- [3] Zalatnay, Zs., Simon, Cs., Maliosz, M., Terza, B., “Managing streaming services in a distributed testbed”, *The 5th International Conference on Recent Achievements in Mechatronics, Automation, Computer Sciences and Robotics, MACRo 2015*, Târgu Mureş, Romania, March 2015.
- [4] Akan, O. B., Isik, M. T., Buyurman, B., “Wireless passive sensor networks”, *IEEE Communications Magazine*, vol. 47, nr. 8, pp. 92-99, 2009.
- [5] Simon, Cs., Maliosz, M., “Network Coding Based Caching for Near Real-Time Streaming Media”, To appear in: *Infocommunications Journal: a publication of the Scientific Association for Infocommunications (HTE)*, vol. 7, nr. 1, pp. 7-14, 2015.
- [6] Li, B., et al, “Random network coding in peer-to-peer networks: From theory to practice”, 2011.
- [7] Gajic, B., Riihijarvi, J., Mhnen, P., “Performance evaluation of network coding: Effects of topology and network traffic for linear and xor coding”, *Journal of Communication*, vol. 4, nr. 11, pp. 885-893, 2009.
- [8] Chachulski, S., and Katti, S., “Trading structure for randomness in wireless opportunistic routing”, in *Proc. of ACM SIGCOMM*, 2007.
- [9] Katti, S., Katabi, D., Hu, W., Rahul, H., and Medard, M., “The importance of being opportunistic: Practical network coding for wireless environments”, in *Proc. 43rd Annual Allerton Conference on Communication, Control, and Computing*, 2005.
- [10] Gkantsidis, C., and Rodriguez, P. R. “Network coding for large scale content distribution”, in *Proc. of IEEE INFOCOM 2005*, vol. 4, 2005.
- [11] Traskov, D., Lenz, J., Ratnakar, N. and Médard, M., “Asynchronous Network Coded Multicast”, in *Proc. of ICC Communication Theory Symposium*, 2010.

-
- [12] Zhang, X., Neglia, G., Kurose, J., “Network Coding in Disruption Tolerant Networks, Network Coding: Fundamentals and Applications”, Elsevier Science (Ed.), 2011.
 - [13] Liu, J., and Xu, J., “Proxy caching for media streaming over the Internet”, *IEEE Communications Magazine*, vol. 42 nr. 8, pp. 88-94, 2004.
 - [14] Tewari, R., Vin, H. M., Dan, A., and Sitaram, D. “Resource-based caching for Web servers”, in *Proc. of SPIE/ACM Conf. on Multimedia Computing and Networking (MMCN’98)*, San Jose, CA., 1998.
 - [15] Sen, S., Rexford, J., and Towsley, D., “Proxy prefix caching for multimedia streams”, in *Proc. of IEEE INFOCOM’99*, New York, NY, 1999.
 - [16] Wu, K. L., Yu, P. S., and Wolf, J. L., “Segment-based proxy caching of multimedia streams”, in *Proc. of WorldWideWeb Conference (WWW10)*, Hong Kong, 2001.
 - [17] Miao, Z., and Ortega, A., “Scalable proxy caching of video under storage constraints”, *IEEE Journal on Selected Areas in Communications*, vol. 20, no. 7, pp. 1315-1327, September 2002.
 - [18] Fahmi, H., Latif, M., Sedigh-Ali, S., Ghafoor, A., Liu, P., and Hsu, L., “Proxy servers for scalable interactive video support”, *IEEE Computer*, 43(9): 54-60, 2001.
 - [19] Zhang, Z.-L., Wang, Y., Du, D., and Su, D., “Video staging: A proxyserver-based approach to end-to-end video delivery over wide-area networks”, *IEEE/ACM Transactions on Networking*, vol. 8 nr. 4, pp. 429-442, 2000.
 - [20] Zhang, M. et al., “A Peer-to-Peer Network for Live Media Streaming - Using a Push-Pull Approach”, in *Proc. of ACM Multimedia*, 2005.
 - [21] Kőrösi, A., Székely, B., Császár, A., Lukovszki, Cs., “High quality P2P-Video-on-Demand with download bandwidth limitation”, in *17th IEEE International Workshop on Quality of Service*, Charleston, USA pp. 1-9, July 2009.
 - [22] Adhikari, V. K., et al., “Unreeling Netflix: Understanding and Improving Multi-CDN Movie Delivery”, in *Proc. IEEE INFOCOM*, 2012.
 - [23] Wu, Y., et al., “CloudMedia: when Cloud on Demand Meets Video on Demand”, in *Proc. IEEE ICDCS*, 2011.
 - [24] Wang, M., Li, B., “R2: Random Push with Random Network Coding in Live Peer-to-Peer Streaming”, *IEEE Journal on Selected Areas in Communications*, 2007.
 - [25] Wong, W., Wang, L., and Kangasharju, J., “Neighborhood search and admission control in cooperative caching networks”, in *IEEE Global Communications Conference (GLOBECOM)*, pp. 2852-2858, 2012.
 - [26] Montpetit, M.-J., Westphal, C., and Trossen, D., “Network coding meets information-centric networking”, in *ACM MobiHoc workshop NOM’12*, pp. 31–36, June 2012.
 - [27] Sourlas, V., Gkatzikis, L., Flegkas, P., and Tassiulas, L., “Distributed cache management in information-centric networks”, *IEEE Transactions on Network and Service Management*, vol. Early Access Online, 2013.
 - [28] Li, B., Wang, Z., Liu, J., and Zhu, W., “Two decades of internet video streaming: A retrospective view”, *ACM Transactions on Multimedia Computing, Communications and Applications (TOMCCAP)*, 9(1s), 33. 2013.
 - [29] Karp, R. M., “Reducibility Among Combinatorial Problems”, in *Proc. Sympos. Complexity of Computer Computations*, IBM Thomas J. Watson Res. Center, Yorktown Heights, N.Y. New York: Plenum, pp.85-103, 1972.
 - [30] IOIO library basic documentation, <https://github.com/ytaioio/wiki/IOIOLib-Basics>, Sparkfun 2012.
 - [31] RTP: A Transport Protocol for Real-Time Applications, IETF RFC 3550, available from: <http://tools.ietf.org/html/rfc3550>.
 - [32] Official page of the VLC media player, available form: <https://www.videolan.org/vlc/index.html>.

- [33] International Telegraph Union - Telecommunication Standardization Sector, Recommendation H.222.0 (07/95), available from: <http://www.itu.int/rec/T-REC-H.222.0-199507-S/en>.
- [34] WiFi package for Android, available from: <http://developer.android.com/reference/android/net/wifi/package-summary.html>.
- [35] Wi-Fi Alliance, Wi-Fi Direct, available from: <http://www.wi-fi.org/discover-and-learn/wi-fi-direct>.



New Approaches Analyzing Usage of the Telecommunication Services

László MOLNÁR¹, Szilárd ANDRÁS²,
Ibolya KOTTA³, Iuliu SZÉKELY⁴

¹Department of Electrical Engineering, Faculty of Technical and Human Sciences,
Sapientia Hungarian University of Transylvania, Tg. Mureş,
e-mail: laszlo.molnar@ms.sapientia.ro

²Faculty of Mathematics and Computer Science, Babeş-Bolyai University, Cluj,
e-mail: andraszko@yahoo.com

³Faculty of Psychology and Education Sciences, Babeş-Bolyai University, Cluj,
e-mail: kottabambi@yahoo.com

⁴Department of Electrical Engineering, Faculty of Technical and Human Sciences,
Sapientia Hungarian University of Transylvania, Tg. Mureş,
e-mail: gszekely@ms.sapientia.ro

Manuscript received September 04, 2014; revised December 18, 2014.

Abstract: In this paper we analyze the media usage of students and the relation between the media usage and known psychological factors. Using hierarchical clustering, we identified three main categories: the socializing, the pragmatic and the all-consuming categories. Our results show that the media usage is also highly age and gender dependent even inside a very tight age group (19-22 years old students). Using PCA, discriminant analysis, and a special transformation that highlights the consentaneous reactions to different questions we also obtained some positive results that can be used to create an artificial intelligent agent for a posteriori clustering and some negative results related to the relation between most of the studied psychological factors and the media usage.

Keywords: Media usage, psychological factors, PCA, discriminant analysis, simultaneous bursts.

1. Introduction

The present telecommunication activities are converging in at least three ways: telecommunication and computer networks convergence; converging towards the Next Generation Network (NGN) architectures (all IP) [13]; convergence of electronic media and telecommunication services. Radio and television changed deeply the psycho-social background of life. They are

accessible by Internet today, but there are much more services accessible by Internet, which are deeply transforming usual life relations [5], [6], [7].

We study the development of the telecommunication services taking into account their psycho-social effects. The research has been intended to have two main stages. At the first stage, a statistical study was achieved concerning the correlation between the usage of the telecommunication services and the user's personality traits. At the second stage, methods of selective telecommunication services and contents delivery according to the individual and group users' profile are to be defined and developed.

The present paper relates the first stage. Selectively delivering of telecom content according to the user's personality traits is our final target.

The phenomena resulting from the usage of telecommunication services are studied mainly by psychology and/or telecommunication marketing.

The first approach studies the effects of using the different telecommunication services, which are considered mainly negative and undesirable (dependence, addiction, anxiety, fear, depression, etc.). The resulted recommendations are mainly targeted to avoid using or to reduce the time to be connected to telecommunication services.

The second approach aims to maximize the usage time of offered services, maximizing the profit which is realized.

These two approaches are rather contradictory.

Studies made after year 2000, show that young people aged between 15 and 24 years spend daily 1-3 hours on Internet. Main purposes are music listening, entertainment and searching for informational contents.

There are several models to evaluate human personality traits. All these models are grounded on the (lexical) hypothesis, which states that building and maintaining inter-personal relations are coded in language, through the human habits describing concepts.

After Howard (2004), the factors of the Big-Five Model are:

1. Neuroticism - N
2. Extraversion - E
3. Openness to experience - O
4. Agreeableness - A
5. Conscientiousness - C

A very interesting direction of the research is in which the main character traits are described by studying the preferences in accessing Internet contents. It is confirmed in this way too, the existence of 5 main character groups (clusters) [9].

The effects of the usage of the telecommunication services are very important to be studied. In order to develop telecommunication services according to their psycho-social effects, deeper knowledge of relationship is

required. A questionnaire to measure this relationship with the youth has been elaborated using an adapted version of the Delphi consultation ([16]). Instead of asking to estimate the exact number of calls, or exact duration of service usage, 6 quantified possible answers were introduced:

0 = not at all, 1= very little, 2 = little, 3 = average, 4 = much, 6 = very much.

This combined questionnaire [17] has been applied on a sample of students. Having been suggested by psychologists, we carried out the survey through handouts, not online. From the total of 1100 students of Tg. Mures Faculty of the Sapientia University about 300 students have been randomly chosen to respond to the questionnaire. For processing the results, we used multi-linear regression [3], [8], [18], cluster analysis [1], discriminant analysis for the cluster classification [2], Principal Component Analysis (PCA) [10], and a newly introduced model based on simultaneous bursts [14], [15].

To identify the different types of behaviour in using the telecommunication services we have applied the clustering method and thus succeeded in identifying three significantly different types:

1. The socializing;
2. The pragmatic;
3. The all-consuming.

Having used the discriminant analysis we have studied the relationship between the psychological factors obtained from the standard psychological tests and the classification obtained from the clustering technique as well as from identifying the different age and gender categories from the information related the usage of the telecommunication services. We have noticed that:

- Psychological factors explain a minor part of the classification;
- There is a significant difference between the very close age groups like 19-20 years and 21-22 years of age;
- There are significant differences between men and women what media usage concerns;

Using the factorial analysis we have chosen 6 principal components (with the varimax method) out of the data related to the media usage. These factors could be used to conduct a new poll with much fewer questions and also with relevant results.

To strengthen the explicit power of the information of the survey we have created a series of transformed variables which expresses the existence of coincidences in the responses given to the pairs of questions. Using these transformed variables we managed to build a model which can explain about 85% of the classification with the help of 19 such coincidences.

2. Cluster analysis of the data related to the usage of media

Cluster classification was made on the basis of media usage and of the media contents, 61 possibilities in 5 groups. For the obtained data through the questionnaire on media usage we adopted different clustering techniques (hierarchical, K-mean) and different types of distances (Euclidian, s-Euclidian, etc.) to compare the obtained classifications. These numeric experiences were intended to identify the number of the categories adopted at classification and to study (at least on intuitive level) the stability of the created categories with respect to the parameters of the method we have used of the created categories. We have found that the number of the significantly different categories and which are not reduced to very small groups (with changed classification techniques) is between 2 and 4.

We calculated the mean (m) and dispersion (s) within each category related to each question for two classifications: one with three (*Table 1*) and one with four categories. Owing to the hierarchical categorizing method the three categories in the first group may be obtained from those four in the second group by merging two groups. Consequently the second category in the first group (where we have 3 categories) is obtained by merging categories 2 and 3 in the second group (where we have 4 categories).

Table 1: Mean and dispersion in the structures with 3 categories (clusters).

	cl1	cl2	cl3	cl1	cl2	cl3
	Soc (97)	Cons (102)	Prag (63)	Soc (97)	Cons (102)	Prag (63)
<i>Mobile calls</i>	m	m	m	s	s	s
Solving personal problems	2.60	2.45	2.21	1.24	1.32	1.14
Brief personal communication	2.88	2.54	1.97	1.06	1.31	1.27
Long personal communication	1.94	2.16	1.24	1.27	1.22	1.10
Long communication	0.93	1.69	0.41	1.14	1.23	0.69
SMS	3.05	2.83	1.56	1.46	1.62	1.54
<i>Mobile</i>	m	m	m	s	s	s
Music	1.23	1.81	0.75	1.26	1.40	1.22
Internet browsing	1.05	1.88	0.86	1.36	1.52	1.19
Internet chat	0.46	1.50	0.40	0.99	1.49	0.91
Internet e-mail	0.56	1.25	0.41	1.00	1.24	0.85
Games	0.73	1.34	0.48	0.99	1.29	0.91

	c11	c12	c13	c11	c12	c13
	Soc (97)	Cons (102)	Prag (63)	Soc (97)	Cons (102)	Prag (63)
<i>Radio</i>	<i>m</i>	<i>m</i>	<i>m</i>	<i>s</i>	<i>s</i>	<i>s</i>
Information	1.09	1.77	0.32	1.11	1.24	0.62
News	1.22	1.78	0.38	1.14	1.27	0.61
Politics	0.37	1.14	0.13	0.86	1.15	0.42
Culture	0.90	1.69	0.17	1.16	1.28	0.52
Science	0.73	1.70	0.19	1.13	1.33	0.47
Music	2.56	2.94	0.78	1.68	1.60	1.05
Sports	0.52	1.45	0.16	0.93	1.38	0.54
Quiz	0.20	0.99	0.13	0.51	1.09	0.42
<i>TV</i>	<i>m</i>	<i>m</i>	<i>m</i>	<i>s</i>	<i>s</i>	<i>s</i>
News	0.81	2.19	0.40	1.03	2.36	0.77
Politics	0.28	1.44	0.08	0.64	1.10	0.33
Culture	0.66	1.96	0.17	0.98	1.15	0.58
Science	0.99	2.32	0.68	1.31	1.22	1.16
Music	1.06	2.52	0.16	1.31	1.38	0.48
Sport	0.67	2.03	0.48	1.21	1.45	1.22
Quiz	0.26	1.24	0.03	0.77	1.24	0.25
Interactive programs	0.44	1.84	0.29	0.92	1.31	0.83
Video clips	0.53	2.14	0.02	0.97	1.27	0.13
Feature film	0.40	1.70	0.08	0.95	1.34	0.41
Movie serials	0.64	2.40	0.30	1.16	1.53	0.75
Documentaries	1.11	2.15	0.40	1.38	1.41	0.93
Action films	0.57	2.12	0.29	1.06	1.40	0.71
Comedies	1.04	2.82	0.27	1.36	1.28	0.70
Plays	0.25	1.37	0.00	0.69	1.22	0.00
Romance films	0.48	2.05	0.11	1.06	1.35	0.44
Reality show	0.38	1.73	0.11	0.89	1.53	0.44
Horror	0.32	1.68	0.03	0.90	1.54	0.25
Erotic	0.16	1.31	0.02	0.55	1.47	0.13
<i>Internet</i>	<i>m</i>	<i>m</i>	<i>m</i>	<i>s</i>	<i>s</i>	<i>s</i>
Professional resource	2.58	2.61	2.16	1.25	1.20	1.46

	cl1	cl2	cl3	cl1	cl2	cl3
	Soc (97)	Cons (102)	Prag (63)	Soc (97)	Cons (102)	Prag (63)
E-mail	2.30	2.42	1.54	1.09	1.21	1.19
Games	1.06	1.88	0.89	1.43	1.54	1.43
Messenger (e.g. Yahoo)	3.13	2.82	1.57	1.44	1.42	1.15
Socialization sites (e.g. Facebook)	3.18	2.97	1.63	1.38	1.45	1.39
Information	2.57	2.82	1.79	1.26	0.98	1.35
E-books, e-textbooks	1.84	2.18	1.06	1.35	1.30	1.26
Encyclopedia (e.g. Wikipedia)	1.71	2.25	1.08	1.32	1.15	1.04
E-shopping	0.53	1.22	0.27	0.98	1.18	0.65
News	1.20	2.05	0.48	1.28	1.20	0.82
Politics	0.27	1.21	0.27	0.65	1.21	0.77
Culture	1.26	1.77	0.37	1.37	1.24	0.77
Science	1.52	2.29	1.19	1.46	1.22	1.33
Music	2.98	3.43	1.83	1.40	1.16	1.67
Sport	0.75	1.88	0.46	1.16	1.51	1.06
Matrimonial ads	0.26	0.92	0.02	0.79	1.20	0.13
Video clips	1.61	2.48	1.03	1.48	1.36	1.49
Feature film	0.94	1.46	0.16	1.38	1.45	0.63
Documentaries	1.41	1.80	0.59	1.53	1.46	1.10
Action films	1.35	2.01	0.49	1.59	1.47	1.05
Comedies	1.99	2.75	0.78	1.64	1.32	1.18
Romance films	0.98	2.16	0.16	1.43	1.45	0.60
Horror	0.87	1.71	0.24	1.40	1.48	0.76
Erotic	0.34	1.23	0.17	0.78	1.41	0.55

The table shows that those belonging to the first category use the services mainly for socialization and for this reason we called this type socializing behaviour. Those in the last category use these services mainly to solve current problems and for professional activities. For this we called the type pragmatic behaviour. Second category can be called all-consumers.

These categories can be differentiated at each type of services, moreover, at the majority of the questions of the questionnaire. The dispersion does not differ significantly (it has been tested by F test), and the means are significantly different (Students's t test): $p < 0.05$.

For a suggestive visualization we have calculated the centroids, the equation of the plane defined by these three centroids, and we projected each individual on this plane. This step has been realized with MATLAB because the adopted application for the rest of the calculations (SPSS ver.21) has not got this function. Thus the data from SPSS has been exported to EXCEL and from there imported to MATLAB ([4], [12]) for processing.

Thus we obtained *Fig. 1* where the green spots correspond to the socializing category, the blue ones to the consumers and the yellow spots to the pragmatists. The red circles mark the centroids.

These categories generate an avalanche of problems related to future research: how can these individuals' opinions be used to create a psychological index of the contents based on "face recognition" and "voice recognition" concerning the extraction of the users' reactions? Is it true that the pragmatists first choose the content and only afterwards the form of the service?

Concerning the possibility of identifying the age and sex categories we analyzed the cluster categorization, too, on the following subcategories: women aged 19-20 (21), women aged 21-22 (22), men aged 19-20 (11) and men 21-22 (12). For the first two categories we had to eliminate some data in order to obtain substantial categories. So for category 21 we excluded 11 persons, from category 22 we excluded 6 persons.

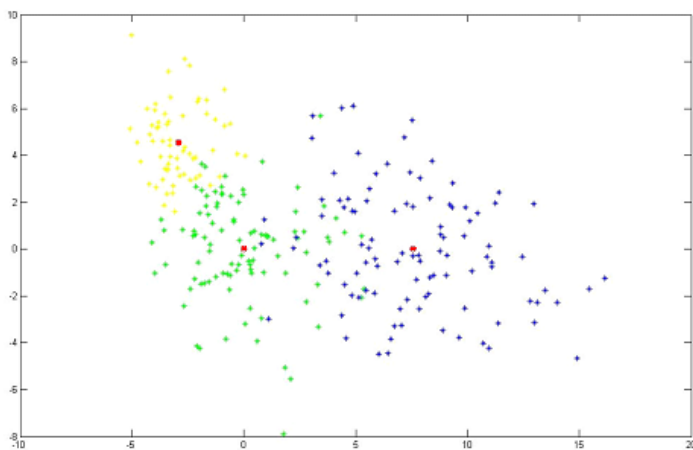


Figure 1: Projection of each individual on the plane defined by the three centroids. Values are coordinates in this plane.

Both classifications (with two classes) show that on subcategory level two behaviours can be identified (compared with the three behaviors identified for the whole population). At subcategory 21 a more emphatic socializing behavior can be identified for a part of the population and the rest of the population (including a part of the socializing category, all pragmatics and all consumers from this subcategory) can be considered as a separate category. At subcategory 22 the emphatic socializing group becomes more significant and includes a part (small) of the consumers and the other part is formed by a significant nucleus of pragmatists, a part of consumers and a negligible part of the socializing category.

It can be noticed with the women a radical change as regards the structure of the population even at this slight age difference.

Analyzing from the same point of view the subpopulation composed of men we have noticed that it is not necessary to exclude any data (without individuals with exaggerated “individualism”) and it cannot be noticed the change of the structure either. Certainly these results raise a series of questions: how this structure of usage of services evolves in time, which are the external parameters the evolution depends upon, what kind of relations exist between this structure and other social characteristics (for example whether one is involved in a relationship or not) etc.

3. Discriminant analysis of the classification obtained from cluster analysis using psychological factors

The discriminant analysis between the factors of the psychological tests and of the results of the cluster analysis obtained in the previous paragraph offers a model which shows the explicative power of the psychological factors in the classification obtained from the usage of the media. From *Table 2* results that two functions are sufficient and these have a relatively big explanatory power in case of the target variable (59% respectively 41%).

Table 2: Eigenvalues.

Function	Eigenvalue	% of Variance	Cumulative %	Canonical Correlation
1	.370a	59.0	59.0	.520
2	.257a	41.0	100.0	.452

Note: First 2 canonical discriminant functions were used in the analysis.

The values obtained with the Wilks’ Lambda test (*Table 3*) show that there are significant differences between the constructed functions. We applied the Box test also for the equality of the covariance matrices and the results show that the discriminant analysis can be applied.

Table 3: Wilks' Lambda

Test of Function(s)	Wilks' Lambda	Chi-square	df	Sig.
1 through 2	.580	86.492	54	.003
2	.795	36.400	26	.085

The following two tables contain discriminant function coefficients and correlated coefficients of the initial variables (psychological factors) and values created through discriminant functions.

Table 4: Standardized Canonical Discriminant Function Coefficients.

	Coefficients of the functions	
	1	2
STAI_S	-.114	.188
STAI_T	-.099	.504
BECK_DEPR	-.150	.111
SBQ	.083	-.183
COP_PROBLEM	-.343	.051
COP_EMOTION	.680	.284
COP_AVOID	.474	-.301
PISI_01	-.413	.478
PISI_02	.048	-.358
PISI_03	.339	-.182
PISI_04	-.403	-.022
PISI_05	-.116	-.182
PISI_06	.173	.010
PISI_07	.198	-.536
PISI_08	-.240	.673
PISI_09	.287	-.366
PISI_10	.027	-.068
PISI_11	.670	.321
PISI_12	.003	-.104
PISI_13	-.008	.107
PISI_14	-.170	-.628
PISI_15	.540	1.014
PISI_16	.047	-.132
EPQ_P	-.196	.147
EPQ_E	.134	-.151
EPQ_N	.226	-.084
EPQ_L	-.096	.463

The functions are in fact the linear combinations from the explicative variables values, and the values in the tables are the coefficients of these

combinations. The values of these functions will give us a categorization based on the explicative variables and this categorization will be compared with the initial one defined through the target variable. *Table 4* also shows the impact of the initial variables on the two discriminant functions. The green color marks the factors with raised share in the discriminant function 1, and the yellow marks the high share in the discriminant function 2.

Table 5 contains the correlated coefficients between the psychological factors and the discriminant functions.

Table 5: Structure Matrix.

	Function	
	1	2
COP_AVOID	.558*	-.018
PISI_11	.490*	.140
PISI_14	-.390*	-.341
COP_EMOTION	.361*	.111
PISI_16	-.336*	-.114
EPQ_E	.319*	-.148
PISI_07	.282*	-.241
EPQ_N	.239*	.090
PISI_12	-.237*	-.190
EPQ_L	-.230*	.149
PISI_10	.216*	-.092
PISI_15	-.216*	.001
PISI_13	-.181*	-.085
PISI_06	.179*	.135
SBQ	.143*	.003
PISI_04	-.133*	.031
PISI_09	.066*	-.056
BECK_DEPR	.108	.227*
STAI_S	-.003	.208*
PISI_05	-.173	-.205*
PISI_08	.199	.203*
STAI_T	.092	.196*
COP_PROBLEM	-.017	-.174*
PISI_03	-.084	-.140*
EPQ_P	.027	.122*
PISI_02	.028	-.098*
PISI_01	-.028	.065*

The calculated discriminant function values on the mean of the three categories (*Table 6*) show that these have different compartment (these types of compartment can be identified with plane vectors having different directions,

the first being in the first quadrant, the second in the fourth one and the third in the second one).

Table 6: Functions at Group Centroids.

Cluster	Function	
	1	2
1.00	.473	.454
2.00	.124	-.646
3.00	-1.107	.244

Fig. 2 shows the values of the discriminant functions and the classification obtained based on them. The discriminant function values for each member of the population: each circle represents an individual of the population, the two coordinates are the values of the two discriminant functions, and the color is obtained by categorizing based on these functions.

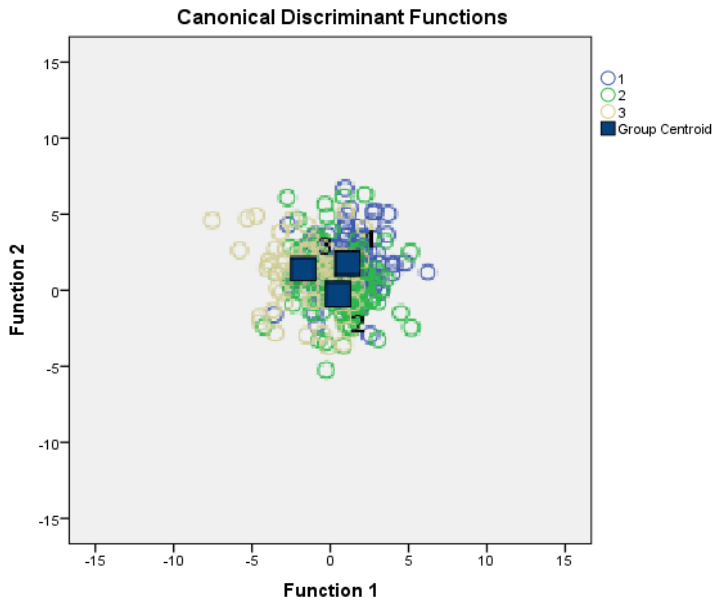


Figure 2: Discriminant function values for each member of the population.

Table 7 shows the fact that on the basis of the calculated factors of the psychological tests we can correctly classify 55.7 % of the whole population.

Studying the structure of the discriminant functions we can see that not all the psychological factors are relevant in this analysis.

For this we construct two more models, the first based on the PISI test and COPING and the second on just some factors selected from these.

Certainly through selecting these variables we will lose from the explanatory power but we will get a correct classification for 48.5% of the population based on only 4 psychological factors instead of 27.

Table 7: Classification Results.

		Cluster	Predicted Group Membership			Total
			1.00	2.00	3.00	
Original	Count	1.00	70	24	8	102
		2.00	35	47	15	97
		3.00	18	16	29	63
	%	1.00	68.6	23.5	7.8	100.0
		2.00	36.1	48.5	15.5	100.0
		3.00	28.6	25.4	46.0	100.0

Note: 55.7% of original grouped cases correctly classified

4. Discriminant analysis, Model based on PISI and COPING factors

The Wilks' Lambda, Chi-square and Box gave positive results. Coefficients calculated (Table 8):

Table 8: Standardized Canonical Discriminant Function Coefficients.

	Function	
	1	2
COP_PROBLEM	-.299	.316
COP_EMOTION	.504	.014
COP_AVOID	.458	.714
PISI_01	-.249	-.410
PISI_02	.028	.278
PISI_03	.304	.179
PISI_04	-.346	.062
PISI_05	-.237	.262
PISI_06	.169	-.048
PISI_07	-.016	.612
PISI_08	.031	-.578
PISI_09	.293	-.018
PISI_10	.254	-.114
PISI_11	.479	-.037
PISI_12	-.021	.347
PISI_13	.032	.038

	Function	
	1	2
PISI_14	-.330	.342
PISI_15	.558	-.311
PISI_16	-.156	.203

From this table we can extract the factors with relatively high contribution (green colour). The next model will be constructed on these four factors.

Also in this case the calculated discriminant functions in the centroids of the three categories separated out into 3 quadrants (*Table 9*):

Table 9: Functions at Group Centroids.

Cluster	Function	
	1	2
1	.527	-.288
2	-.033	.471
3	-.821	-.341

Each circle in *Fig. 3* represents an individual of the population.

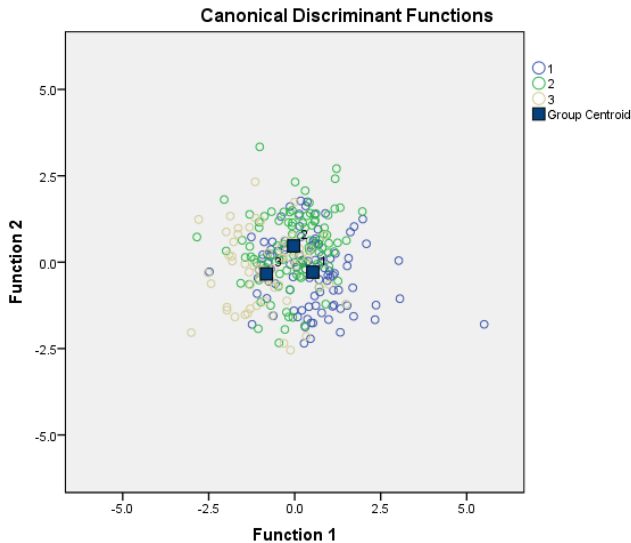


Figure 3: Discriminant function values, COPING and PISI models.

The 2 coordinates are the values of the 2 discriminant functions, and the colors are obtained by categorizing based on these functions.

In the previous model where 55.7% could be classified, in this situation still 54.6% of the cases can be classified (*Table 10*).

Table 10: Classification results.

		Cluster	Predicted Group Membership			Total
			1.00	2.00	3.00	
Original	Count	1.00	57	36	9	102
		2.00	27	57	13	97
		3.00	10	24	29	63
	%	1.00	55.9	35.3	8.8	100.0
		2.00	27.8	58.8	13.4	100.0
		3.00	15.9	38.1	46.0	100.0

5. Discriminant analysis, Model based on the 4 most relevant factors

- COP_EMOTION- Coping centered on emotions (Coping is an active process through which an individual can deal successfully with a stressful situation and succeeds in controlling it [19]).
- COP_AVOID-coping centered on avoiding
- PISI_11 - The power of social creation
- PISI_15 - Controlling sentiments

Similarly the previous steps were remade starting just from the four most relevant factors.

In this case too, the discriminant function values calculated in the centre of centroids of those three categories separated into 3 quadrants (Table 11).

Table 11: Functions at Group Centroids

Cluster	Function	
	1	2
1.00	.350	.136
2.00	.100	-.172
3.00	-.722	.066

Each circle in Fig. 4 represents an individual of the population, the 2 coordinates are the values of the 2 discriminant functions, and the color is obtained by categorizing based on these functions.

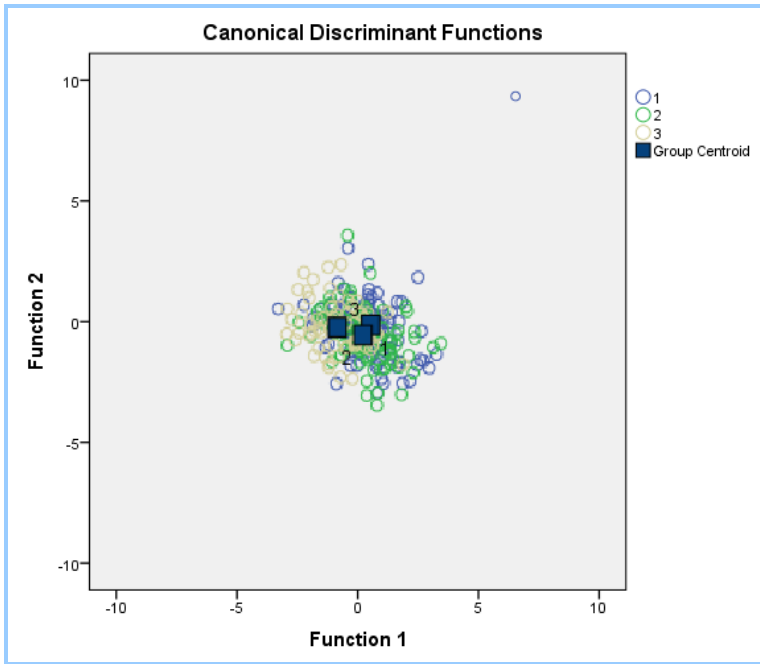


Figure 4: Discriminant function values, model with 4 factors.

In the previous model 54.6% could be classified. In this situation 48.5% of the cases can be classified (Table 12):

Table 12: Classification results.

		Cluster	Predicted Group Membership			Total
			1.00	2.00	3.00	
Original	Count	1.00	47	42	13	102
		2.00	32	52	13	97
		3.00	12	23	28	63
	%	1.00	46.1	41.2	12.7	100.0
		2.00	33.0	53.6	13.4	100.0
		3.00	19.0	36.5	44.4	100.0

Note: 48.5% of original grouped cases correctly classified

Consequently by reducing the psychological factors from 27 to 4 we lose only 7.2% from the explanatory power.

6. Principal component analysis

The value for the Bartlett test and Kaiser-Meyer-Olkin measure show that the correlation matrix is significantly different from the identity matrix and that the correlative coefficients can be explained relatively well through partial correlates, so there is no need for Anti-Image Correlation Matrix and the factorial analysis can be used.

The table of the communalities (not included) shows how much per cent of each variant of the initial variable can be explained by using the 6 factors drawn out through the PCA method (and the rotation of these using the Varimax process).

Table 13, contains the global explanation of the factors and shows the factors extracted on the bases of Cattell criterion (Scree test).

The graph obtained from eigenvalues (Scree plot) explains 50.65% of the total variants.

Table 13: Eigenvalues for extracted components (fragment).

Component	Initial Eigenvalues		
	Total	% of Variance	Cumulative %
1	15.706	25.748	25.748
2	4.170	6.837	32.584
3	3.736	6.124	38.709
4	2.722	4.463	43.171
5	2.672	4.381	47.552
6	1.892	3.101	50.653
7	1.766	2.895	53.548
8	1.504	2.466	56.014
9	1.434	2.351	58.365
10	1.376	2.256	60.621
11 ...			

Certainly the analysis can be repeated to extract more factors, but in this case we will have two problems: we are either notable to explain the factors or the methods of calculating the optimal rotations are not convergent.

For this reason we kept just 6 factors and in the annexed table we included just the first 36 values (which are necessary to be able to explain 90% of the total variant).

The Cattell (scree test) is a pseudo-empirical test to establish the number of relevant factors. Consequently the eigenvalues, which line up along a straight line, will not be taken into consideration.

In this case, after the 6th eigenvalue the others are practically on a straight line, so according to the Cattell criterion the extraction of 6 values is recommended (*Fig. 5*).

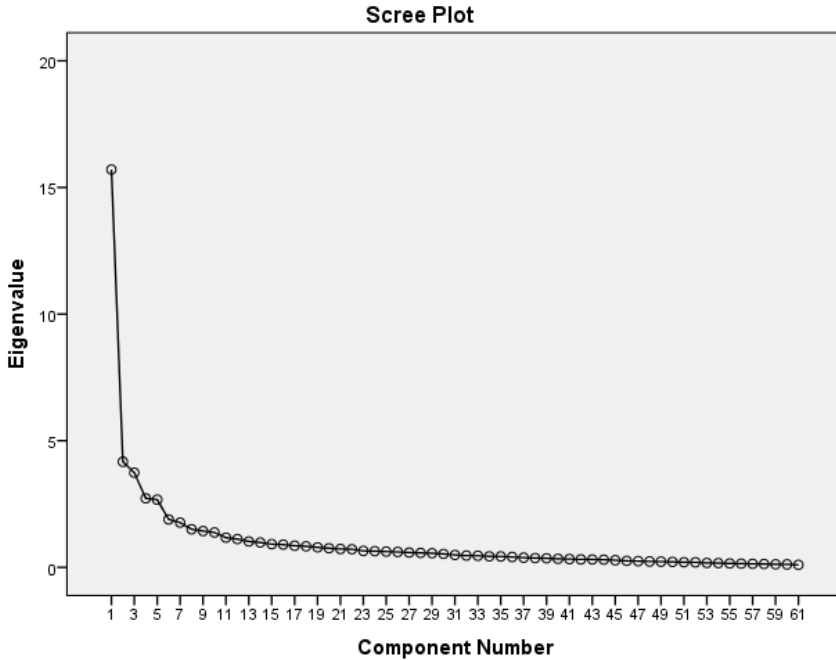


Figure 5: Eigenvalues for Cattell test.

To obtain a more suggestive correlation between the initial variables and obtained components, and to point out the possible interpretations of gained factors we rotated them using the Varimax process (we took just the relevant parts where the coefficient of correlation is at least 0.6).

We obtained 6 new components (*Table 14*).

The first factor includes the usage of cultural services on a large scale (culture, plays, films, music etc.).

The second factor is mainly linked to information (information, politics, science, sport, news).

The third factor refers to the information accessed electronically.

The fourth factor refers to Internet usage for mail, chatting, searching, the fifth one is related to action and horror films and the sixth to socializing.

Table 14: Rotated Component Matrix, relations between components and initial variables.

	Component					
	1	2	3	4	5	6
Mobile						
Internet browsing				.778		
Internet chat				.758		
Internet e-mail				.720		
Radio						
Information		.719				
News		.697				
Politics		.621				
Culture		.711				
Science		.699				
Sports		.633				
TV						
Culture	.602					
Music	.693					
Video clips	.692					
Movie serials	.708					
Comedies	.746					
Plays	.604					
Romance films	.747					
Reality show	.661					
Internet						
E-mail			.654			
Socialization sites (e.g. Facebook)						.635
E-books, e-textbooks			.720			
Encyclopedia (e.g. Wikipedia)			.686			
Culture			.625			
Action films					.725	
Horror					.689	

Notes: Extraction Method: Principal Component Analysis

Rotation Method: Varimax with Kaiser Normalization

Rotation converged in 8 iterations

7. Model based on coincidences (simultaneous bursts)

To increase the explanatory power of the initiative classification we constructed for each pair of initial variables ($K_{x,y}$ in *Table 15*) a new variable which measures the simultaneous bursts of the two initial variables.

So the new variable can take the values of -2, -1, 0, 1 or 2 depending on the values of the initial variables according to the following rules:

- The value is 2 if the initial variables have the same value;
- The value is 1 if the modulus of the difference between the initial variables is 1;
- The value is -1 if the modulus of the difference between the initial variables is one unit smaller than the possible maximal value;
- The value is -2 if the modulus of the difference between the initial variables is maximum possible;
- The value is 0 in all the other cases.

So of the 61 initial variables we constructed $61 \times 60 / 2 = 1830$ new variables (using the syntactic programming of SPSS - [11]) to which we attached the factors too, obtained from evaluating the psychological tests.

After this by constructing some successive regressive models we eliminated the variables which did not present a significant contribution to the explanatory power of the module.

As a consequence of this interactive process (after 9 steps) we obtained a set of 21 significant variables which together have an explanatory power of 85%. These variables being numbered in order of their automatic generation we decoded them and we obtained the decoding table (*Table 15*):

To select from these variables those which have a significant contribution in the explanation of categorization it was calculated the coefficient of correlation among these variables and the target variable and the significance of each test was tested.

Thus 9 variables were eliminated from the model and it was obtained a model of linear regression which has an explanatory power of 74% based on 2 psychological factors (PISI_11, COP_EMOTION) and 10 coincidences to the questions referring to the usage of telecommunication services.

To select from these variables those which have a significant contribution in the explanation of categorization it was calculated the coefficient of correlation among these variables and the target variable and the significance of each test was tested.

Table 15: Decoding table for the new variables.

NewVar	i			j
384	7	K.2.2	K.5.15	52
422	8	K.2.3	K.5.1	38
423	8	K.2.3	K.5.2	39
429	8	K.2.3	K.5.8	45
579	11	K.3.1	K.5.8	45
646	13	K.3.3	K.3.7	17
739	15	K.3.5	K.4.1	19
757	15	K.3.5	K.4.19	37
767	15	K.3.5	K.5.10	47
806	16	K.3.6	K.5.5	42
1463	35	K.4.17	K.5.16	53
1492	36	K.4.18	K.5.21	58
1502	37	K.4.19	K.5.8	45
1508	37	K.4.19	K.5.14	51
957	20	K.4.2	K.4.9	27
961	20	K.4.2	K.4.13	31
978	20	K.4.2	K.5.11	48
993	21	K.4.3	K.4.6	24
1628	43	K.5.6	K.5.17	54

After this analysis *Table 16* was obtained and thus in the decoding table the significant variables were marked with green.

Thus 9 variables were eliminated from the model and it was obtained a model of linear regression which has an explanatory power of 74% based on 2 psychological factors (PISI_11, COP_EMOTION) and 10 coincidences to the questions referring to the usage of telecommunication services.

For the rest of the variables the significance level (Sig) is bigger than 0.05, so we omitted these variables.

These results can be used for both designing a new questionnaire and for identifying the belonging of some individuals to the identified categories.

Beside these practical aspects the above described process raises a series of theoretical questions related to the possibility of generalizing this process to obtain factors based on creating variables of coincidences in general,

respectively the a priori testing of the possibility of some improvement by creating variables of coincidence type.

Table 16: Correlation among significant variables and the target variable.

Model	Unstandardized Coefficients		Stand-ized Coeffic	t	Sig.	95.0% Confidence Interval for B	
	B	Std. Error	Beta			Lower Bound	Upper Bound
(Constant)	4.108	.435		9.435	.000	3.248	4.967
NewVar423	-.291	.068	-.273	-4.279	.000	-.425	-.157
PISI_11	-.036	.009	-.187	-3.798	.000	-.055	-.017
NewVar422	.198	.055	.191	3.621	.000	.090	.307
NewVar757	-.194	.056	-.212	-3.490	.001	-.303	-.084
NewVar1463	-.169	.054	-.173	-3.119	.002	-.276	-.062
NewVar993	-.151	.054	-.162	-2.778	.006	-.258	-.044
NewVar429	.158	.060	.158	2.651	.009	.040	.276
NewVar384	-.115	.044	-.119	-2.581	.011	-.203	-.027
NewVar961	-.172	.068	-.185	-2.516	.013	-.306	-.037
NewVar767	-.111	.044	-.119	-2.507	.013	-.199	-.024
NewVar978	-.139	.056	-.119	-2.493	.014	-.250	-.029
NewVar579	-.122	.053	-.123	-2.289	.023	-.228	-.017
NewVar1492	-.135	.063	-.154	-2.150	.033	-.260	-.011
NewVar1628	.098	.046	.098	2.124	.035	.007	.189
NewVar739	.122	.059	.127	2.056	.041	.005	.238
COP_EMOTION	-.009	.005	-.135	-2.043	.043	-.019	.000
NewVar957	-.112	.057	-.114	-1.971	.050	-.224	.000

3. Conclusion

The majority of the psychological factors (from clinical tests) do not have a significant relevance for the usage of telecommunication services apart from COP_EMOTION, PISI_11 factors. For further research the identification of other psychological factors is needed.

In the usage of telecommunication services three big categories of users can be identified: the socializing, the all-consuming and the pragmatic. These

categories represent a quite interesting dynamics if we analyze the different subcategories (women-men, age categories). A more detailed study of this phenomenon would deserve a supplemental attention.

To construct content filters it is advisable to exclude the pragmatists (or to start working with them in an alternative, more conscientious way).

References

- [1] András, Sz., and Baricz, Á., “Statisztika közgazdászoknak (Statistics for Economists)”, Editura Státus, Miercurea Ciuc, 2010.
- [2] Andrews, N. O., and Fox, E. A., “Recent Developments in Document Clustering”, *Technical Report TR507535, Computer Science*, Virginia Tech., 2007.
- [3] Bilodeau, M., and Brenner, D., “Theory of Multivariate Statistics”, Ed. Springer, 1999.
- [4] Blaga, P., “Statistică prin Matlab”, Ed. Presa Universitară Clujeană, 2002.
- [5] Bromley, R., V., and Bowles, D., “Impact of Internet on use of traditional news media”, *Newspaper Research Journal*, Department of Journalism, University of Memphis 16(2), 1995.
- [6] Chan, K.; and Fang, W., “Use of the internet and traditional media among young people, Young Consumers: Insight and Ideas for Responsible Marketers”, *Emerald* 8(4) pp. 244-256, 2007.
- [7] Chen, R, Su, E., Shen, V., Wang, Y., “Introduction to IP Multimedia Subsystem (IMS), Part 1: SOA Parlay X Web services”, IBM, <http://www.ibm.com/developerworks/webservices/library/ws-soa-ipmultisub1/>, 2006.
- [8] Ezekiel, M., Fox, K. A., “Korreláció és regresszióanalízis (Correlation and Regression Analysis)”, Közgazdasági és Jogi Kiadó, Budapest, 1970.
- [9] Faber, M. A., Mayer, J. D., “Resonance to archetypes in media: There’s some accounting for taste”, *Journal of Research in Personality*, 43(3): pp. 307-322, 2009.
- [10] Jackson, J. E., “A User’s Guide to Principal Components (Wiley Series in Probability and Statistics)”, Ed. Wiley-Interscience, 2003.
- [11] Landau, S., Everitt, B. S., “Handbook of statistical analysis using SPSS”, Chapman&Hall/CRC, 2004.
- [12] Martínez, W. L., Martínez, A. R., “Computational Statistics Handbook With MATLAB”, Chapman and Hall/CRC Computer Science and Data Analysis Series, Taylor and Francis, 2008.
- [13] Milne, R., “ICT quality of service regulation: practices and proposals”, ITU website, 2006, [Online]. Available on 1st March 2013, http://www.itu.int/ITU-D/treg/Events/Seminars/2006/QoS-consumer/documents/SI-2_QOS-bkgpaper-presentation.pdf. 2006.
- [14] Molnár, L., “Development of the Telecommunication Services According to their Psycho-Social Effects”, PhD thesis, Transilvania University, Brasov, Romania, 2013.
- [15] Molnár, L., András, Sz., Székely, I., “Relation between media content usage and known psychological factors”, *4th International Conference on Recent Achievements in Mechatronics, Automation, Computer Science and Robotics (MACRo2013)*, Sapientia University, Tg. Mureș, 2013.
- [16] Molnár, L., Székely, I., “Adapted Delphi Consultation to Elaborate a Questionnaire for Measuring the Usage of Different Telecommunication Services”, in *The 6th edition of the Interdisciplinarity in Engineering International Conference (InterEng)*, “Petru Maior” University of Tîrgu Mureș, pp. 388-393, 2012.

-
- [17] Molnár, L., Székely, I., “Simultaneously Measurement of the Usage of some Telecommunication Services and some Psycho Factors”, *XXIInd Conference on Computers and Education - SzámOkt*, Alba Iulia, pp. 319-324, 2012.
- [18] Mundruczó, Gy., “Alkalmazott regressziószámítás (Applied Regression Analysis)”, Akadémiai Kiadó, Budapest, 1981.
- [19] MUT_VITCU&Asociatii, “Index de termeni”, <http://www.mutvitcu.ro/index-de-termeni/coping/20>.



Two-Stage Kalman Filtering for Indoor Localization of Omnidirectional Robots

Lőrinc MÁRTON, Katalin GYÖRGY

Department of Electrical Engineering,
Faculty of Technical and Human Sciences,
Sapientia Hungarian University of Transylvania, Tg. Mureş,
e-mail: martonl@ms.sapientia.ro

Manuscript received March 20, 2014; revised December 15, 2014.

Abstract: In this study a sensor fusion technique was developed for indoor localization of omnidirectional mobile robots. The proposed sensor fusion method combines the measurements made by an indoor localization system (e.g. ultrasound based localization) with the measurements that comes from an IMU (Inertial Measurement Unit). It was taken into consideration that the measurements made by the ultrasonic sensor are available with lower measurement rate than the IMU measurements. To tackle this problem a two-stage Kalman filter was developed. The first stage estimates the orientation of the robot at the measurement rate of the IMU using a linear Kalman filter. The second stage estimates the position and velocity of the robot. The prediction of the robot's position is performed based on the robot model at the update rate of the IMU. The correction phase is performed at the update rate of the external localization system using nonlinear Kalman filtering techniques. All the measurements were considered noisy and in the case of the IMU the measurement biases were also taken into consideration. For the implementation of the nonlinear Kalman filter, a discretized nonlinear omnidirectional robot model was developed. It was necessary as the classic unicycle model cannot be directly applied in the case of the omnidirectional robot. Simulation measurements were performed to evaluate the performances of the proposed two-stage filter. For the implementation of the second stage, two approaches were tested namely the Extended Kalman Filter and the Unscented Kalman Filter.

Keywords: Robot sensing systems, Motion estimation, Kalman filtering, Sensor Fusion.

1. Introduction

The sensor fusion is an effective method to solve the precise localization problem of mobile robots. According to this technique more than one sensor are applied to obtain the position of the robot and to combine effectively the

different measurements to generate the estimated system states. The sensor fusion allows the mitigation of the limitations of different sensor, obtaining a more accurate position of the robot.

The Kalman Filtering technique is an efficient way for sensor fusion in robotic applications [1]. When the measurement model of the robot is linear the Linear Kalman Filter is suitable to solve the sensor fusion problem. In the case of nonlinear robot models Extended Kalman Filtering techniques of the Unscented Kalman Filtering can be applied. An alternative to the Kalman Filter can be the Particle Filter based robot state estimation [2].

There are several ways to solve the indoor localization of the robot; the most common is the vision based localization [3]. Another promising approach is based on ultrasonic signal receiver - emitter pairs. The emitters or receivers are placed over the robot's workspace and its pair is placed on the robot. These systems measure the Time of Flight of the signals traveling between the synchronized receivers and transmitters. By assuming that the spatial positions of the receivers are known, multiple measurements can be combined with trilateration to find the location of the robot [4].

The orientation of a mobile robot related to a given axis can be determined using dedicated sensors such as magnetometers [5].

If precise time synchronization and effective signal detection is provided, a well calibrated ultrasound based localization system can provide sub-centimeter position accuracy. However the standard Time of Flight ultrasonic range finders are only able to provide tens of readings per second. This update rate is not enough for fast robot control applications. To handle this problem, the Time of Flight measurement based position computation can be fused with inertial measurements to provide much faster position estimation. These sensor fusion methods use the model of the robot and measurements from accelerometers and gyroscope sensors [6].

The goal of the current work is to develop a sensor fusion technique for omnidirectional mobile robots which combines the measurements of a robot localization system having low measurement update rate with the measurements of the Inertial Measurement Unit (magnetometer, accelerometer, gyroscope). The two-stage Kalman filter introduced in this work is similar to the quadrotor helicopter localization method presented in [7].

2. Robot Modeling for Sensor Fusion

2.1. Unicycle robots

Consider a unicycle-type robot that moves in a horizontal plane. The coordinates of the robot's position (x, y) are given in an inertial reference frame (x_w, y_w) , see *Fig. 1*. Another frame is attached to the robot's body (x_R, y_R) which origin is in the center of gravity of the robot. The orientation of the robot in the reference frame is defined as the angle between the x axes of the reference frame and robot's frame (θ).

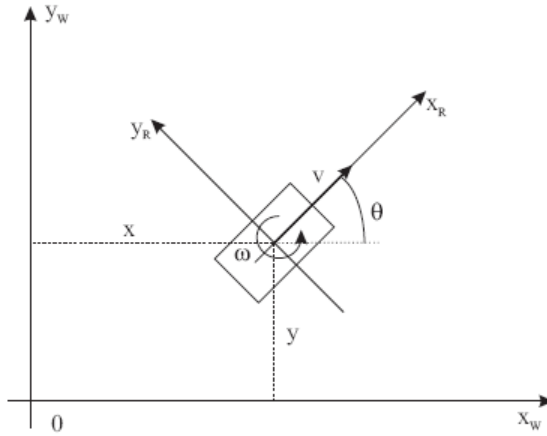


Figure 1: Unicycle robot.

Due to the kinematic constraint in the unicycle-type robot's motion, the robot cannot generate velocity along the $0y_R$ axis. The direction of the robot's velocity vector always corresponds to the x axis of the robot's frame. The motion of the mobile robot in a two dimensional reference frame is described by:

$$\begin{cases} \dot{x} = \cos(\theta) \cdot v, \\ \dot{y} = \sin(\theta) \cdot v, \\ \dot{\theta} = \omega, \\ \dot{v} = a. \end{cases} \quad (1)$$

Here v is the velocity of the mobile robot, ω denotes the angular velocity of it. The notations x and y stand for the robot's coordinates in the reference frame and the angle θ denotes the robot's orientation. The acceleration of the robot along the $0x_R$ axis (a) is the first order derivative of v .

2.2. Omnidirectional robots

In the case of the omnidirectional robot model it has to be considered that this type of robot can generate angular velocity and linear velocity independently. This fact makes the control design of the omnidirectional robot simpler. However, during the model development for sensor fusion the inter-influence of the independent linear and rotational motions has to be taken into consideration.

Consider an omnidirectional robot that moves in a horizontal plane. The coordinates of the robot's position (x, y) are given in an inertial reference frame (x_w, y_w) , see Fig. 2. Another frame is attached to the body (x_R, y_R) of the robot. The orientation of the robot in the reference frame is defined as the angle between the x axes of the reference frame and robot's frame (α).

The robot can generate velocity along both $0x_R$ and $0y_R$ axes, i.e. the direction of the robot's velocity vector does not necessarily correspond to the x axis of the robot's frame. The motion of the mobile robot in a two dimensional reference frame is described by:

$$\begin{cases} \dot{x} = \cos(\theta) \cdot v, \\ \dot{y} = \sin(\theta) \cdot v, \\ \dot{\alpha} = \omega. \end{cases} \quad (2)$$

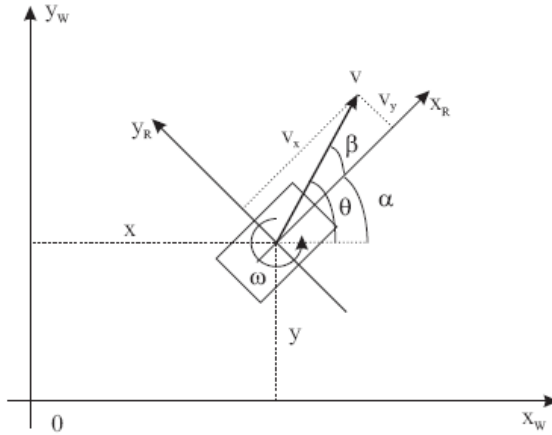


Figure 2: Omnidirectional robot.

Here θ is the angle between the velocity vector and the x axis of the reference frame.

In the robot's frame the components of the velocity vector are denoted by v_x and v_y . The relation between θ and α is:

$$\theta = \alpha + \beta = \alpha + \arctan\left(\frac{v_y}{v_x}\right) \quad (3)$$

The kinematic relationship between acceleration measurements and velocity components can generally be formulated as [9]:

$$\begin{cases} \dot{v}_x = a_x + \omega \cdot v_y \\ \dot{v}_y = a_y - \omega \cdot v_x \end{cases} \quad (4)$$

Consider an Inertial Measurement Unit (IMU) mounted in the robot's center which contains accelerometer, gyroscope and a magnetometer. The magnetometer is applied for orientation measurement. Using the IMU acceleration of the robot along the x and y axes (a_x , a_y), the angular velocity around the axis perpendicular to the robot's frame (ω) and the orientation of the robot (α) is measured. The IMU measurements are corrupted by noise:

$$\begin{cases} a_{xMEASURED} = a_x + b_{ax} + w_{ax}, \\ \dot{b}_{ax} = 0, \\ a_{yMEASURED} = a_y + b_{ay} + w_{ay}, \\ \dot{b}_{ay} = 0, \\ \omega_{MEASURED} = \omega + b_{\omega} + w_{\omega}, \\ \dot{b}_{\omega} = 0, \\ \alpha_{MEASURED} = \alpha + w_{\alpha}, \end{cases} \quad (5)$$

where b_{ax} , b_{ay} and b_{ω} are constant unknown biases and the stochastic noise components w_{ax} , w_{ay} , w_{ω} and w_{α} are assumed zero mean with normal distribution: $w_{ax}, w_{ay} \sim N(0, \sigma_a)$, $w_{\omega} \sim N(0, \sigma_a)$, $w_{\alpha} \sim N(0, \sigma_a)$.

The coordinates x and y are measured by a localization system and the measurements are also considered to be affected by zero mean value stochastic noise with normal distribution ($N(0, \sigma_x)$).

2.3. Discretized Two-Stage Model for Sensor Fusion

Consider that the IMU provides the measurements with T measurement period and the external localization system has a measurement period kT , where k is a strictly positive integer. To deal with multiple measurement rates a two-stage discrete time modeling is proposed. For the numerical approximation of

the continuous time model, the Euler integration method can be applied, i.e. $\dot{\alpha} \approx (\alpha[k] - \alpha[k-1]) / T$.

Stage 1. The angular position and the bias of the velocity offset are estimated:

$$\begin{cases} \alpha[k] = \alpha[k-1] + T \cdot (\omega[k-1] + b_\omega[k-1]) \\ b_\omega[k] = b_\omega[k-1] \end{cases} \quad (6)$$

As measured output, the orientation of the robot is considered; the input is the angular velocity.

Stage 2. Based on the estimated orientation in Stage 1, from the model and measurement equations the position yields the model for robot pose estimation

$$\begin{cases} x[k] = x[k-1] + T \cdot \cos\left(\alpha[k-1] + \arctan\left(\frac{v_y[k-1]}{v_x[k-1]}\right)\right) \cdot \sqrt{v_x[k-1]^2 + v_y[k-1]^2}, \\ y[k] = y[k-1] + T \cdot \sin\left(\alpha[k-1] + \arctan\left(\frac{v_y[k-1]}{v_x[k-1]}\right)\right) \cdot \sqrt{v_x[k-1]^2 + v_y[k-1]^2}, \\ v_x[k] = v_x[k-1] + T \cdot (a_x[k-1] + b_{ax}[k-1] + \omega[k-1] \cdot v_y[k-1]), \\ v_y[k] = v_y[k-1] + T \cdot (a_y[k-1] + b_{ay}[k-1] - \omega[k-1] \cdot v_x[k-1]), \\ b_{ax}[k] = b_{ax}[k-1], \\ b_{ay}[k] = b_{ay}[k-1]. \end{cases} \quad (7)$$

The measured outputs are the coordinates $x[k]$, $y[k]$ the inputs are the acceleration components of the robot ($a_x[k]$, $a_y[k]$) and the orientation and angular velocity measurements ($\omega[k]$, $\alpha[k]$). As the position measurement update rate is lower than the IMU measurement update rate, between two position measurements the model above is used for prediction. When a new position measurement is available, the update phase of the estimation is executed.

In the case of the localization task the states, outputs and inputs are defined as:

$$\begin{aligned} X &= (x \ y \ v_x \ v_y \ b_x \ b_y)^T \\ Y &= (x \ y)^T \\ U &= (a_x \ a_y)^T \end{aligned} \quad (8)$$

Note that the proposed modeling technique presented here for omnidirectional robots can also be applied to the unicycle robots introduced in subsection 2.1.

3. A short review of the Linear, Extended and Unscented Kalman Filter

The general framework for nonlinear state estimation methods is based on a nonlinear discrete time state space model

$$\begin{cases} X[k] = f(X[k-1], U[k-1]) + w[k-1] \\ Y[k] = h(X[k], U[k]) + v[k] \end{cases} \quad (9)$$

where $X[k]$ is the n -dimensional state vector, $U[k]$ is the m -dimensional input vector and $Y[k]$ is the noisy output vector (p -dimensional) of the system. The f and h are nonlinear continuous functions. The $w[k]$ is an n dimensional process noise sequence and $v[k]$ is a p dimensional observation (measurement) noise sequence. Both noises (vectors) are Gaussian (normal distribution), independent random processes with zero means and known time invariant covariance matrices:

$$\begin{aligned} w &\sim N(0, \sigma_w) & \text{cov}\{w\} &= Q & E\{w\} &= 0 \\ v &\sim N(0, \sigma_v) & \text{cov}\{v\} &= Q & E\{v\} &= 0 \end{aligned} \quad (10)$$

The objective of the estimation process is to calculate the $X[k]$ recursively from the output measurements $Y[k]$. In accordance with Bayesian theory this means to determine recursively the estimation of $X[k]$ if the following data is given: $Y[1], \dots, Y[k]$ (up to time k). We consider that the initial *probability distribution function* (pdf) of the state vector $\text{pdf}(X[0]/Y[0])$ is known and the $\text{pdf}(X[k]/Y[1:k])$ is obtained recursively in two steps: prediction step and update (correction) step.

The linear Kalman filter (KF) can be used just for linear dynamic systems and this method propagates the mean and covariance of the *pdf* of the model states in an optimal way.

The Extended Kalman filter (EKF) in many ways is similar with simple Kalman filter. In this case the state distribution is propagated analytically through a linear approximation of the system around the working point. The linear approximation of the nonlinearities may introduce errors in the estimated states. The state matrix of the linear approximation is computable as:

$$F(X[k], U[k]) = \frac{\partial f(X[k], U[k])}{\partial X} \quad (11)$$

The Unscented Kalman Filter (UKF) is a derivative free method, and it resolves the estimation problem using a deterministic sampling approach [8]. The state distribution is also represented by Gaussian random variables, but this algorithm is using a minimal set of sample points, called sigma points. The sigma points are calculated in each step and they completely capture the true

mean and covariance of the states and are propagated through the nonlinearity. For calculating the statistics of a random variable which undergoes a nonlinear transformation we can use the unscented transformation.

4. Simulation measurements

4.1. Simulation environment

The proposed sensor fusion algorithm was tested in a simulation environment that was developed in Matlab environment. The Matlab implementation of the omnidirectional robot model has the form:

```
T = 0.01; %sec
time = 1:T:20;
% robot acceleration
ps = 0.5;
a_xr = -cos(ps*time)*ps^2;
a_yr = -sin(ps*time)*ps^2;
% robot orientation
omega_r = -0.1572;
alpha_r = alpha_r + T*omega_r;
% robot motion
v_xr = v_xr + T*(a_xr + omega_r*v_yr);
v_yr = v_yr + T*(a_yr - omega_r*v_xr);
x_r = x_r + T * cos(alpha_r + atan2(v_yr, v_xr)) *
    .. sqrt(v_xr^2 + v_yr^2);
y_r = y_r + T * sin(alpha_r + atan2(v_yr, v_xr)) *
    .. sqrt(v_xr^2 + v_yr^2);
```

The measurement update period of the IMU was chosen $T = 10ms$. The inputs of the robot were the acceleration signals, which were generated as sinusoidal both along the x and y axis. As the two accelerations are shifted with a phase $\pi/2$ the robot motion is almost circular. A constant angular velocity was assumed during the robot's motion.

The measurement noises were assumed in the form:

```

% Orientation measurement
offset_omega = 0.2;
noise_alpha = 0.1*(rand(1,1) - 0.5)/2;
alpha = alpha_r + noise_alpha;
noise_omega = 0.3*(rand(1,1) - 0.5)/2;
omega = omega_r + noise_omega + offset_omega;
% Acceleration measurements
offset_ax = 0.2;
noise_ax = 0.5*(rand(1,1) - 0.5)/2;
a_x = a_xr + noise_ax + offset_ax;
offset_ay = 0.2;
noise_ay = 0.5*(rand(1,1) - 0.5)/2;
a_y = a_yr + noise_ay + offset_ay;

```

As it can be seen, both on the acceleration and on the angular velocity measurements high frequency noises and measurement biases were assumed.

The position measurements that come from the ultrasonic measurement system were taken with an update rate which is ten times smaller than the IMU's update rate, i.e. 100ms. The x , y position measurements were also assumed to be affected by high frequency noises.

```

noise_x = 0.025*(rand(1,1) - 0.5)/2;
noise_y = 0.025*(rand(1,1) - 0.5)/2;
p_x = x_r + noise_x;
p_y = y_r + noise_y;

```

Firstly, the angular position and the bias of the angular velocity were estimated, these were taken as system states in the first stage of the sensor fusion: $(\alpha \ b_\omega)$. For the implementation of this first stage a linear Kalman filter was applied in which the Q , R and $P_{kk}[0]$ matrices were chosen as:

```

% stage 1
fi_omega = 1;
Q_1 = fi_omega*eye(2); % covariance matrix of the states
fi_theta = 10;
R_1 = fi_theta^2*eye(1); % covariance of the output
L = 1;
Pkk_1 = L*eye(2); % covariance of the initial estimation error

```

According to the equation (6) the matrices for the linear system to be estimated can be written as:

```

F_1 = [1 T; 0 1];
G_1 = [T; 0];
H_1 = [1 0];

```

For the implementation of stage 2 in the prediction phase of the Extended Kalman Filter the model (7) was directly applied. The states of the estimator for the second stage are $(x \ y \ v_x \ v_y \ b_x \ b_y)$, the measured outputs are $(x \ y)$, the inputs are $(a_x \ a_y)$. The angular position (α) estimated in stage 1 and the angular velocity (ω) of the robot were also considered known parameters for stage 2. In the update phase the nonlinear system was linearized around the current estimated state. The linearized state matrix has been implemented as (see equation (11)):

```
F_2(1,:) = [1 0 T*d_f_x_per_d_v_x T*d_f_x_per_d_v_y 0 0];
F_2(2,:) = [0 1 T*d_f_y_per_d_v_x T*d_f_y_per_d_v_y 0 0];
F_2(3,:) = [0 0 1 T*omega T 0];
F_2(4,:) = [0 0 -T*omega 1 0 T];
F_2(5,:) = [0 0 0 0 1 0];
F_2(6,:) = [0 0 0 0 0 1];
```

The partial derivatives in the first two lines of the system matrix F_2 were obtained using symbolic derivation for the first two lines of the model (7):

```
syms v_x v_y alpha
f_x = T*sqrt(v_x^2 + v_y^2)*sin(alpha + atan(v_y/v_x));
f_y = T*sqrt(v_x^2 + v_y^2)*cos(alpha + atan(v_y/v_x));
d_f_x_per_d_v_x = diff(f_x, v_x);
d_f_x_per_d_v_y = diff(f_x, v_y);
d_f_y_per_d_v_x = diff(f_y, v_x);
d_f_y_per_d_v_y = diff(f_y, v_y);
```

For the implementation of this second stage the Q , R and $P_{kk}[0]$ matrices were chosen as:

```
% covariance matrix of the state noises
fi_a = .5;
Q_2 = fi_a*eye(6);
% covariance matrix of the output noises
fi_p = 0.025;
R_2 = fi_p^2*eye(2);
% covariance of the initial estimation error
L = 1;
Pkk_2 = L*eye(6);
```

These values were chosen both in the case of the Extended Kalman Filter and the Unscented Kalman Filter.

4.2. Simulation results

For sensor fusion the simulation ran for 2000 IMU measurement periods, i.e. 20s.

Fig. 3 shows the behavior of stage 1 of the estimation. As the figure shows, the Linear Kalman Kilter can offer a precise estimate of the angular position and angular velocity bias in spite of noisy measurements.

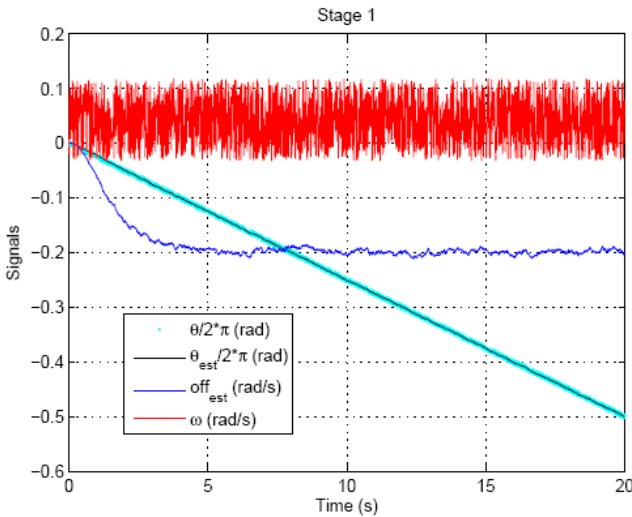


Figure 3: Stage 1: Inputs, measured outputs, estimated states.

Fig. 4 shows the estimated states generated by the Extended Kalman filter. These measurements also show that the EKF can cope with measurement noises of the accelerometer. Between the measurements the model based prediction can offer a good estimate of the robot's motion for the time intervals between the measurement update.

The resulting motion of the robot is presented in *Fig. 5*. During the localization measurements the robot moved on an almost circular trajectory, which assures that all the states of the system change in time.

The performances of the Extended Kalman Filter were compared with the performances of the Unscented Kalman Filter applying the same Q and R matrices during the simulation. The *Fig. 6 and 7* show that the UKF approach has longer transients in the estimation errors. On the other hand, when the estimation transients lapse, the average of the estimation errors are smaller in the case of the UKF, see *Fig. 8*. The measurements shown in this figure take into account the last 1000 measurement iterations to get rid of the estimation transients.

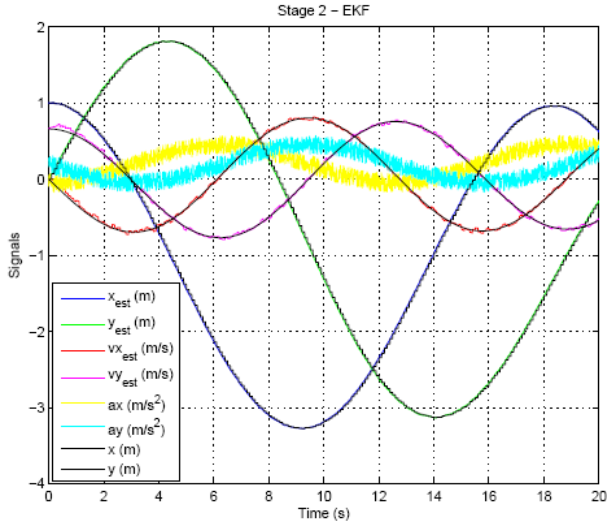


Figure 4: Stage 2: Inputs, measured outputs, estimated states.

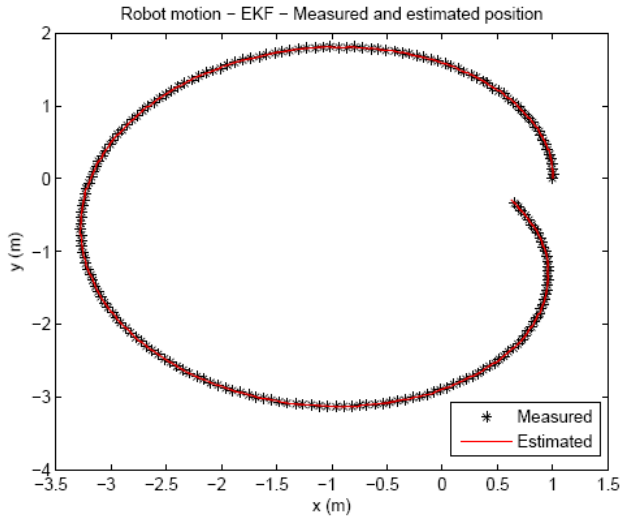


Figure 5: Robot's motion in plane during the simulation experiments.

The beneficial effects of the UKF can also be seen in *Fig. 9 and 10*. The UKF has a much pronounced filtering capability as the EKF and it mitigates the effect of the measurements noises more efficiently.

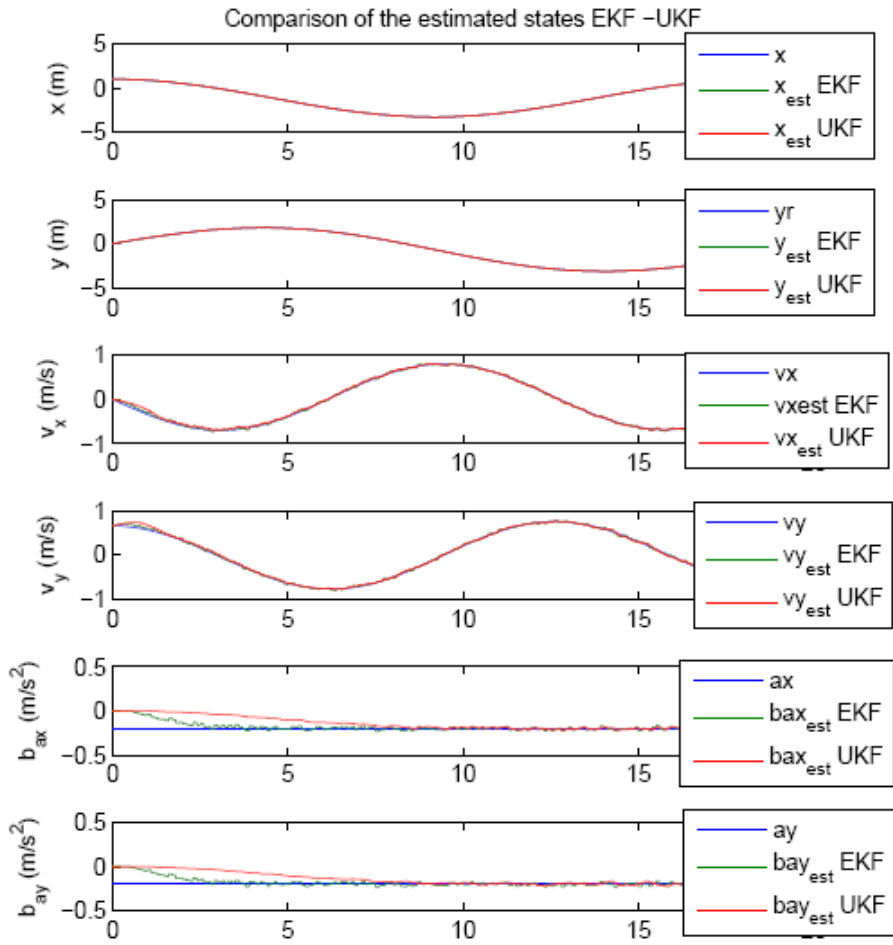


Figure 6: Comparison of UKF and EKF: estimated states.

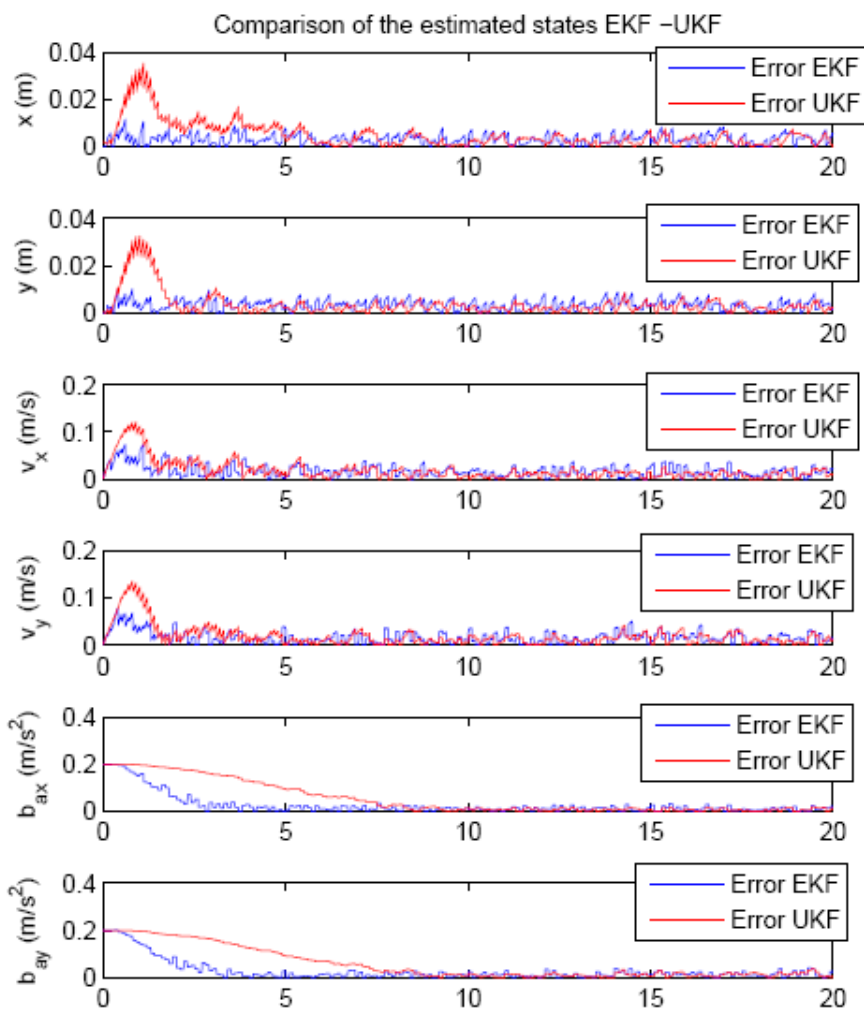


Figure 7: Comparison of UKF and EKF: estimation errors.

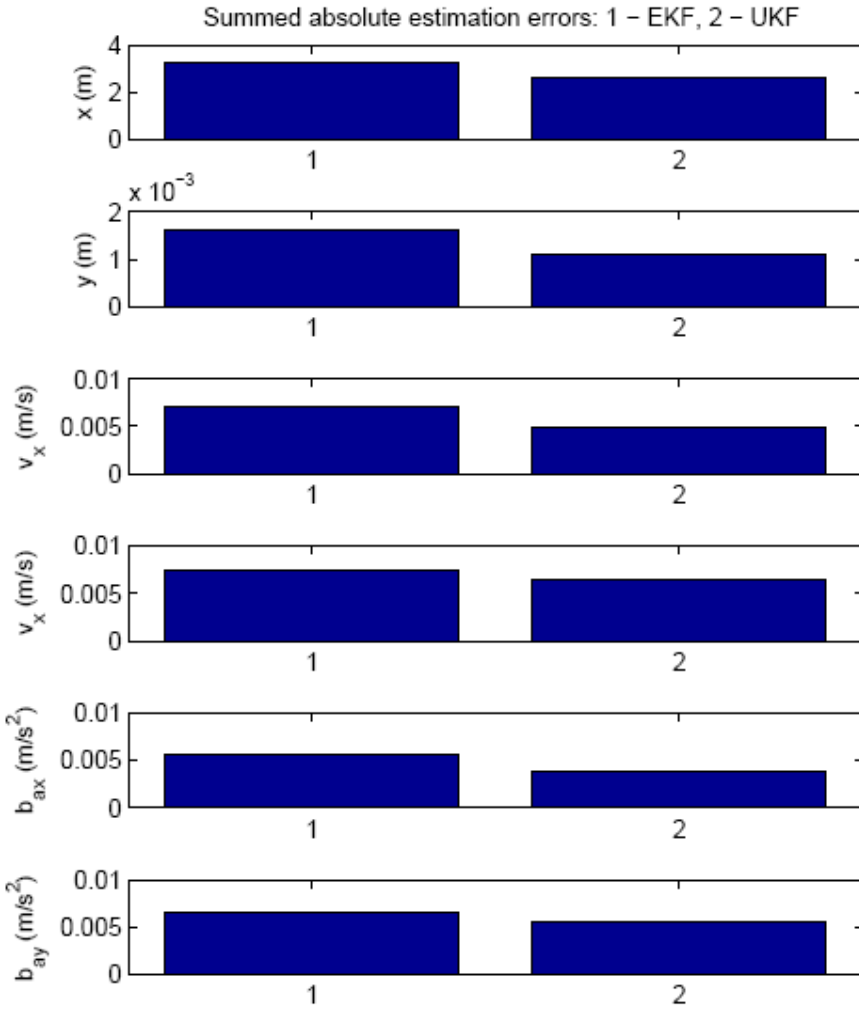


Figure 8: Comparison of UKF and EKF after the transients: sum of the normalized absolute values of estimation errors.

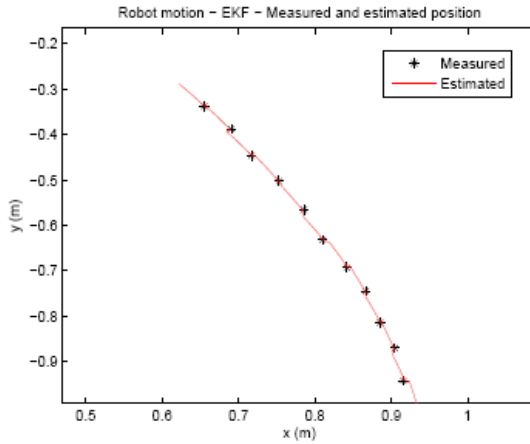


Figure 9: Position estimation with EKF.

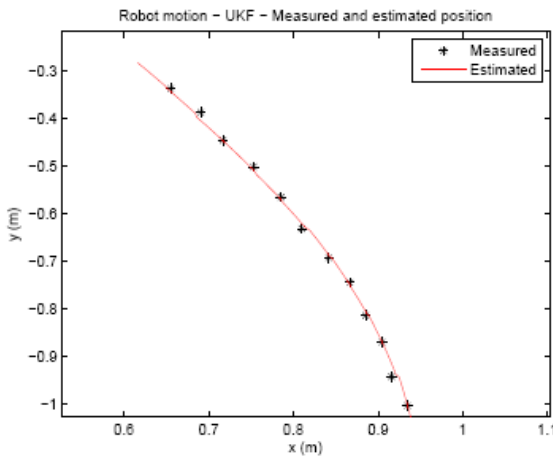


Figure 10: Position estimation with UKF.

5. Conclusions

In this work a sensor fusion method was introduced to improve the performances of indoor mobile robot localization systems (such as ultrasonic, radio signal based). To handle the slow measurement update rate of the localization system the position measurements are extended with a position predictor that applies the robot sensor model which input is given by IMU measurements. The obtained solution is a combination of a linear and an Extended Kalman filter, a two-stage Kalman filter. The Linear Kalman Filter

works with the update rate of the IMU and it provides the orientation of the robot. The second stage is an Extended Kalman Filter provides the planar position and the linear velocity components of the omnidirectional robot. The effectiveness of the method is shown through simulation examples. The simulation experiments show that applying Unscented Kalman Filter instead of Extended Kalman Filter could lead to more accurate position estimation.

Acknowledgements

The research and publication has been supported by the European Union and Hungary and co-financed by the European Social Fund through the project TAMOP-4.2.2.C-11/1/KONV-2012-0004 - National Research Center for Development and Market Introduction of Advanced Information and Communication Technologies (subproject I.6).

The research work was also supported by a grant of the Romanian National Authority for Scientific Research, CNCS - UEFISCDI (project number PN-II-RU-TE-2011-3-0005).

References

- [1] Simon, D., “Kalman filtering with state constraints: a survey of linear and nonlinear algorithms”, *Control Theory Applications*, IET 4(8), pp.1303–1318, August 2010.
- [2] Rekleitis, I., Dudek, G., Milios, E., “Probabilistic cooperative localization and mapping in practice”, in: *Proc. of IEEE International Conference on Robotics and Automation*, pp. 1907–1912, September 2003.
- [3] Tamas, L., Lazea, G., “Pattern recognition and tracking dynamic objects with LIDAR.”, in: *41st International Symposium on Robotics (ISR) and 6th German Conference on Robotics (ROBOTIK)*, pp. 1–6, 2010.
- [4] Burguera, A., Gonzalez, Y., Oliver, G., “Sonar sensor models and their application to mobile robot localization”, *Sensors* 9, pp. 10217 – 10243, 2009.
- [5] Kis, L., Lantos, B., “Development of state estimation system with INS, magnetometer and carrier phase GPS for vehicle navigation”, *Gyroscopy and Navigation* 5(3), pp. 153–161, 2014.
- [6] Font-Llagunes, J.M., Batlle, J.A., “Consistent triangulation for mobile robot localization using discontinuous angular measurements”, *Robotics and Autonomous Systems* 57(9) pp. 931 – 942, 2009.
- [7] Lantos, B., Marton, L., “Nonlinear Control of Vehicles and Robots” Springer, London, UK 2011.
- [8] Kandepu, R., Foss, B., Imsland, L., “Applying the unscented Kalman filter for nonlinear state estimation”, *Journal of Process Control* 18(78), pp. 753 – 768, 2008.
- [9] Ryu, J., and Gerdes, J. C., “Integrating inertial sensors with Global Positioning System (GPS) for vehicle dynamics control”, *Journal of Dynamic Systems, Measurement, Control*, 126, pp. 243 – 254, 2004.



Heat-Treatment of 16MnCr Steel in a Linear Non-Isotherm Plasma Reactor

Lajos KENÉZ, Nimród KUTASI, Emőd FILEP,
László JAKAB-FARKAS, Imre Árpád SZŐCS

Department of Electrical Engineering,
Faculty of Technical and Human Sciences,
Sapientia Hungarian University of Transylvania, Tg. Mureş,
e-mail: l_kenez@yahoo.com, kutasi@ms.sapientia.ro

Manuscript received February 20, 2013; revised November 20, 2013.

Abstract: Over the last few years a Direct Current Plasma Nitriding (DCPN) equipment has been built at the Sapientia-University. This equipment was built on the basis of an older linear plasma reactor. Over the years the vacuum-system and vacuum-measurement, gas feeding system was upgraded and a brand new modern voltage supply was developed to generate and sustain the plasma discharge. Using the upgraded DCPN equipment we treated 16MnCr steel pieces at 530 degrees Celsius, for one, two, three, four and 6 hours long, respectively. We present optical- and electron microscopy investigation and the Vickers-hardness study of the prepared treated pieces. The results of the DCPN experiments reported in this paper serve as comparison basis for the following ASPN (Active Screen Plasma Nitriding) experiments, which will be performed at the same sample temperature and time-span conditions.

Keywords: plasma, nitriding, heat treatment, coating.

1. Introduction

Plasma nitriding is one of the most efficient, environment and health-friendly coating and hardening techniques.

Plasma nitriding is widely used in case of industrial applications and it is also object of many developments and plasma physics studies [1-6]. There are two different plasma nitriding methods, the DCPN (Direct Current Plasma Nitriding) and the ASPN (Active Screen Plasma Nitriding) method. In case of the DCPN method the nitrated pieces represent the cathode of the plasma discharge, thus the pieces are heated directly by the discharge. In case of the ASPN method there is a separate metallic screen which plays the role of the cathode, the screen is heated by the discharge while the nitrated pieces are

heated by heat transfer. Starting from the basis of a linear plasma reactor, we developed a modern DCPN equipment which is suitable for heat treatment of different steels in nitrogen-hydrogen plasma. Steels are treated at 530 degrees Celsius, for about 1-6 hours, at working pressure 2 torr, depending on the industrial requirements. The equipment is also suitable for dedicated local plasma diagnostics research, involving different types of electrostatic (Langmuir) probes such as cylindrical-, double- and emitting probes. In the present paper the construction of the equipment is presented, along with detailed description of the constructing modules, first nitriding experiments involving *16MnCr* steel pieces, optical- and electron microscopy investigations and Vickers hardness study of the adequately prepared samples.

2. General presentation of the Direct Current Plasma Nitriding (DCPN) equipment

The present DCPN equipment is based on an older DCPN machine called NITRION-10 [7]. We discarded the vacuum-system, electrical-system and gas feeding lines, and retained the discharge chamber which is the anode of the discharge (grounded) and the cathode which holds the pieces to be treated too (the cathode in *Fig.1* is a solid metallic cylinder mounted coaxially with the chamber axis).

The experimental equipment is presented in *Fig.1*. The upper flange and the body of the vacuum-chamber is water cooled. The upper flange is provided with gas-inlet hole, electrical feed-through and the cathode of the plasma discharge is also mounted in the top flange. There is a motion feed-through on the side of the chamber which is used to introduce a Langmuir-probe for plasma diagnostics research. Optionally, a heat shielding metallic cylinder can be coaxially positioned inside the plasma chamber.

We adopted a reasonable vacuum line involving an Alcatel 2105 type fore-vacuum pump and an absolute pressure gauge for pressure measurement. We can reach pressure in the range of 1-0,02 torr, which is by far sufficiently low for plasma nitriding. The working pressure for plasma nitriding is about 3,5 torr which is obtained mixing and introducing gaseous nitrogen and hydrogen.

It is very important to ensure proper and safe gas feeding system for the heat treatment. For this purpose hydrogen and nitrogen is needed, which are provided by a combined nitrogen-hydrogen generator. We provided the nitrogen and the hydrogen outlets of the generator with precision valves to set the proper gas flows. After the valves, the hoses are introduced into a mixing chamber which is connected to the plasma chamber.

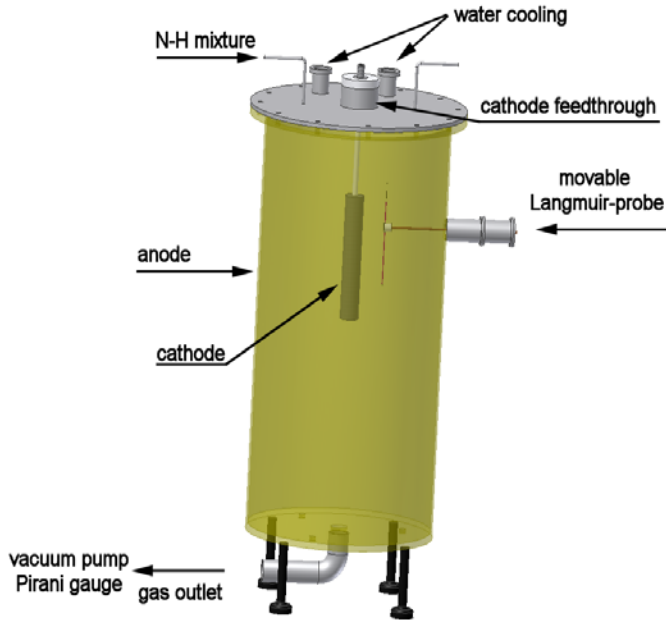


Figure 1: DCPN equipment.

Due to the low pressure obtained by pumping the plasma and mixing chambers, nitrogen and hydrogen can be mixed as ideal gases in the mixing chamber, and can be introduced as perfect mixture suitable for plasma nitriding.

3. Development of a Regulated Direct Current plasma discharge Power Supply (RDC-PS)

A new DC power supply was developed in order to obtain accurate output voltage and current, with 1% precision compared to the set values. The new digitally controlled power supply has several benefits, namely programmable arc management, fast protections, and communication interface with higher level control system. The main characteristics of the power supply are described in *Table 1*.

Table 1: Specifications of the DC power supply.

AC input:	230Vac, 10A
DC Output:	0-1000VDC, 0-2A controllable.
Control:	Fast, DSP based voltage and current control. PLC for process control and external communication. Interface to PC via PLC.
Mode of operation:	Voltage control with current limitation or vice versa. Programmable restart in case of arc discharge (arc management).
Protections:	Fast overcurrent and di/dt protection. Overvoltage protection. Cooling water flow monitoring.
Human-Machine Interf.	Siemens OP3.

According to Fig.2 the DC power supply consists of an input rectifier and a filter circuit, an inverter unit feeding the voltage transformer followed by the rectifier and the output filter. Due to the single-phase mains input voltage, the DC-link has an important role on smoothing the rectified voltage, but the filter has to block also the high frequency noise coming from the inverter.

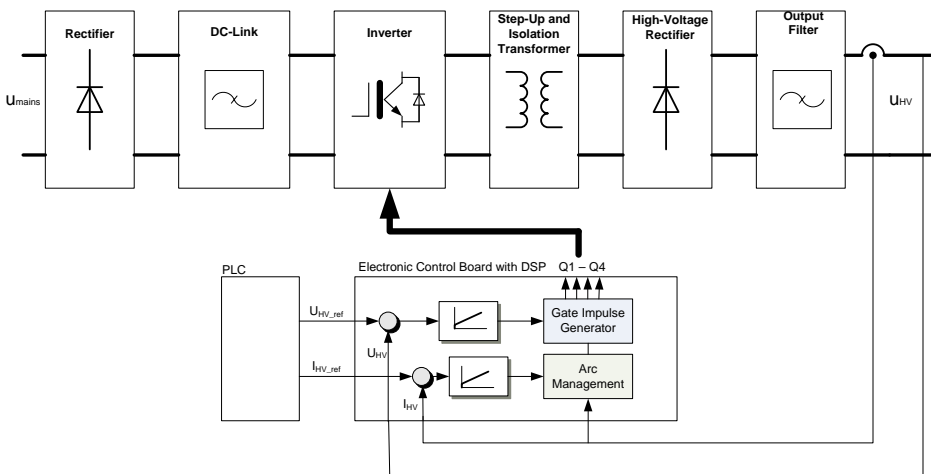


Figure 2: Schematic diagram of the DC power supply.

The inverter and the high-voltage rectifier have been realized with the state of the art semiconductors. In the inverter, two pairs of 40 Amps IGBTs are used, working at 100 kHz. The high-voltage rectifier has been built with Silicon Carbide (SiC) diodes, thus the switching losses can be neglected. With this

technology the cooling demand of the converter is reduced and the size of the reactive elements, mainly the output transformer, is reduced. The output filter has the role of reduction of the HV voltage ripple, but the energy stored in the capacitor has to be considered when the load is a vacuum chamber with plasma discharge. In case of electric arc, the energy of the capacitor (C_p) will be discharged on the surface of the treated part by a DC arc, having a strong erosion effect on the surface. The higher the energy stored in the capacitor, the higher the evaporated metal quantity. In our case a good compromise was to use a capacitor of $1 \mu\text{F}$.

The control of the power supply is based on an inverter control board containing all necessary signal conditioning circuits, a dsPIC30F6010 digital signal controller for all the measurements and control functions, and finally a Lattice type CPLD for gate impulse generation and fast error handling. The control board communicates with a VIPA PLC, where the setvalues are entered and the mode of operation is selected. The user can select between two modes of operation, namely voltage control with current limitation, or vice versa. Beside of these, the arc management can be enabled or disabled from the PLC. In case of enabled arc management, the restart time is programmable. In case if the arc management is disabled, when overcurrent occurs on the output, the power supply stops, reporting overcurrent error. Simulations and practical measurements regarding the power supply operation are presented in [8].

4. Graphic User Interface - Control from PC

The nitriding process is controlled from a process computer, where a LabWindows CVI based software is running.

The process control software has been developed to offer an easy interface for data visualization and logging, controlling of the different process parameters. The most important control problem is the temperature control. Based on a simplified model of the system, a PI controller with anti-windup has been implemented to control the temperature of the treated part. The actual temperature can be seen on the main screen of the GUI and the temperature can be logged for further data processing. The main variable from the DC power supply are displayed (voltage, current, power), the power supply can be controlled through the PC in manual mode or closed loop temperature control mode.

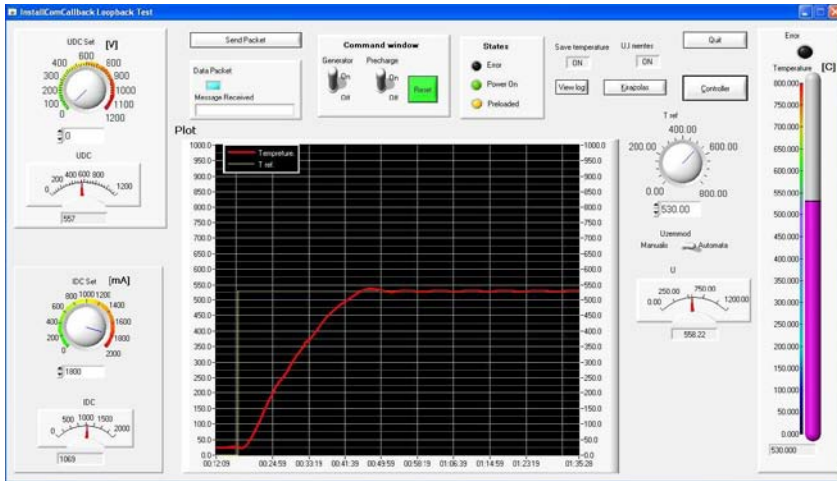


Figure 3: The graphic user interface (GUI) of the process control software.

The startup of the process is an important technological task, namely the temperature of the part has to be increased to the nitriding temperature with a well-defined ramp. The ramp can be set from the GUI of the process control software.

5. Piece holder system – material selection of the treated pieces

For test experiments, we selected a material whose properties are well-known with respect to plasma-nitriding heat treatment. This material is a 16MnCr steel. We planned to perform a series of heat treatments using the same material, same plasma conditions, and same geometry varying only the time-span of the heat treatment. The cathode arrangement used for heat treatment is presented in Fig. 3.

Two identical pieces are shown, which are positioned symmetrically with respect to the plasma chamber axis. This is important to have the same plasma conditions in the vicinity of each piece; hence the pieces reach the same temperature during heat treatment. We measure the temperature of the pieces using a K-type 1,5 mm diameter thermocouple, positioned inside a ceramic insulator tube to ensure galvanic isolation and introduced in Piece “B” through a hole. Piece “A” is changeable; we manufactured 4 identical pieces for this experiment.

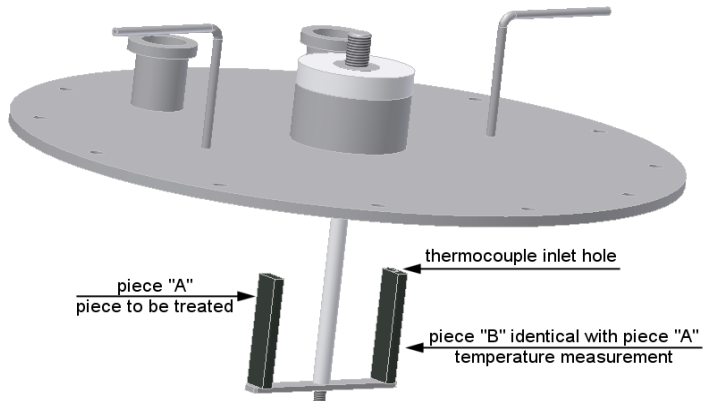
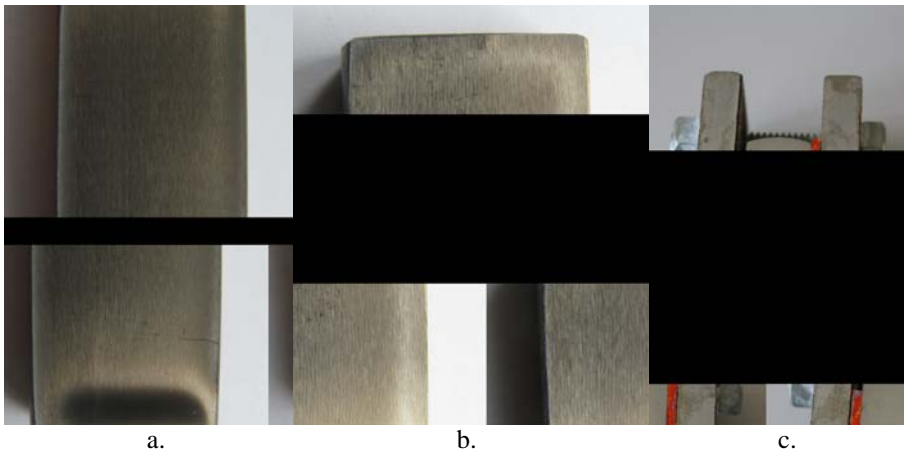


Figure 3: Experimental arrangement. Piece “A” is the piece to be treated; Piece “B” is an identical piece with Piece “A” located in symmetrical position with respect to the chamber axis.

6. Sample preparation for different investigations

It is very important to perform different investigations of the treated pieces, such as optical microscopy, electron microscopy and hardness measurements. For this reason the pieces must be properly prepared.



a.

b.

c.

Figure 4: Heat treated steel piece
a. deposition caused by cathode evaporation
b. edge-effect due to DCPN heat treatment
c. sample preparation for optical and electron microscopy.

At first all treated pieces must be cut perpendicularly to the plane side presented in *Fig. 3*. After cutting the treated pieces the samples were locked between two copper plates. After that the surfaces of the samples must be grinded, and polished in many steps involving different water resistant *SiC* abrasive papers with different grades of granulation, e.g. 100, 250, 500, 1000 until the surface become buff. After polishing, all surfaces were etched using 3% nital solution (solution of alcohol and nitric acid).

7. Conclusions

7.1. Visual observations

Visual observations of the samples provide important information. One can see, that the heat treatment of the pieces is not uniform. The bottom region of the piece in *Fig.4a* is covered by deposition of the evaporated cathode material. This is inevitable, because in DCPN treatment, the piece to be treated is the cathode of the discharge, so it must be in galvanic contact with some piece holder.

One other thing can be seen in *Fig.4b* namely the edge-effect. Also due to the fact that the treated piece is the cathode of the discharge, the appearance of the pieces is not uniform. The electric field distribution in the surroundings of the treated pieces is influenced by the shape of the piece. Of course the electric field is inhomogeneous; it becomes high at the edges of the pieces, leading to higher charge carrier transport to these regions.

7.2. Optical and electron microscopy

The prepared samples were observed using an optical microscope, than photographed. Such photo involving 60×10 optical zoom is presented in *Fig.5*.

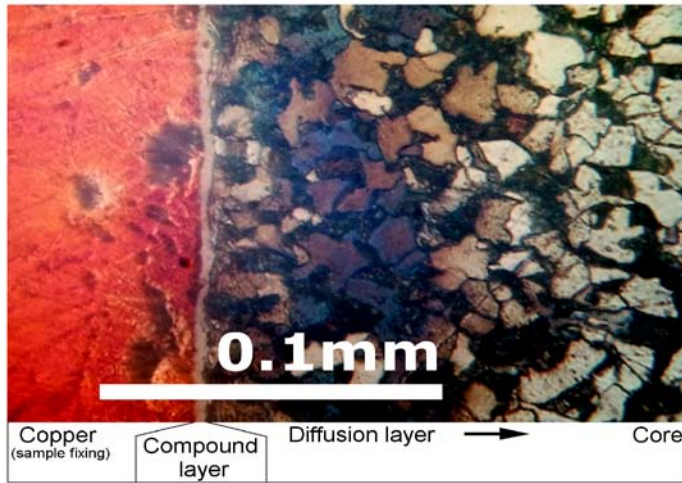


Figure 5: Heat treatment temperature 530°C, time-span 1 hour, magnification of the optical microscope 60x10.

Fig.6 presents a further magnified scanning electron microscope picture of the same sample.

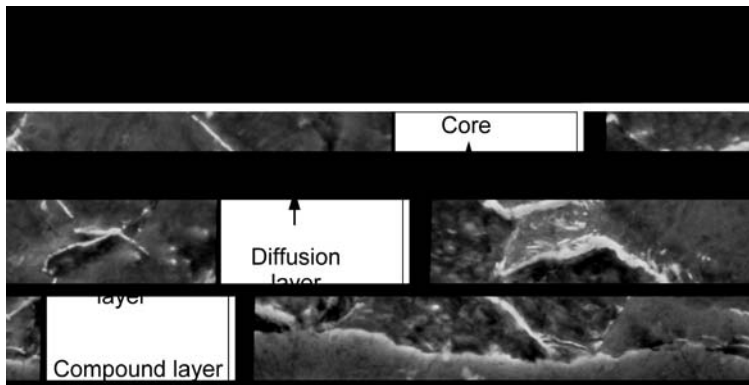


Figure 6: SEM picture using secondary electrons; 2-3 μm thick compound layer-magnification of the electron microscope $\times 5000$.

We prepared all our samples as described in Section 5 and investigated them according Section 6. We measured in each case the thickness of the diffusion layer and obtained the curve presented in Fig. 8. One can conclude, that the diffusion layer thickness (d_{diff}) is proportional to \sqrt{t} .

7.3. Micro-hardness profile measurement (Vickers-hardness)

Another method to measure the thickness of the diffusion layer is to determine the hardness-profile of the cross section of the treated pieces. We applied the Wickers-hardness test using standard 25 gram weight pushed perpendicular to the sectioned surface. The first point to be tested was located 10mm away from the edge of the piece and continued with 25mm steps along a line perpendicular to the edge of the piece toward the inner regions. Usually the distance measured from the edge of the piece to the inflexion point of the micro-hardness profile is used as layer thickness. In case of the steel used in our experiments this point is at about 400MHv, hence we consider as layer thickness the distance measured from the edge of the piece where the hardness of the piece drops to the 400MHV value.

Fig. 7. represents the micro-hardness profile of the piece treated for one hour at 530°C temperature. Similar micro hardness profiles are shown in [9].

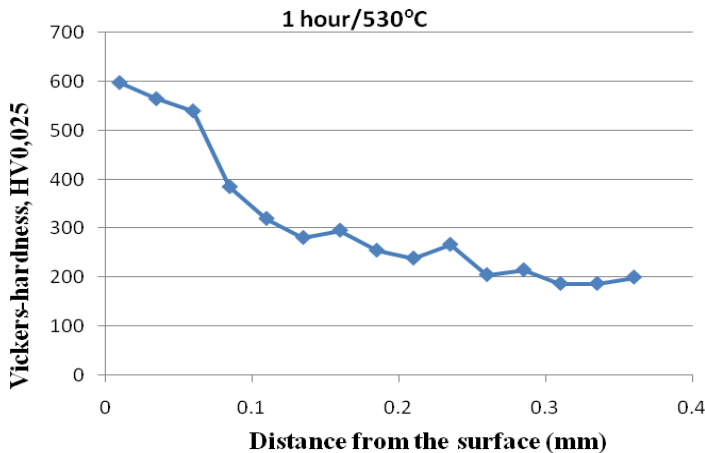


Figure 7: Micro-hardness profile of the piece treated for one hour at 530°C.

The layer thickness values determined using micro-harness test are 10% higher than the ones determined using optical microscopy (*Fig. 8.*). The micro-hardness test is much more reliable than the optical measurements, because the optical ones are influenced by the sample preparation and the time-span of the etching. Evidently the micro-hardness measurements are also loaded by errors caused by inhomogeneous structure of the sample.

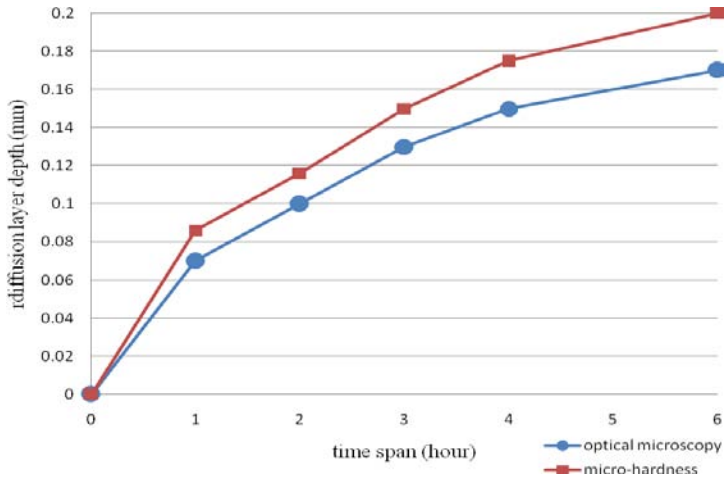


Figure 8: Diffusion layer depth.

Acknowledgement

Among the authors L. Kenéz, N. Kutasi, E. Filep and Szócs I.Á. would like to thank Institute of Research Programs of the Sapientia University (KPI) for supporting the research project and for the accorded scholarships over the years.

References

- [1] Shoaib Shah, M., Saleem, M., Ahmad, R., Zakaullah, M., Qayyum, A., Murtaza, G., “Langmuir probe characterization of nitrogen plasma for surface nitriding of AISI-4140 steel”, *Journal of Materials Processing Technology*, Volume 199, Issues 1–3, 1 April 2008, pp. 363-368.
- [2] Moradshahi, M., Tavakoli, T., Amiri, S., Shayeganmehr, S., “Plasma nitriding of Al alloys by DC glow discharge”, *Surface and Coatings Technology*, Vol. 201, Issues 3–4, 5 October 2006, pp. 567-574.
- [3] Abedi, H. R., Salehi, M., Yazdkhasti, M., “Novel plasma nitriding–oxidizing duplex treatment of AISI 316 austenitic stainless steel”, *Materials Letters*, Vol. 64, Issue 6, 31 March 2010, pp. 698-701.
- [4] Ebrahimi, M., Heydarzadeh Sohi, M., Honarbakhsh Raouf, A., Mahboubi, F., “Effect of plasma nitriding temperature on the corrosion behavior of AISI 4140 steel before and after oxidation”, *Surface and Coatings Technology*, Vol. 205, Supplement 1, 25 December 2010, pp. S261-S266.
- [5] Allenstein, A. N., Lepiński, C. M., Buschinelli, A. J. A., Brunatto, S. F., “Plasma nitriding using high H₂ content gas mixtures for a cavitation erosion resistant steel”, *Applied Surface Science*, Vol. 277, 15 July 2013, pp. 15-24.

- [6] Hannemann, M., Hamann, S., Burlacov, I., Börner, K., Spies, H.-J., Röpcke, J., “Langmuir probe and optical diagnostics of active screen N₂-H₂ plasma nitriding processes with admixture of CH₄”, *Surface and Coatings Technology*, Vol. 235, 25 November 2013, pp. 561-569.
- [7] Farkas, Sz., Filep, E., Kolozsváry, Z., „Plasma Nitriding Improves Service Behaviour of Textil Machine Components”, *J. Heat. Treat*, Vol.1.,Nr.4. 1980, pp. 15-20.
- [8] Kutasi, N., Kenéz, L., Filep, E., Kelemen, A., Mátyási, Sz., “Pulsed power supply design for DC and Active Screen Plasma Nitriding”, *MACRO2013 International Conference on Recent Achievements in Mechatronics, Automation, Computer Science and Robotics*, Sapientia University, Tg. Mures 2013, pp. 115-122.
- [9] Edenhofer, B., “Anwendungen und Vorteile von Nitrierbehandlungen außerhalb des gewöhnlichen Temperaturbereichs, Teil II: Behandlungen bei hohen Temperaturen (oderhalb von 580°C)”, *Härtereitechnische Mitteilungen* 30 [1975] Heft 4, Seite 204-208.



The Single-Parametric Model of the Meshing by Cutting Cylindrical Gears Having Archimedean Spiral Curved Tooth Line

Márton MÁTÉ

Department of Mechanical Engineering,
Faculty of Technical and Human Sciences,
Sapientia Hungarian University of Transylvania, Tg. Mureş,
e-mail: mmate@ms.sapientia.ro

Manuscript received September 15, 2014; revised January 15, 2015.

Abstract: This paper presents a novel method of synthesis of cylindrical gears having opposite curvatures on the contacting flanks. The method is an improved variant of cylindrical gears having Archimedean spiral curved toothline – developed by the author [3, 4]. Due to the increased cutting capacity of the milling head used in the technological variant that will be presented the kinematics of the meshing results more sophisticated like in the simplest case where a single radial feed is applied. Due to the fact that the present technology uses a cutter head with three cutter groups that executes a tangential feed motion the meshing process can be discussed in three variants: single parameter meshing, bi-parametric meshing and a novel method developed by the author – the double meshing model. This paper discusses the most widely used method in the theory of gear meshing, the single parametric method.

The model of the improved cutting tool, the kinematics of meshing, and the mathematical model of gearing are presented in detail.

Keywords: cylindrical gear, curved toothline, spiral, gearing, meshing.

1. Why cylindrical gears with Archimedean spiral shaped toothline?

The improvement of the contact between the tooth flanks and the increase of the load capacity remains a permanent challenge in the world of gear science. The development of cylindrical gears with curved teeth represents one of the possible ways in this direction. Cylindrical gears represent a class of machine elements present in most mechanical power transmission applications. In order to improve their load capacity by given dimensions there exist two tasks that must be fulfilled: the modification of the tooth profile consisting in addendum chamfering and sometimes in admissible dedendum undercut, and the localization of the theoretical contact in a point instead of the theoretical line –

modification defined as localization of the contact patch. This last task is very important to be fulfilled in case of high performance gears of all types. In the case of cylindrical gears there exist two basic types assisted by well suited and robust manufacturing technologies: right teathed and helical teathed cylindrical gears. The localization of the contact patch is realized here by applying high performance but expensive grinding or shaving technologies. By external cylindrical gears –both spur or helical – always convex tooth-surfaces contact.

It is mathematically proved by Hertz's contact theory that better load capacity is reached if the contact occurs between surfaces having opposite curvatures. The idea was applied for the beginning by the bevel gears of automotive power transmission where the flank line of the teeth is a looped epicycloid.

The most famous development regarding the improvement of the load capacity of a cylindrical gear pair is known as the Wildhaber-Novikov teething. This is realized using a set of complementary racks with circular arc shaped tooth profile. As a consequence one of the gears results with convex while the other with concave tooth profile. Despite of the thorough study and research (realized almost in the '60-s) the achieved results weren't reach the expected parameters. It was also remarked that the form and the position of the contact patch modifies intensely with the modification of the axis distance [1], [2].

In order to avoid the disadvantage occurred by Wildhaber-Novikov gear teeth the sense of curvature should be – in the vision of the author – set along the tooth length. In this case the generating element of the gear pair is a self-moving rack with Archimedean spiral curved toothline. The kinematic geometry of the gear pair meshing fulfills Olivier's second principle as it is shown in the right sketch of *Fig. 1*. This represents a plain section through the axis of the milling head. The left sketch of *Fig. 1* present the structure of the milling head. A defined number of profiled cutters are suited on an Archimedean spiral whose pitch is equal to the pitch of the generating rack. The profile of each cutter is corresponding to the profile of the rack defined by DIN 3972. These plain trapezoidal symmetric profiles are included in axial planes of the milling head. As a consequence of the cutter placement defined before, if the milling head rotates, a sliding rack profile appears in the axial plane that slides along a radial direction. If two gears are positioned correspondently to the moving rack, the same geometric dependencies will be reached as in the case of spur gears. However, in parallel sections there exist some delays that lead to the curvature of the generating tooth and finally to the curving of the generated toothline. Finally, the effect consists in the cutting of tooth spaces limited by a concave and a convex surface.

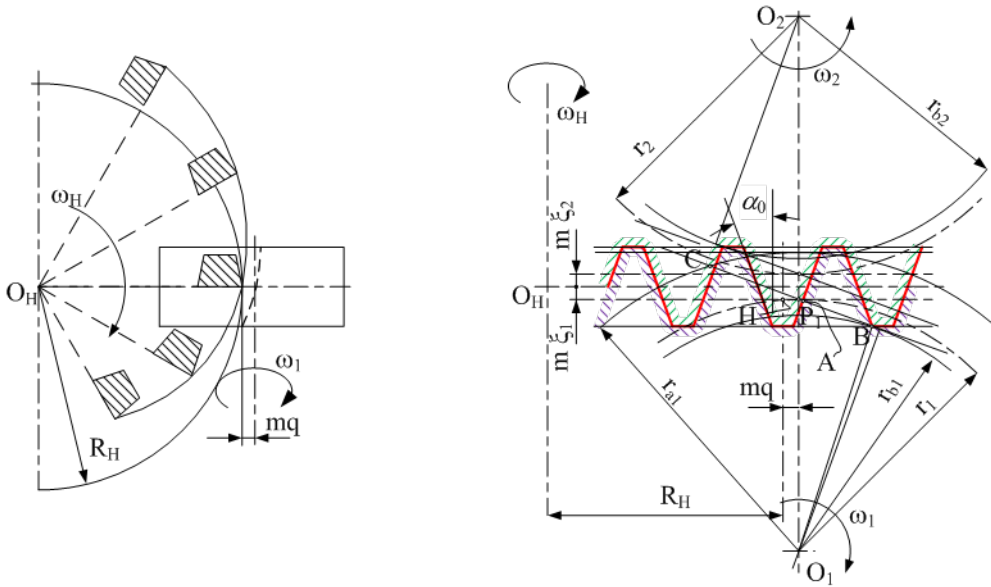


Figure 1: The sketch of the rack generating milling head and the coupling gear pair.

It is proven [3] that one single milling head body is sufficient for the generating of both elements of the gear pair. The problem consists in the changing of the sense of the leading spiral by positioning the cutters on the opposite side as shown in Fig. 2. Due to this a head with symmetric cutter positioning slots solves the problem. This will constitute another advantage versus the Wildhaber-Novikov variant where two distinct cutting tools are necessary to generate the gear-pair. The curvatures on the coupling flanks can be easily adjusted using the tangential shifting parameters q_1, q_2 . The localization of the contact and the relative sliding of the coupling surfaces can be optimized by the rational selection of the profile shifting parameters ξ_1, ξ_2 .

2. The principle of meshing using tangential feed

The gear meshing kinematics presented above uses the radial feed to achieve the complete depth of cut. The cutting process based on this is estimated to be slow. In order to increase the productivity, radial feed will be replaced with tangential feed, and the structure of the milling head will be improved, by considering Z_0 groups of cutters, each of them containing 3 up to 5 cutters.

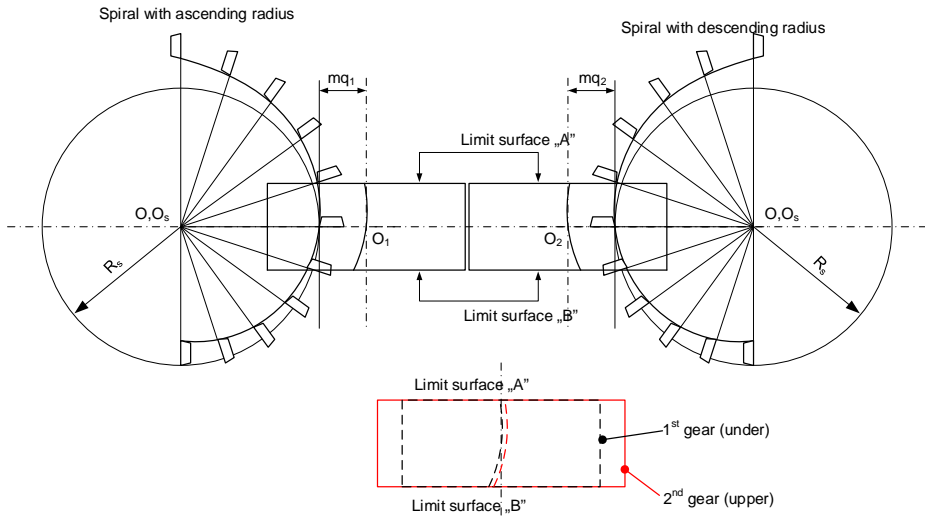


Figure 2: The meshing of the elements of the gear pair using a single cutter head with symmetrical positioning of the inserts.

The sketch of the cutter head and the principle of work is presented in Fig. 3. The cutter groups angularly equidistant positioned in the cutter head. Here cutters with a single edge are used, each of them meshing one surface of the generating rack tooth or gap. The cutters are fitted on equiangular distanced Archimedean spirals with the spiral pitch given by

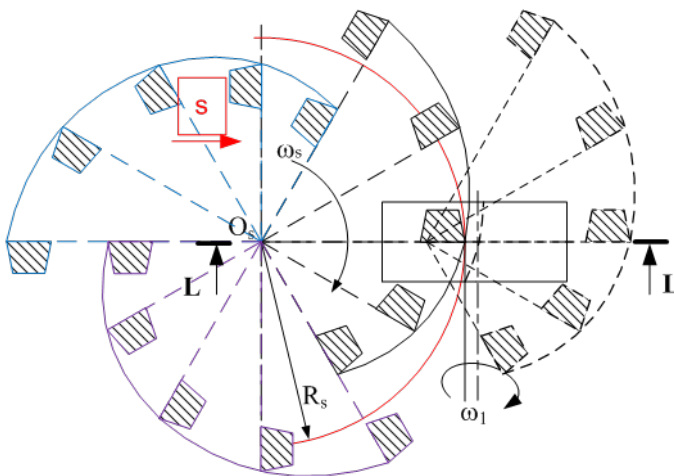


Figure 3: The cutter head and the principle of tangential feed.

$$p_{sp} = Z_0 \frac{\pi m}{2\pi} = Z_0 \frac{m}{2} \tag{1}$$

The magnitude of teeth’s curvature is the reference radius R_s of the spiral.

The reference edge is the central edge e.g. the 3th in each group. Denoting with τ_s the angular distance between two consecutive edges, the limit radius values of the leading spiral are

$$R_s - p_{sp} \frac{z_s - 1}{2} \tau_s \leq \rho \leq R_s + p_{sp} \frac{z_s - 1}{2} \tau_s \tag{2}$$

The kinematics of the meshing is shown on *Fig. 4*. A number of 3 frames are used as follows: frame (x_0, y_0, z_0) of the machine body, considered stationary; frame (x_s, y_s, z_s) of the milling head; finally, frame (x_1, y_1, z_1) bound to the machined gear. The chosen leading parameter in this kinematic model is the rotation angle of the milling head about its own axis φ_s .

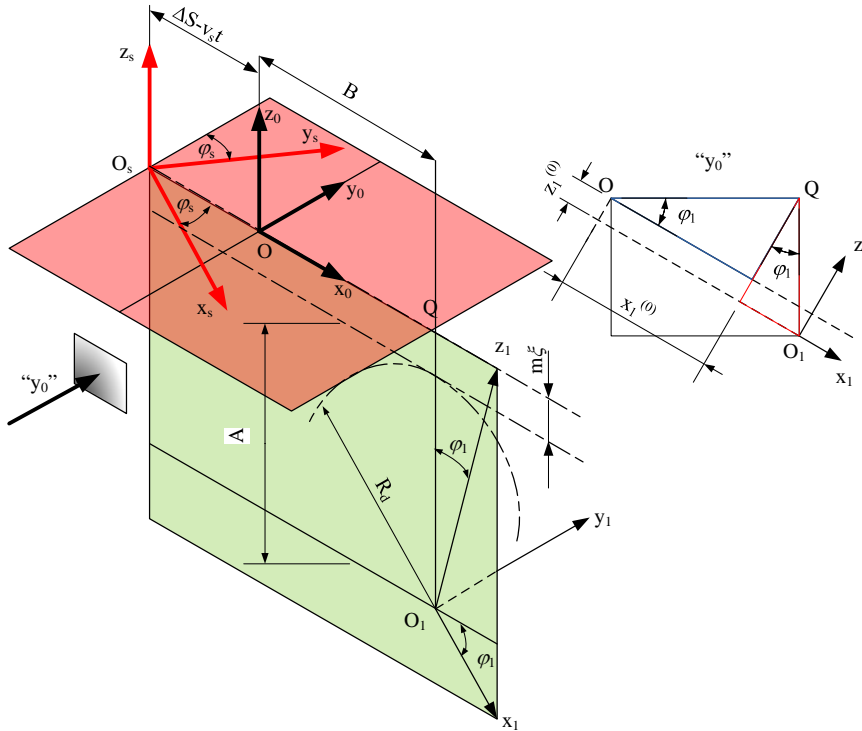


Figure 4: The kinematics of meshing.

The tangential feed can be defined considering the tangential velocity v_s or in dependence with the rotation angle φ_s , meaning in this case the length of tangential sliding. This last definition is more adequate for the next purposes. Finally, the rotation angle φ_1 of the machined gear depends on the rotation angle of the milling head and the corresponding tangential displacement of the milling head $\Delta x(\varphi_s)$. The geometric condition is that of slideless rolling of the pitch circle on the pitch line of the imaginary rack.

In order to prime the function $\Delta x(\varphi_s)$ let's suppose that cutting velocity v_c and tangential feed length pro minute s_1 are known or determined with analogy to other similar cutting processes. In this case, the rotation n of the milling head can be computed with the well-known formula

$$n = \frac{10^3 v_c}{2\pi R_s} \quad (3)$$

Considering that the tangential displacement during one complete rotation amounts s_1/n the sought dependence can be primed as

$$\Delta x = \frac{s_1 \varphi_s}{n 2\pi} = \frac{R_s s_1}{10^3 v_c} \varphi_s = \psi \varphi_s \quad (4)$$

The rotation of the machined gear, considering equation (4) and the pitch of the spiral given by (1) became

$$\varphi_1 = \frac{\varphi_s P_{sp} + \psi \varphi_s}{R_d} = \frac{P_{sp} + \psi}{R_d} \varphi_s \quad (5)$$

Using dependences (4) and (5) the model of the single parametric meshing can be built up.

3. The equations of the single parametric mesching

A. The equations of the generating surfaces

Generating surfaces in the theory of meshing are considered – both one and two parametric cases – the support surfaces of the cutting edges, which can take very variate forms; their definition stats from the presumption that the cutting tool possesses an infinity of edges e.g. a grinding wheel [5], [6], [7]. In the case described in this paper the generating surfaces are the support of the cutting

edges. Generatrix is the straight segment of cutting edge while the directory is is the Archimedean spiral. The equations can be easily written using *Fig. 5*.

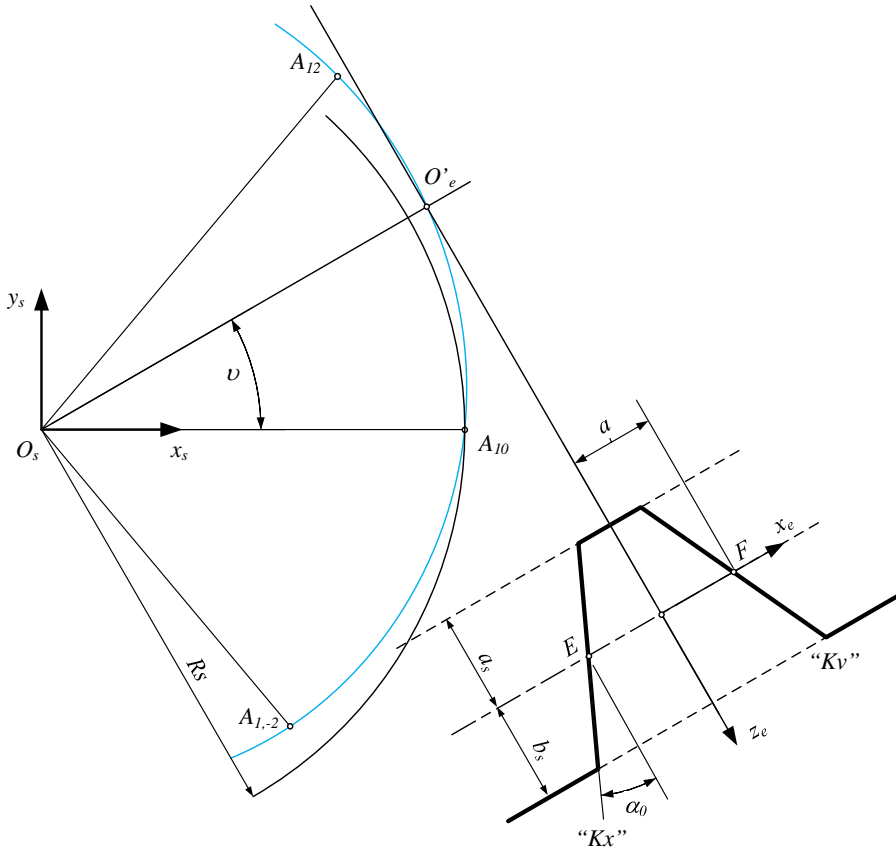


Figure 5: The built-up of the generating surfaces.

Here is to remark that generating surfaces are meshed by the cutting edges when frame $(x_e y_e z_e)$ moves counterclockwise with origin O_e on the Archimedean spiral while axis $O_s z_s$ is still contained in plane $(x_e z_e)$. Notation “ Kx ” denotes the convex toothspace generating edge. By analogy, notation “ Ky ” is used for the concave surface. Using the matrix transformation between the involved frames

$$\mathbf{r}_s = \mathbf{M}_{se} \mathbf{r}_e \Leftrightarrow \begin{pmatrix} x_s \\ y_s \\ z_s \\ 1 \end{pmatrix} = \begin{pmatrix} \cos \nu & -\sin \nu & 0 & (R_s + p_{sp} \nu) \cos \nu \\ \sin \nu & \cos \nu & 0 & (R_s + p_{sp} \nu) \sin \nu \\ 0 & 0 & 1 & 0 \\ 0 & 0 & 0 & 1 \end{pmatrix} \begin{pmatrix} x_e \\ y_e \\ z_e \\ 1 \end{pmatrix} \quad (6)$$

the generalized equations of the generating surfaces result as follows:

$$\begin{cases} x_s(u, \nu) = (i(a + u \operatorname{tg} \alpha_0) + R_s + p_{sp} \nu) \cos \nu \\ y_s(u, \nu) = (i(a + u \operatorname{tg} \alpha_0) + R_s + p_{sp} \nu) \sin \nu, \quad i \in \{-1; 1\} \\ z_s(u, \nu) = u \end{cases} \quad (7)$$

B. The equation of gearing

The equation of gearing will be written using the kinematic model developed by Litvin [8]. First the equations of the generating surface families must be written. This is accessible using geometric dependences emphasized on Fig. 4. The equation of the transformation is

$$\mathbf{r}_1 = \mathbf{M}_{1s} \mathbf{r}_s \quad (8)$$

where the transformation matrix has the following expression:

$$\mathbf{M}_{1s} = \begin{pmatrix} \cos \varphi_1 \cos \varphi_s & \cos \varphi_1 \sin \varphi_s & -\sin \varphi_s & -(B + \Delta s - \psi \varphi_s) \cos \varphi_1 - A \sin \varphi_1 \\ -\sin \varphi_s & \cos \varphi_s & 0 & 0 \\ \sin \varphi_1 \cos \varphi_s & \sin \varphi_1 \sin \varphi_s & \cos \varphi_1 & -(B + \Delta s - \psi \varphi_s) \cos \varphi_1 + A \sin \varphi_1 \\ 0 & 0 & 0 & 1 \end{pmatrix} \quad (9)$$

The relative velocity can be written with help of Fig. 6. First, the tangential velocity component of the milling head is

$$\dot{\mathbf{s}} = \psi \omega_s \mathbf{i}_0 \quad (10)$$

Adding this to the component resulted from the superposition of rotations the relative velocity can be computed as follows:

$$\begin{aligned} \mathbf{v}_{O_s}^{(s,1)} &= \mathbf{v}_{O_s}^{(s)} - \mathbf{v}_{O_s}^{(1)} = \psi \omega_s \mathbf{i}_0 + \boldsymbol{\omega}_{O_s}^{(s)} \times \mathbf{r}_s - \boldsymbol{\omega}_{O_1}^{(1)} \times \mathbf{r}_1 = \\ &= \psi \omega_s (\cos \varphi_s \mathbf{i}_s + \sin \varphi_s \mathbf{j}_s) + (\boldsymbol{\omega}_{O_s}^{(s)} - \boldsymbol{\omega}_{O_s}^{(1)}) \times \mathbf{r}_s - \mathbf{A}_w \times \boldsymbol{\omega}_{O_s}^{(1)} \end{aligned} \quad (11)$$

The normal vectors of the generating surfaces are computed using the classical formula $\mathbf{n} = \mathbf{r}'_u \times \mathbf{r}'_v$. With all partial results, after a long calculus,

$$\begin{aligned}
a' &= \frac{-\operatorname{tg} \alpha_0 \cos(\varphi_s - \nu)}{\cos^2 \alpha_0} \\
2k' &= p_{sp} \sin(\varphi_s - \nu) - \left[(R_s + a + p_{sp} \nu)(1 + 2 \operatorname{tg}^2 \alpha_0) + A \operatorname{tg} \alpha_0 \right] \cos(\varphi_s - \nu) + \\
&\quad + i_{s1} p_{sp} \operatorname{tg} \alpha_0 + (B + \Delta S - \psi \varphi_s) \operatorname{tg}^2 \alpha_0 \\
c' &= A p_{sp} \sin(\varphi_s - \nu) - (p_{sp} \nu + R_s + a) \left[A + (p_{sp} \nu + R_s + a) \operatorname{tg} \alpha_0 \right] \cos(\varphi_s - \nu) + \\
&\quad + \left[i_{s1} p_{sp} + \operatorname{tg} \alpha_0 (B + \Delta S - \psi \varphi_s) \right] (p_{sp} \nu + R_s + a) \\
i_{s1} &= \frac{1}{i_{1s}} = \frac{R_d}{p_{sp} + \psi}
\end{aligned} \tag{13}$$

C. The computing of the meshed surface

The equation of gearing returns solutions of type

$$u_i = f_i(\nu, \varphi_s), \quad i = \overline{1, 2} \tag{14}$$

for both toothspace limiting surfaces. Due to the fact that equation of gearing returns *all* solutions, it is necessary to separate only those that contribute to build up the real materialized part of the machined gear. As a conclusion, some parameter limiting conditions must be defined.

If the width of the machined gear is B_k then y coordinate of the generating surfaces must fulfill the condition:

$$-0.5B_k \leq y_1 \leq 0.5B_k \tag{15}$$

Considering the start position of the frames involved in the mathematical model, it can be easily established the limits of the rolling angle φ_1 considering an analogy with the coupling of a spur involute gear and a rack. After some calculus it results

$$\varphi_{11} = - \frac{\left(\sqrt{r_a^2 - r_b^2} - \sqrt{r_a^2 - R_d^2} \right) \frac{1}{\cos \alpha_0} + (a - m\xi \operatorname{tg} \alpha_0)}{R_d} \tag{16}$$

$$\varphi_{12} = \frac{h_{0a}^* + c_a^* - m\xi}{\sin \alpha_0 \cos \alpha_0} - (a - m\xi \operatorname{tg} \alpha_0) \tag{17}$$

Finally, the value of the edge parameter moves within the interval $u \in [-a_s, b_s]$, while the spiral parameter $\nu \in [-\pi/Z_0, \pi/Z_0]$.

Considering two sets of N_i respectively N_j equidistant values on the intervals mentioned before, the generating surface can be approximated as a system of nodes $(x_1^{(i,j)}, y_1^{(i,j)}, z_1^{(i,j)})$. Now the equation of gearing will be brought on the following particular form:

$$u_i - f\left(v_j, \frac{R_d}{p_{sp} + \psi} \varphi_1^{(i,j)}\right) = 0 \quad (18)$$

The angle $\varphi_1^{(i,j)}$ results numerically for each (u_i, v_j) parameter combination. If the solution meets the interval defined by the limit values given through expressions (16) and (17) a real point results on the meshed surface.

Another possible way to compute the points of the meshed surface consists in the determination of the contact curve on the generating surface. In this case, the gear's rolling parameter φ_1 will be represented as a set of N_i values on the rolling interval. For each φ_1^i and each v_j a correspondent value $u_{i,j}$ is obtained through solving equation (12). With this, the contact curve on the generating surfaces are written using equations (7). The meshing surface results with the transposing of the contact curve in the frame (x_1, y_1, z_1) using the matrix transformation (8).

Acknowledgements

Publishing of this journal is supported by the Institute for Research Programmes of the Sapientia University.

This research was supported by the European Union and the State of Hungary, co-financed by the European Social Fund in the framework of TÁMOP-4.2.4.A/2-11/1-2012-0001 'National Excellence Program'.

Unspecified notations

α_0 – the rack profile angle

m – the module

R_d – the radius of the pitch circle

r_a – the radius of the addendum circle

r_f – the radius of the dedendum circle

r_b – the radius of the involute basic circle

a – the half width of the generating rack profile on the pitch line

ξ – profile shifting coefficient

ω_s – angular velocity vector of the milling head

ω_1 – angular velocity vector of the machined gear

References

- [1] Litvin, F.L., Pin-Hao, F., Lagutin, S. A. “Computerized Generation and Simulation of Meshing and Contact of New Type of Novikov-Wildhaber Helical Gears”, R—2000-209415"Online]. Available: http://gearexpert.free.fr/fichiers_pdf/engrenage_Novikov_Wildhaber_NASA_report.pdf [Accessed: 30-Jun-2012].
- [2] Nacy, S. M., Abdullah, M. Q., Mohammed, M. N. “Generation of Crowned Parabolic Novikov Gears”, Adept Scientific Knowledge Base. Available: <http://www.adeptscience.co.uk/kb/articleprint.php?noteid=6E9E>. [Accessed: 19-Mar-2012].
- [3] Máté, M., Hollanda, D., “The Cutting of Cylindrical Gears Having Archimedean Spiral Shaped Tooth Line”, *13th International Conference on Tools*, 27-28 March 2012, Miskolc, pp. 357-362.
- [4] Máté, M., Hollanda, D., Tolvaly-Rosca, F., Popa-Müller, I., “The localization of the contact patch by cylindrical gear having an Archimedean toothline using the method of setting the tangential displacement”, in *Conference Proceedings of the XXI-th International Conference of Mechanical Engineers*, Arad, 25-28 apr. 2013, pp.265-268.
- [5] Dudás, I. “The Theory and Practice of Worm Gear Drives”, Penton Press, 2005.
- [6] Dudás, I., Bányai, K., Varga, G., “Simulation of meshing of worm gearing”, American Society of Mechanical Engineers, Design Engineering Division (Publication) DE 88, pp. 141-146, 1996.
- [7] Varga, G., Balajti, Z., Dudás, I., “Advantages of the CCD camera measurements for profile and wear of cutting tools”, *Journal of Physics: Conference Series* 13 (1), pp. 159-162, 2005, “Zotero Style Repository”, Roy Rosenzweig Center for History and New Media. [Online]. Available: <http://www.zotero.org/styles>. [Accessed: 19-Mar-2012].
- [8] Litvin, F. L., Fuentes, A. , “Gear geometry and applied theory. (Romanian translation by prof. Vencel Csibi)”, Ed. Dacia, Cluj-Napoca, 2009.



Characterization Methods of a 2 DOF Micro Positioning Compliant Mechanism

Daniel LATEȘ¹, Simona NOVEANU², Vencel CSIBI³

Technical University of Cluj-Napoca,
Department of Mechatronics and Machine Dynamics,
Cluj-Napoca, Romania,

¹e-mail: danielates@yahoo.fr

²e-mail: simona.noveanu@mdm.utcluj.ro

³e-mail: csibiven@yahoo.com

Manuscript received October 15, 2014; revised December 15, 2014.

Abstract: This paper presents a micro positioning plain mechanism with two degrees of freedom. The mechanism is compliant with rectangular joints for profile sections. The actuation of the mechanism is performed using two piezoelectric actuators. The limit positions of the final effector mechanism are determined by two experimental methods. The first method is an optical method that uses a CNC and CMM Aberlink program. The second method uses the same CNC probing, but the equipment is completed with the Aberlink 3D program and a testing head. At the end of the paper the comparison of the results obtained by the above methods are analyzed.

Keywords: compliant mechanisms for positioning, displacement, CNC, Aberlink CMM, Aberlink 3D.

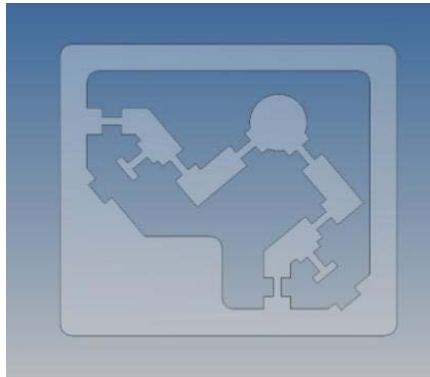
1. Introduction

Plan positioning mechanisms have been studied in different variants [9], [15], [16]. For micro and nano positioning systems made with joints and/or flexible elements having limited motions but suitable for miniaturization are used [1], [2], [7], [8]. Their actuation is effected by the use of unconventional actuators [5], [6], [17], [18].

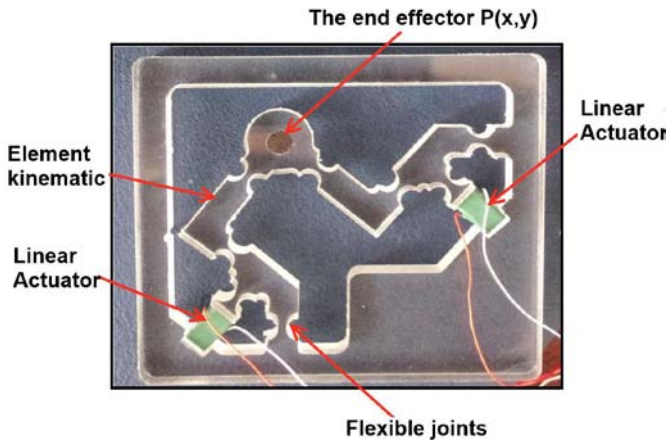
This paper presents the design of a positioning mechanism with flexible joints created of one single piece. The characterization of the compliant mechanism is performed by a piezoelectric drive activated through two methods: the first is optical using a CNC and CMM Aberlink program; the second method uses the palpation and is assisted by the same CNC with the 3D Aberlink program.

2. Design and implementation of the micro positioning mechanism

The compliant micro positioning mechanism is actuated by two linear piezoelectric actuators each capable of a $9,1 \mu m$ maximum stroke. The structure constituent elements are represented in *Fig. 1*, [3], [4]. The projections on axes x, y of the motions of the “ P ”- end effector are calculated separately for each actuator and finally totalized. The 3D model of the micro positioning system design is shown in *Fig. 1*.



a) 3D Model



b) Model made practical

Figure 1: Description of structure.

Finite element analysis is performed for 1, 3, 5, 7 and 9 μm stroke values admitting the following constants of the mechanism constituting material: Poisson's ratio $\nu = 0,39$ and Young's modulus $E = 0,39 \text{ MPa}$.

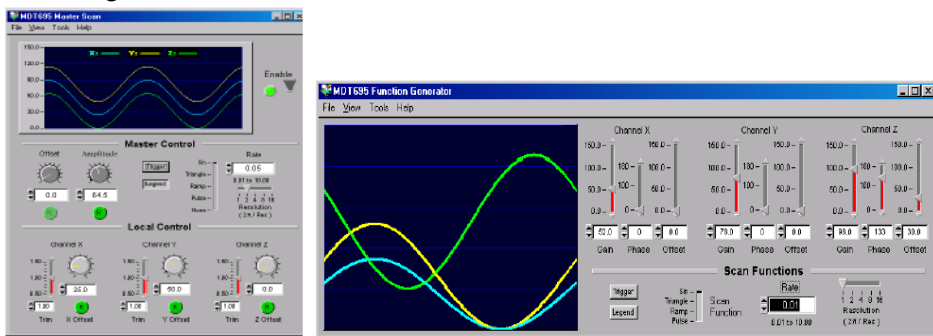
The obtained results are presented in Table 1.

Table 1.

Test nr.	Actuator 1 (Left)	Actuator 2 (Right)	Force on actuator (N)	Displacement of the actuator (μm)	FEM Analysis Displacement of endpoint "P" (μm)		
					x	Y	comp
1.	x	-	0,038	1	1,3	0,4	1,4
2.	x	-	0,116	3	4,0	1,5	4,1
3.	x	-	0,194	5	6,5	2,6	7,0
4.	x	-	0,272	7	8,7	3,9	9,6
5.	x	-	0,350	9	12	4,8	13
6.	-	x	0,07	1	0,5	0,8	0,9
7.	-	x	0,210	3	1,5	2,4	2,9
8.	-	x	0,350	5	2,6	4,1	4,8
9.	-	x	0,490	7	3,7	5,7	6,8
10.	-	x	0,650	9	4,9	7,6	9,1

3. The control of the micro positioning mechanism

Micro positioning mechanism control is achieved through an MDT693A controller that has the ability to interact and control through a Master Scan screen. Here the desired settings can be made for controlling the motions of the actuators. Fig. 2a presents the arrangement of the buttons. Fig. 2b, shows the function generator window [12].



a) Master Scan screen

b) The window function generator

Figure 2: MDT693A controller Interface.

4. The characterization of the micro positioning mechanism

The characterization of the mechanism is performed using the following two investigative methods:

- measurements on a stand using the Aberlink CNC and CMM software (method 1);
- measurements on a CNC machine using the 3D Aberlink program (method 2).

4.1 *The realization of the measurement on stand Aberlink with CNC and CMM software (method 1)*

The measurements using the experimental stand were realized with the help of an image acquisition camera designed for this type of machine and a special program called “Aberlink color CMM Camera”. With this equipment small or dedicated parts can be measured, acquiring two-coordinate data (2D). The use of this method provides high-resolution and non-contact control. The camera disposes of light setting, edge detection and optical scanning tools, which are fully programmable, having the possibility to use also the tactile method within the program, [10].

The infrastructural characteristics of this method are:

- Fully compatible with Aberlink’s easy-to-use measurement software;
- Swap between touch probe and CMM camera in seconds;
- Use touch and vision technology within the same inspection program;
- Unique dual light ring with UV LED’s to back light parts on the CMM;
- High speed optical scanning - up to 5000 points/second;
- High precision edge detection for feature inspection;
- Thread measurement - min/max/mean pitch, left/right angles, effective diameter;
- Screen overlays - XY/angular crosshairs, align to mouse, align to edge;
- Large stand-off for measuring over tall features;
- Fully programmable digital zoom (no need to change lens);
- Directional overhead lights and back light for profile and surface feature inspection;
- Telecentric lens measures accurately even when the feature is out of focus [10].

Fig. 3 shows the stand built for these types of measurements. The main components that act in the main experiment are also detailed.

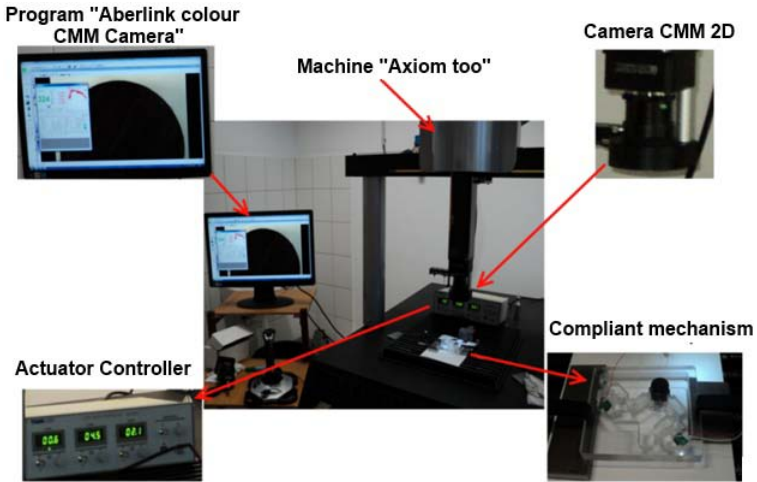


Figure 3: CMM 2D camera measurement stand.

Fig. 4 presents a screen capture obtained during the measurement. The end effector appears black colored due to the contrast (between rear view and track measured) needed for performing the measurements. After the measurement area is delimited, (2 mm from the outer edge of the end effector, in this case), the program allows 342 points of measurement in which it computes the motion from the displacement between the scanned images.

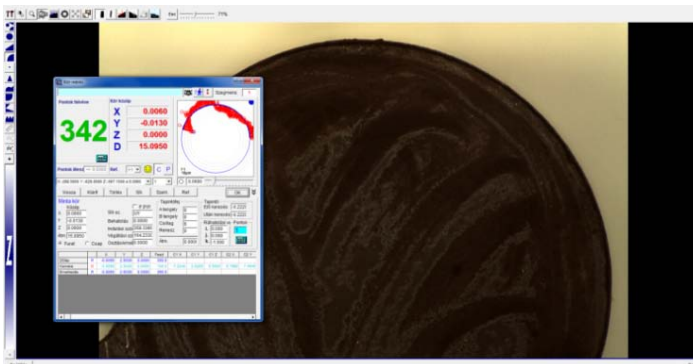


Figure 4: Computing of the displacement.

Fig. 5 shows the measurement points detected by the program after scanning and calculating the motions from the area of interest. The radial lines that start from the circumference of the blue semicircle represent the motions of the measuring points scored by the program. Quite large deviations between the measurement points appear.

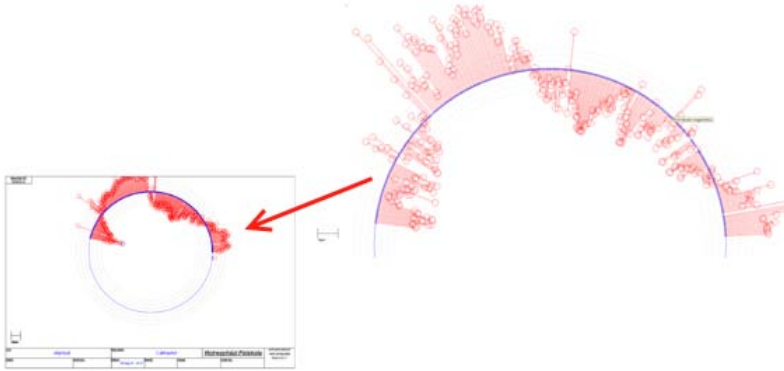


Figure 5: Displacement points made by the mechanism.

4.2 The measuring stand with CNC and Aberlink 3D (Method 2)

For this set of measurements the CNC machine from AXIOM and the 3D Aberlink program was used. Aberlink 3D is an innovative software package for manual designing, CNC and CMMs. This program is one of the favorites for producers of measurement devices. Aberlink provides a complex and easy explorable interface for the user [11].

The characteristics of the second method are the followings:

- Reliable high accuracy 3D inspection;
- Aberlink's easy-to-use measurement software (now standard on many OEM systems);
- Individual locks and fine adjust hand wheels on each axis;
- Suitable for the workshop environment;
- Anti-vibration protection from local machine tools as standard;
- Temperature compensation and other correction options for workshop environments.

Fig. 6 shows the main acting elements of the experimental stand during the measurements. Before starting the measuring process the machine must be calibrated. This procedure uses particular specimens. The 3D Aberlink software starts while the reference specimens are inserted on the x , y and z directions for the compliant mechanism.

Initially 6 measuring points situated on the circumference of the end effector were chosen. After a few attempts, 20 other measurement points are added in order to obtain the best possible measurement accuracy. The measuring points are placed manually, and then the machine memorizes them automatically. After the palpation process is complete in each of the 20 points situated on the circumference of the end effector, the program automatically calculates the center of the circle that defines the area of interest.

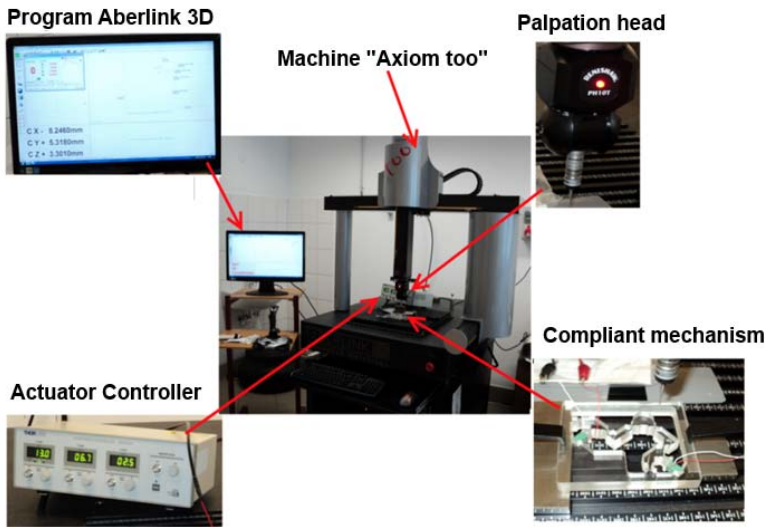


Figure 6: The stand equipped with the specimen.

5. The obtained results and their experimental comparison

5.1. The results

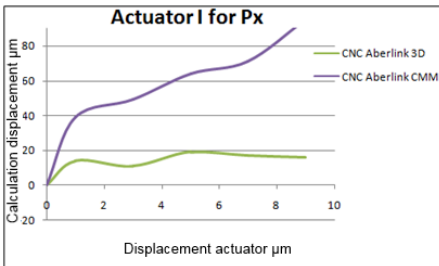
The results obtained through the two experiments performed with the equipment described in the previous chapter are presented in Table 2.

Table 2.

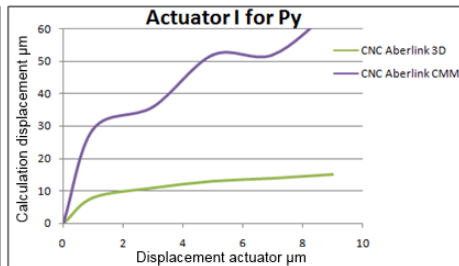
No test	Actuator 1 (Left)	Actuator 2 (Right)	Voltage Control Actuator (V _L)	Actuator displacement (µm)	Displacement "P" Method 1 (µm)		Displacement "P" Method 2 (µm)	
					x	y	x	y
1.	x	-	13	1	39	29	14	8
2.	x	-	40	3	49	36	11	11
3.	x	-	66	5	64	52	19	13
4.	x	-	93	7	71	52	17	14
5.	x	-	120	9	95	66	16	15
6.	-	x	13	1	39	29	14	13
7.	-	x	40	3	49	36	14	15
8.	-	x	66	5	64	52	15	17
9.	-	x	93	7	71	52	16	18
10.	-	x	120	9	95	66	16	19

5.2. The symmetrical joints micro positioning mechanism with rectangular section (rectangular symmetry)

The comparative data are shown in the four graphs presented in Fig. 7. Here a smaller measurement error for the y-axis can be observed: when the displacement of the actuator reaches 6 microns, the experimenting part has a slight increase, compared to the numerical FEM.



a)



b)

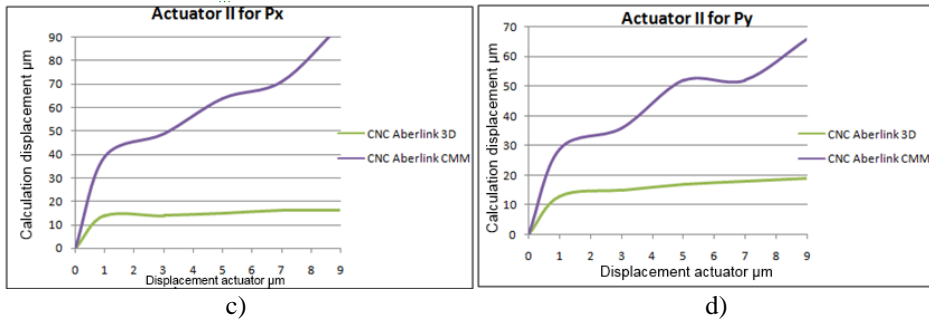


Figure 7: The graph with the results of the “Px” and “Py” end-effectors for actuator no. 1 and 2.

5.3. CNC and CN probe optical linearization method

If linearizing the curves, presented in Fig. 7, a better operable instrument will be gained. Results of the linearization are shown in Fig. 8.

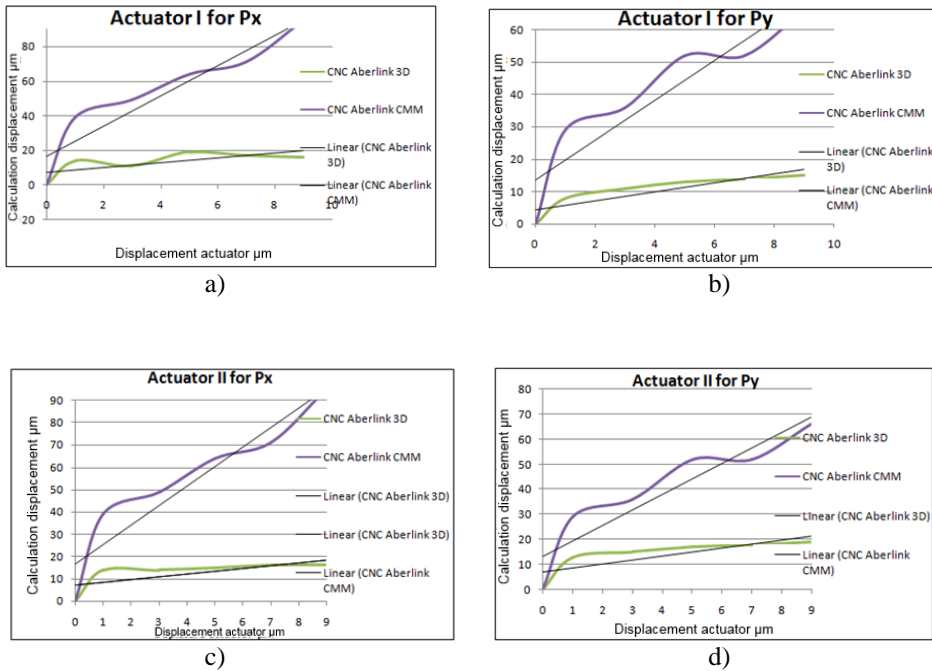


Figure 8: The linearization for the CNC optical and the probe CN methods.

5.4. The errors for the two measurement methods using the error bars with the standard error

As well as knowing the standard error (SE) is the standard deviation of the sampling distribution of a statistic. The term may also be used to refer to an estimate of that standard deviation, derived from a particular sample used to compute the estimate, [13].

Error bars express potential error amounts that are graphically relative to each data point or data marker in a data series. The error bars displayed were realized using the MS Excel admitting a standard significance level of 95% for both experiments. Standard Error and Standard Deviation are figured on the charts below (Fig. 9), [14].

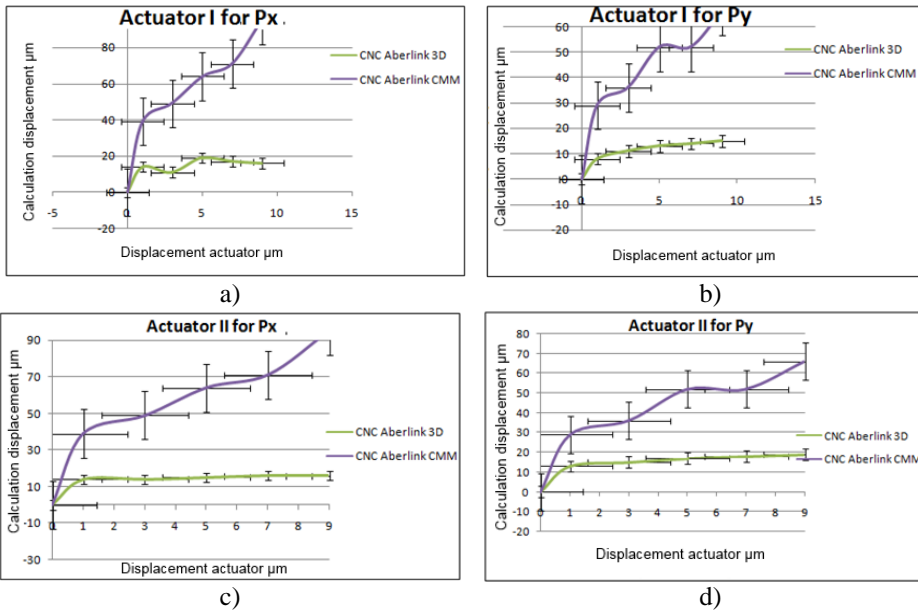


Figure 9: The standard error of the four statistics regarding the positions x , y of the actuators no. 1 and 2.

6. Conclusion

Regarding the facts and experiments presented above several conclusions can be stated:

The compliant micro-positioning mechanism subject of the study above is able to ensure a greater number positions of required accuracy than classical

jointed mechanism. It results in the same simplicity of structure positions characterized by higher accuracy.

The micro-positioning mechanism presented in this paper may be used easily to realize without any difficulties the imposed displacements according to directions x , y in the functional plane. This is available due to the work of the compliant joints and the linear piezoelectrical actuators.

Comparing the two experimental methods presented in this paper it can be concluded that palpation method ensures a higher accuracy of displacements due to the direct measuring realized on the periphery of the final effector (a circle).

The advantage of the optical method accompanied by image processing offers the advantage of a larger number of measuring points. In spite of this the measuring errors are larger leading to a bigger value of the dispersion.

From this can be concluded that the optical method is recommended when a short time experiment is needed for rapid data acquisition or estimating the working space of the mechanism. High precision measurements or control are recommended to be realized using the palpation method.

Acknowledgements

This work is supported by the Sectorial Operational Program Human Resources Development HRD / 159 / 1.5 / S / 137516 financed by the European Social Fund and by the Romanian Government.

References

- [1] Chao, D., Liu, R., Wu, Y., Shi, L., Zong, G., "Manufacturing error analysis of compliant 3-DOF microrobot", *Front. Mech. Eng. China*, 2006, pp. 299–304.
- [2] Huy, H. P., Chen, I. M., "Optimal Synthesis for Workspace and Manipulability of Parallel Flexure Mechanism", *Proceeding of the 11th World Congress in Mechanism and Machine Science*, August 18-21, 2003, Tianjin, China.
- [3] Lateş, D., Noveanu, S., Csibi, V., "Caracterizarea mecanismelor compliante cu două grade de libertate prin metoda preluării de imagine", *Conferința a II-a, Națională multidisciplinară, profesorul Ion D. Lăzărescu*, Alba Iulia, 2014, pp. 105-114.
- [4] Lateş, D., Noveanu, S., Zah, M., "Analytical study on compliant joints with asymmetrical profiles", *21th International Conference on Mechanical Engineering (OGET)*, Arad, 2013.
- [5] Lobontiu, N., Garcia, E., "Mechanics of Microelectromechanical Systems", Kluwer Academic Publishers New York, Boston, Dordrecht, London, Moscow, 2005.
- [6] Mătieş, V., Dan, M., Olimpiu, T., Mihai, M., Csibi, V., "Actuatori in Mecatronica", Editura Mediamira, Cluj-Napoca, 2000.
- [7] Polit, S., Jingyan, D., "Design of high-bandwidth high-precision flexure-based nanopositioning modules", *Journal of Manufacturing Systems*, Vol. 28, Issues 2–3, July 2009, pp. 71-77.

-
- [8] Tien-Fu, L., Handley D. C., Yuen, K. Y., Craig, E., “A three- DOF compliant micromotion stage with flexure hinges”, *Industrial Robot: an International Journal*, 2004, Vol. 31 Iss: 4, pp. 355-361.
 - [9] Weiwei, S., Shuang, C., Yaoxin, Z., “Symposium on Robot Control Nonlinear friction compensation of a 2-DOF planar parallel manipulator”, *Special Section of Revised Papers from the 8th International IFAC Symposium on Robot Control 8th International IFAC*, Vol. 18, Issue 7, Sept. 2008, pp. 340–346.
 - [10] <http://www.aberlink.com/products/cmm/camera-system/>
 - [11] <http://www.aberlink.com/products/cmm/axiom-too-manual/>
 - [12] <http://www.thorlabs.de>
 - [13] http://en.wikipedia.org/wiki/Standard_error
 - [14] <http://office.microsoft.com/en-us/excel-help/add-change-or-remove-error-bars-in-a-chart-HP010007462.aspx>
 - [15] <http://www.bg.ic.ac.uk/research/e.burdet/parallel.php>
 - [16] <http://charm.stanford.edu/ME327/JaredAndSam>.
 - [17] <http://www.clubafaceri.ro/22432/motoare-pas-cu-pas-2958446.html>
 - [18] <http://webbut.unitbv.ro/Carti%20on-line/BSM/BSM/capitol5.pdf>



Gripping Compliant Systems Operated with Bellows Actuators Used in Biomedical Engineering

Vasile Sergiu JISA¹, Daniel LATEȘ²

Technical University of Cluj-Napoca,
Department of Mechatronics and Machine Dynamics,
Cluj-Napoca, Romania,

¹e-mail: vasile_sergiu_jisa@yahoo.com

²e-mail: daniellates@yahoo.fr

Manuscript received July 23, 2014; revised September 15, 2014.

Abstract: The purpose of this paper is to analyze a set of developed gripper prototypes operated by bellow actuators that can be utilized in biomedical engineering. The main role of these grippers is catching small and big objects, their main advantage being to remove the complexity of structures using flexible couplings. Experimental results will be compared with numerical results obtained by finite element method.

Keywords: compliant mechanisms, bellows actuators, grippers, finite element analysis.

1. Introduction

Nature is a real and inexhaustible source of optimal solutions for a variety of technical problems of great interest. Trends of miniaturization of compatible products with modern technology open new perspectives for micro grippers, for the manipulation of samples in mechatronics, robotics, biomedical engineering and other technical fields, where the required force is provided by micro actuators [1], [2].

This paper presents a structured set of grippers that can be miniaturized in the future, which highlights the multiple possibilities offered by compliant elements operated by corrugated tubular elements (bellows). The first part presents a few concepts about compliant mechanisms, followed by presenting flexible couplings which are having a major importance for the functionality of compliant structures. The importance of using bellow actuators in mechatronics/robotics and biomedical engineering is covered in chapter three, while chapter four is dedicated to the CAD model of proposed prototypes, which have two, three respectively four fingers (fasteners). The finite element

method for the developed models is presented in the next chapter and finally, the comparing results obtained by numerical and practical methods are submitted.

Mini grippers are covered in various articles pertaining to specialty literature, such as [2], [3] and [4]. The authors create models and present aspects regarding robotic micro-manipulation systems, an artificial finger from polymer and metal composite used for micro gripping and debate about the control and the driver system for the proposed actuators.

2. Synthesis of mechanisms with elastic elements

Due to technological progress and the miniaturization of structure mechanisms that tend to get the best possible performance in terms of motion control, positioning systems were also part of the ongoing development and change. Transition from a positioning system based on mechanisms using couplings and classical elements to in one piece mechanisms with flexible joints is due to different material characteristics and related studies. Compliant mechanisms are those mechanisms that transmit the motion or force due to material elasticity, as shown *Fig. 1* [5].



Figure 1: Principle of compliant motion mechanisms.

The elasticity of the material is exerted on the flexible coupling. A flexible coupling consists of a thin member that provides rotation between two members through bending, like in *Fig. 2* [6], [13].



Figure 2: Classical coupling (a), Flexure hinges (b).

The compliant mechanisms use elastic displacements due to forward movement, are reversible and remain within the validity limit of Hooke's law [12]. These mechanisms are designed for miniaturization and are accurate systems because they contain elements of rigid solid character, the connection between them being made by elastic type links which provide a certain unequivocally relative movement between elements [14].

Since the performance of compliant mechanisms is highly dependent on the characteristics of the materials from which they are made, the analysis of these unconventional mechanisms requires knowledge from several fields. Motions allowed by these mechanisms are more restrictive and highly dependent on the topology of the mechanism. Mechanisms with elastic joints have recently experienced a spectacular development due to advances in micro-technologies [7].

3. Bellows based actuators

Bellow elements are also called corrugated-tubes with thin walled shells of revolution, which are precision engineering constructive elements, frequently used as sensorial elements. They falls into the energy accumulation and signal translation categories. Bellows are curved on the side and can elongate or compress under axial force or internal/external pressure. Their activation is based on elastic deformation of corrugated elements, having high performances versus weight and they have a simple design and low cost [8].

Bellows are frequently used in pneumatics and hydraulics, their geometrical dimension, shape and material determining a clear dependency between the inside or outside installed pressure and deformation produced by it [9].

The performances of different mechatronic systems are influenced by their actuators which convert the input energy into controllable motion. The actuation effect is achievable by: induced limited strains, interactions of the magnetic field, electrical current and electrical charges, respectively, mechanical interaction. The last one involves the presence of a liquid or gas, whose pressure or flow determines the movement and/or deformation of the active elements. The actuators based on inflatable elements may be classified as: variable stiffness actuators, actuators with asymmetrical pressurization, artificial muscles and other types, including bellow actuators [10].

The bellows which will activate the grippers are made from nickel alloy with 20 mm length in normal state and 0.08 mm wall thickness, a number of 24 convolutions powered with pneumatic pressure at a maximum value of 20 bar for the FC-1 bellow (*Fig. 3*) and 27bar for the FC-9 bellow. Tensile Strength for these types of bellows is 930 MPa and Yield strength is 910 MPa, according to Servometer manufacturer's catalog [11].

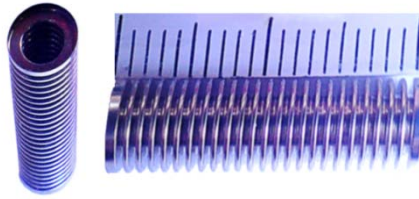


Figure 3: FC-1 bellow.

4. Constructive variants of grippers used in biomedical engineering

Fig. 4 presents CAD gripper models, each one being operated by only one bellow. For the constructive models presented in Fig. 4 a), c) and d), the role of the corrugated tube element is to spread the clamps of the gripper. Their return into the initial position is achieved by releasing the pressure from the transducer. Fig. 4 c) presents the structure of a gripper with three arms disposed at 120° from each other, which are operated simultaneously by one bellow disposed along the axis of the structure. In Fig. 4 d) the fingers are disposed at an angle of 90° for bigger objects and better grasping.

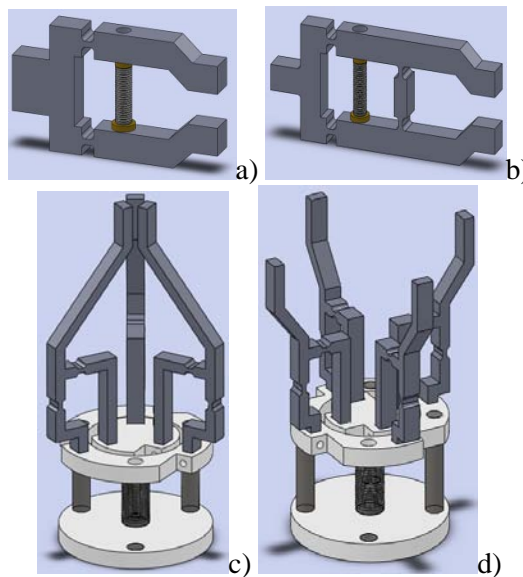


Figure 4: a) Normal gripper, b) Reverse operated gripper, c) Gripper with three fingers, d) Gripper with four fingers.

The model from *Fig. 4 b)* differs from the previous one by introducing an element between the bellows and the gripping claw. Introducing an internal pressure inside the bellow will lead to the closure of the gripping claws.

5. Finite element analysis for the compliant mechanisms

FEA begins with CAD modeling within the Design Module of the Ansys software. Ansys offers a suite of arithmetical and logical operations with the purpose of obtaining fast, efficient and approximate results and provides access to almost any field of engineering simulation which requires a design process [15].

The main advantage of FEM is reducing the complexity of the studied problem, making possible different types of analyses (linear and nonlinear static, dynamic, buckling, and fatigue). Also the shape and material optimization can be studied.

Analysis starts with establishing of the boundary condition and the material properties of the parts and is continued with the discretization of the models using different specific methods for each obtained element. *Fig. 5* shows the discretization of the normal gripper. Within this meshing the hex dominant method was used for the gripping claw. Size of the used elements does not exceed 2 mm for the gripping claw (exception: maximum size of the joints is 0.5 mm) and 0.2 mm shell elements for the corrugated tube.

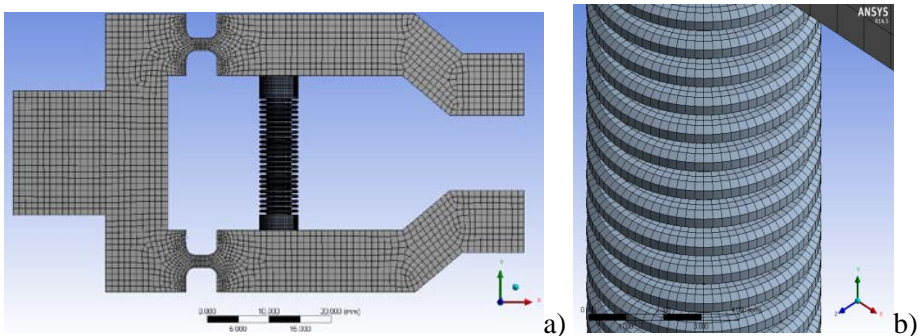


Figure 5: Discretization of the: a) normal gripper, b) FC-1 bellow.

Fig. 6. Presents the discretization for grippers with four fingers and details about FC-9 meshing with shell elements.

The discretization of the other structures was done in the same manner, the total number of obtained nodes and elements being shown in *Table 1*.

Table 1: Number of Nodes and Elements obtained by FEM method.

	Normal gripper	Reverse actuating gripper	Gripper with 3 fingers	Gripper with 4 fingers
Number of Nodes	240786	346016	226214	269707
Number of Elements	83575	107400	75110	83393

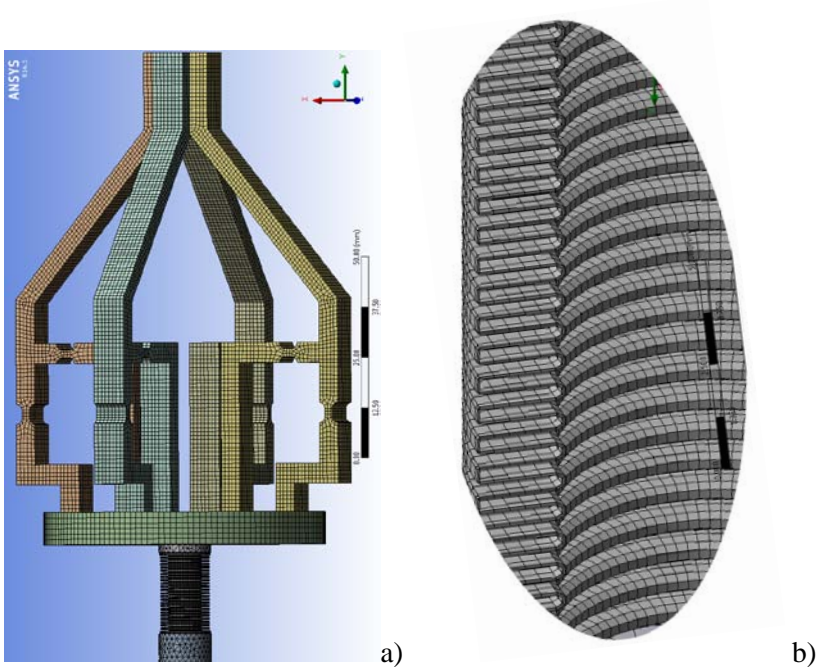


Figure 6: a) Mesh of the gripper with four fingers; b) Detail view regarding discretization of the FC-9 bellows.

All models have been tested using pressures between 0.1 and 0.7 MPa, with the purpose of studying joints' and bellows' behavior, total displacements, equivalent elastic strain and equivalent stress, of the model's structures.

Fig. 7 a) presents the total displacement of the normal gripper's claw, the bellows being pressurized with 0.2 MPa. The value of the equivalent elastic strain of the gripper joint can be observed in Fig. 7 b). Details regarding values of equivalent stress of the FC-1 bellows are in Fig. 7 c). Fig. 7 d) presents a comparison between the initial position and the total displacement of the gripping elements at the pressure of 0.7 MPa. 7 e) and 7 f) show the values obtained for the equivalent elastic strain of all four fingers of the gripper and also for the equivalent stress of the FC-9 bellows which activates the gripper.

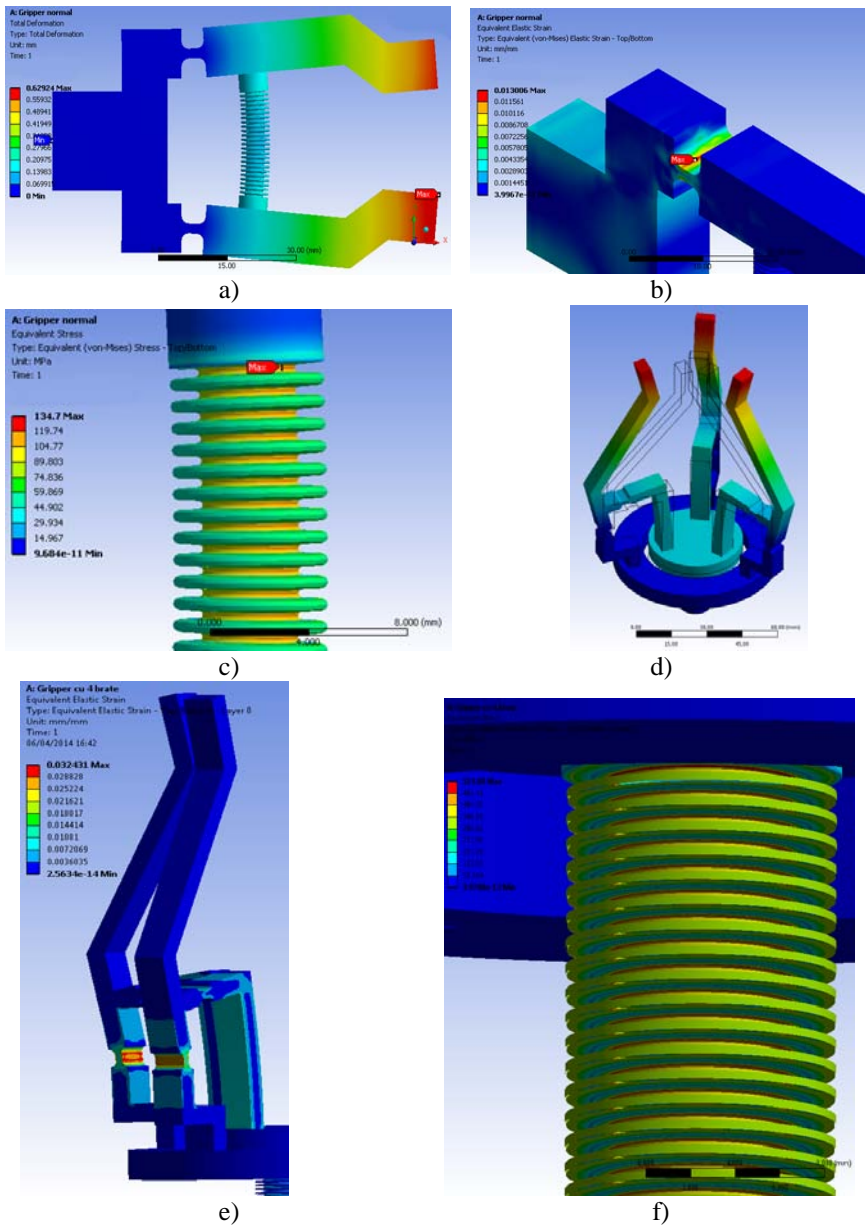


Figure 7: a) Total deformation of the normal gripper; b) Equivalent elastic strain of the joint; c) Equivalent stress for the FC-1 bellow; d) Normal vs. Total deformation of the gripper with three fingers; e) Equivalent elastic strain of the gripper with four fingers joints; f) Equivalent stress for the FC-9 bellow.

6. Experimental results

Compliant grippers made of PMMA, with aid of a CNC 3 axis mill (ISEL – CPM 2018) are presented in *Fig. 8*.



Figure 8: Compliant grippers: a) Normal and reverse actuating grippers
b) Gripper with three and four fingers.

Fig. 9 shows the components of the experimental stand where the measurements were performed on each gripper with a high speed camera and with VEDDAC software used for digital images correlation. The points of reference and arrows that show the starting and the final position of the fingers' free ends can be observed in *Fig. 10*.

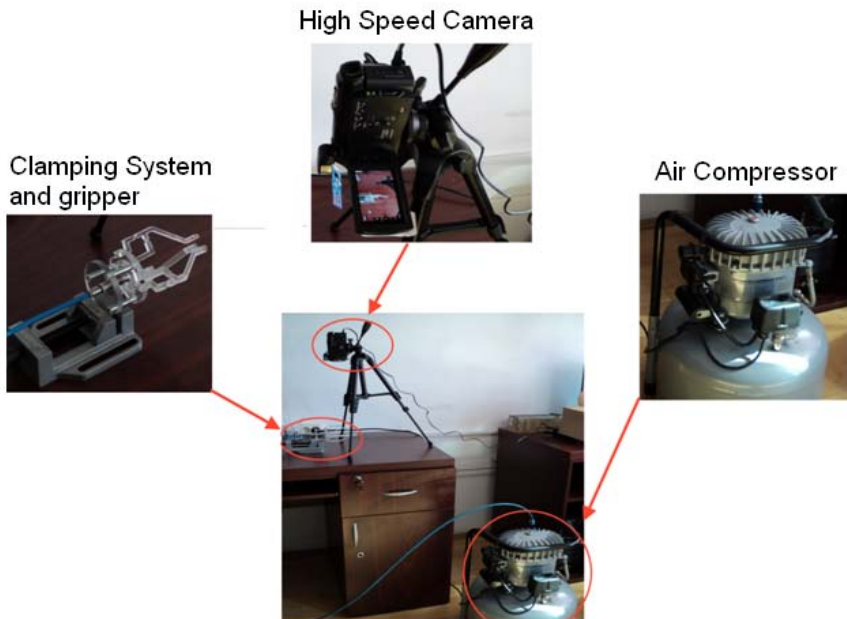


Figure 9: Experimental stand for displacement measurements.

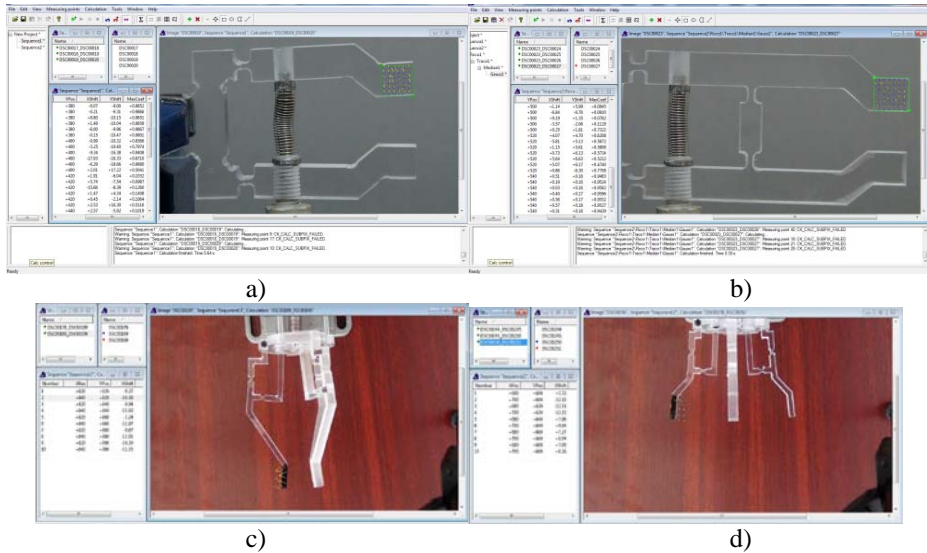


Figure 10: Correlated images from VEDDAC software with the results in the left side of the image. a) Normal gripper; b) Reverse actuating gripper; c) Gripper with three fingers; d) Gripper with four fingers.

Table 2: Experimental results obtained using Veddac software.

Gripper Type	Test No.	Pressure [MPa]	Maximum displacement [mm]
Normal gripper	1	0.2	0.62
Normal gripper	2	0.3	0.93
Normal gripper	3	0.6	1.24
Reverse gripper	4	0.2	244×10^{-3}
Gripper with 3 fingers	5	0.2	7.8
Gripper with 3 fingers	6	0.3	13
Gripper with 3 fingers	7	0.4	14.52
Gripper with 3 fingers	8	0.5	15.44
Gripper with 3 fingers	9	0.6	18.16
Gripper with 3 fingers	10	0.7	20.4
Gripper with 4 fingers	11	0.2	1.5
Gripper with 4 fingers	12	0.3	3.5
Gripper with 4 fingers	13	0.4	8.5
Gripper with 4 fingers	14	0.5	9.5
Gripper with 4 fingers	15	0.6	11
Gripper with 4 fingers	16	0.7	13

In order to determine the values for the displacements, one must know the pressure corresponding to each gripper type, the size of the flexible couplings and the limits within which it moves its active elements. *Table 2* presents the experimental results for each gripper, having applied pressures between 2 and 7 bars by taking into account the gripper's structure.

Table 3 shows the total displacement, equivalent elastic strain and equivalent stress obtained using the FEM method for each gripper at 0.6 MPa. The 10 mm thick PMMA has the following properties: Young's Modulus 1920 MPa and Poisson's Ratio 0.39, while the 8 mm thick one is characterized by: Young's Modulus 1811 MPa and Poisson's Ratio 0.38. These were determined by performing measurements on PMMA check bars on a servo hydraulic tensile testing machine.

Table 3: Results obtained by using FEM method.

	Normal gripper	Reverse actuating gripper	Gripper with 3 fingers	Gripper with 4 fingers
Total displacement [mm]	1,80	0,325	21	20,038
Equivalent elastic strain	0,005	0,016	0,038	0,036
Equivalent Stress [MPa]	230,68	120,14	682,08	657,28

7. Conclusions

The authors were able to combine and develop a set of grippers with elastic joints operated by bellow actuators and they made a comparison between the results obtained using the numerical method with FEM and experimental method with precise measuring. For the first types of grippers, actuated by FC-1 bellows, the difference between the obtained results are due to underestimating the stiffness of the elastic joints (the actuators start bending from the middle when being pressurized with more than 0.2MPa). Instead, the numeric results obtained for the grippers actuated by the FC-9 bellow can be improved by modifying the quality of the mesh elements.

One can state that the designed and tested prototypes present certain advantages in comparison with classical grippers, as they are more compact, do not require lubrication and the friction from couplings is missing. Due to miniaturization, they can work in special environments requiring high precision, accuracy reliability and small workspaces.

Gripper operation through elastic elements like bellows provides the desired control of the structure over the manipulated object, depending on input and output parameters of the bellow and the compliant mechanisms.

Acknowledgements

This paper is supported by the Sectoral Operational Programme Human Resources Development POSDRU/159/1.5/S/137516 financed from the European Social Fund and by the Romanian Government.

References

- [1] Volland, B. E., et al, “Duo-action electro thermal micro gripper”, *Microelectronic Engineering*, Vol. 84, pp. 1329-1332, 2007.
- [2] Mândru, D., Tătar, O., Rusu, C., Crişan, R., “Contribuţii privind proiectarea dispozitivelor de prindere miniaturizate (minigripere)”, *Proc. of the VII-th National Symposium PRASIC'02*, Braşov, Vol. I, pp. 145-150, 2002.
- [3] Kim, B-S., et al, “Fabrication and property analysis of a MEMS micro-gripper for robotic micro-manipulation”, *Robotics and Computer Integrated Manufacturing*, Vol. 28, pp. 50-56, 2012.
- [4] Jain, R. K., Datta, S., Majumder, S., “Design and control of an IPMC artificial muscle finger for micro gripper using EMG signal”, *Mechatronics*, Vol. 23, pp. 381-394, 2013.
- [5] Noveanu, S., “Contribuţii privind studiul mecanismelor compliante specifice sistemelor mecatronice”, Teza de doctorat, 2009.
- [6] Lates, D, Noveanu, S, Csibi, V, “Micropositioning system with flexure hinges for microfactories”, *7th International Congress of Precision Machining (ICPM)*, Miskolc, Hungary, 2013.
- [7] Lobontiu, N., “Compliant Mechanisms: Design of Flexure Hinges”, Library of Congress Cataloging-in-Publication Data.
- [8] Jişă, V. S., Mândru, D., “Synthesis and Analysis of the Bellows Actuators”, *14th Symposium on Experimental Stress Analysis and Materials Testing*, Book of abstracts, A3, Timişoara, 2013.
- [9] Jişă, V. S., Chetran, B., Noveanu, S., Crişan, N., “Actuating systems based on two bellows”, *Journal Fiability and Durability*, No. 1/2013, pp. 141–145, 2013.
- [10] Mândru, D., Tătar, O., Crişan, R., Noveanu, S., “Acţionări în mecanică fină şi mecatronică”, Editura Alma Mater, Cluj-Napoca, 2004.
- [11] <http://www.servometer.com/wp-content/uploads/2011/12/Electroforms-metal-bellows-web.pdf>
- [12] Lobontiu, N., and Epherahim, G., “Mechanics of Microelectromechanical Systems”, Kluwer Academic Publishers New York, Boston, Dordrecht, London, Moscow, 2005.
- [13] Lates, D., Noveanu, S., Zah M., “Analytical study on compliant joints with asymmetrical profiles”, *21th International Conference on Mechanical Engineering (OGET)*, Arad, 2013.
- [14] Csibi, V., Noveanu, S., Mândru, D., “Research concerning analysis of compliant joints with parabolic and hyperbolic profiles”, OGET, 2005.
- [15] Lee, H. H., “Finite Element Simulation with ANSYS Workbench 14, Theory, Applications, Case Studies”, ISBN 978-1-58503-725-4.

Acta Universitatis Sapientiae

The scientific journal of Sapientia University publishes original papers and surveys in several areas of sciences written in English.

Information about each series can be found at

<http://www.acta.sapientia.ro>.

Editor-in-Chief

László DÁVID

Main Editorial Board

Zoltán A. BIRÓ
Ágnes PETHŐ

Zoltán KÁSA

András KELEMEN
Emőd VERESS

Acta Universitatis Sapientiae Electrical and Mechanical Engineering

Executive Editor

András KELEMEN (Sapientia University, Romania)
kandras@ms.sapientia.ro

Editorial Board

Tihamér ADÁM (University of Miskolc, Hungary)
Vencel CSIBI (Technical University of Cluj-Napoca, Romania)
Dénes FODOR (University of Pannonia, Hungary)
Dionisie HOLLANDA (Sapientia University, Romania)
Maria IMECS (Technical University of Cluj-Napoca, Romania)
Zsolt LACZIK (University of Oxford, United Kingdom)
Géza NÉMETH (Budapest University of Technology and Economics, Hungary)
Ștefan PREITL (“Politehnica” University of Timișoara, Romania)
Gheorghe SEBESTYÉN (Technical University of Cluj-Napoca, Romania)
Iuliu SZÉKELY (Sapientia University, Romania)
Imre TIMÁR (University of Pannonia, Hungary)
Mircea Florin VAIDA (Technical University of Cluj-Napoca, Romania)
József VÁSÁRHELYI (University of Miskolc, Hungary)



Sapientia University



Scientia Publishing House

ISSN 2065-5916

<http://www.acta.sapientia.ro>

Information for authors

Acta Universitatis Sapientiae, Electrical and Mechanical Engineering publishes only original papers and surveys in various fields of Electrical and Mechanical Engineering. All papers are peer-reviewed.

Papers published in current and previous volumes can be found in Portable Document Format (PDF) form at the address: <http://www.acta.sapientia.ro>.

The submitted papers must not be considered to be published by other journals. The corresponding author is responsible to obtain the permission for publication of co-authors and of the authorities of institutes, if needed. The Editorial Board is disclaiming any responsibility.

The paper must be submitted both in MSWord document and PDF format. The submitted PDF document is used as reference. The camera-ready journal is prepared in PDF format by the editors. In order to reduce subsequent changes of aspect to minimum, an accurate formatting is required. The paper should be prepared on A4 paper (210 × 297 mm) and it must contain an abstract of 200-250 words.

The language of the journal is English. The paper must be prepared in single-column format, not exceeding 12 pages including figures, tables and references.

The template file from <http://www.acta.sapientia.ro/acta-emeng/emeng-main.htm> may be used for details.

Submission must be made only by e-mail (acta-emeng@acta.sapientia.ro).

One issue is offered to each author free of charge. No reprints are available.

Contact address and subscription:

Acta Universitatis Sapientiae, Electrical and Mechanical Engineering
RO 400112 Cluj-Napoca
Str. Matei Corvin nr. 4.
E-mail: acta-emeng@acta.sapientia.ro

Printed by Digital Color Company
www.digitalcolorcompany.ro